COMPUTATIONAL ANALYSIS OF PHOTOCATALYTIC NITROGEN FIXATION ON OXIDE SURFACES

A Dissertation
Presented to
The Academic Faculty

By

Benjamin M. Comer

In Partial Fulfillment
of the Requirements for the Degree
Doctor of Philosophy in the
School of Chemical and Biomolecular Engineering

Georgia Institute of Technology

December 2020

COMPUTATIONAL ANALYSIS OF PHOTOCATALYTIC NITROGEN FIXATION ON OXIDE SURFACES

Approved by:

Dr. Andrew Medford, Advisor
School of Chemical and
Biomolecular Engineering
Georgia Institute of Technology

Dr. David Sholl
School of Chemical and
Biomolecular Engineering
Georgia Institute of Technology

Dr. Christopher Jones
School of Chemical and
Biomolecular Engineering
Georgia Institute of Technology

Dr. Marta Hatzell
School of Mechanical Engineering
Georgia Institute of Technology

Dr. David Sherrill
School of Chemistry
Georgia Institute of Technology

Date Approved: October 6, 2020

ACKNOWLEDGEMENTS

I would like to aknownledge my advisor, Andrew (A.J.) Medford for the mentoring and advisiement that helped me produce this work, as well as the full Medford Group for their support. I would also like to acknowledge my collaborators, in Marta Hatzel's group, the international fertilizer development center (IFDC), and Dr. Realff for their help in the work presented in this thesis. Funding for this work has come from the School of Chemical & Biomolecular Engineering at Georgia Tech, The U.S. Department of Energy (DE-SC0019410), and the National Science Foundation (1943707).

TABLE OF CONTENTS

LIST OF TABLES

LIST OF FIGURES

NOMENCLATURE

DFT	Density Functional Theory
NRR	Nitrogen Reduction Reaction
RHE	Reversible Hydrogen Electrode
UHV	Ultra High Vacuum
GGA	Generalized Gradient Approximation
SHE	Standard Hydrogen Electrode
VCR	Value Cost Ratio
PV	Photovoltaic
OER	Oxygen Evolution Reaction
CHE	Computational Hydrogen Electrode
BEEF-vdw	Bayesian Error Estimation Functional with Van Der Waals corrections
O-br	Bridging Oxygen
XPS	X-Ray Photoelectron Spectroscopy
AP-XPS	Near Ambient Pressure X-Ray Photoelectron Specroscopy
ALS	Advanced Light Source
PBE	Perdew–Burke-Ernzerhof

SUMMARY

The fixation of nitrogen is of great importance for the production of chemicals and fertilizers and is performed primarily through the Haber-Bosch process. This thesis explores the potential of photocatalysis to produce fixed nitrogen in a less intensive, more distributed manner, with a focus on analyses of the surface reactions using ab inito calculations. Chapter 1 provides a brief introduction to fundamentals of N_2 fixation reaction kinetics, and provides an overview of the current literature on TiO_2. Chapter 2 focuses on the technological prospects of photocatalysis for nitrogen fixation, while Chapters 4-6 focus on the surface reaction on the TiO_2 surface. In total, this work shows that photocatalytic nitrogen fixation can be a viable technology, and elucidates the reaction pathways of nitrogen fixation on rutile TiO_2.

Chapter 1 provides an overview of the Haber-Bosch process's current impact, both economically and environmentally, as well as the basics of the reaction kinetics, thermodynamics, and photocatalysis highlighting the different pathways nitrogen fixation can take. Chapter 1 also reviews the experimental literature on TiO_2 surfaces, which is the primary system of interest, in addition to an overview of the literature on photocatalytic nitrogen fixation. The latter section notes the long history of this field. It highlights the issues around measurement and contamination, concluding with a review of the current consensus on how such ambient nitrogen fixation reactions should be carried out, and summarizes the current best protocols for experimental measurements.

Haber Bosh is highly efficient but also has among the most substantial carbon impacts of all industrial processes. By contrast, the photocatalytic production of fixed nitrogen for fertilizer would not incur such a significant carbon impact, reducing global carbon emissions. Chapter 2 examines the technological prospects of solar fertilizer production through photocatalysis and alternative routes. We find that photocatalytically producing fertilizers would lead to a more decentralized supply chain due to the global distribution of solar

energy. Additionally, fertilizer produced by this method will likely be of a much lower nutrient concentration than traditional fertilizers. However, lower concentration fertilizers may be beneficial for crop yields and environmental nitrogen pollution if adequately integrated with agricultural infrastructure. We outline preliminary performance targets for solar fertilizer production, finding that the requirements are on the order of 0.1% solar-to-chemical conversion efficiency if the process uses ambient pressure air as a feedstock and the resulting solution can be directly applied as fertilizer.

Chapter 3 covers the computational methods used for the remainder of the thesis. Chapters 4-6 analyze the surface mechanism of nitrogen fixation on a model surface, rutile (110). Chapter 4 uses density functional theory (DFT) calculations to show that the pristine and oxygen vacancy sites of rutile (110) have large thermochemical barriers for the nitrogen reduction reaction. We also explore oxidizing nitrogen on the rutile (110) surface, finding it to be thermodynamically feasible, but kinetically challenging. Chapter 5 covers the application of computational screening to examine the possibility of doping transition metals into the rutile (110) surface to improve the surface kinetics and the thermodynamics of dopant site formation. We find correlations between the metal substitution energy of the dopant metal and the *d*-band center of the bulk metallic form of the dopant metal. We also show that the binding energies of nitrogen species are correlated with the metal's *d* band contribution to cohesive energy. We additionally find that none of the proposed metals are predicted to improve the surface reaction significantly. Finally, in Chapter 6, we explore the possible role of adventitious surface carbon in the nitrogen reduction reaction on rutile (110). We find experimental evidence of the confluence of reduced nitrogen and surface carbon under illumination. We also show that a surface-bound carbon radical exhibits remarkable nitrogen reactivity, and propose a thermodynamically plausible path to reduce nitrogen on this active site.

CHAPTER 1

INTRODUCTION AND SIGNIFICANCE

1.1 Fixed Nitrogen

Fixed nitrogen is required for biological life and is a crucial feed-stock to many chemical processes. The increase in the production of fixed nitrogen, primarily in the form of ammonia has led to a significant decrease in the percentage of the world's population that is undernourished (see Figure 1.1) even as the world's population has increased.

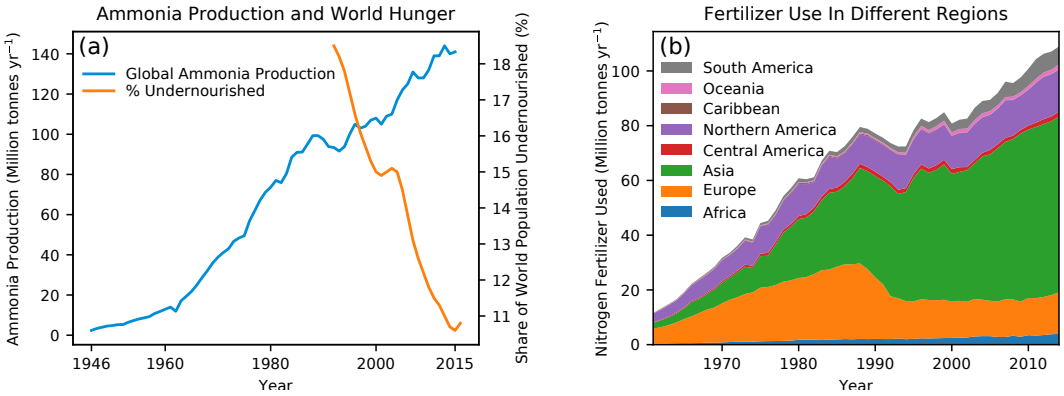

Figure 1.1: (a)The worldwide ammonia production each year since 1946 [1] and % of individuals who are undernourished globally [2]. (b) the use of nitrogen fertilizer over time denominated by region [3]

The standard method of producing ammonia at an industrial scale is through the thermochemical synthesis with the well-known Haber-Bosch process [4]. This process transformed the global fertilizer industry during the early 1900s and is a critical enabler of the continued expansion of the human population [5]. The impact of the increase in fertilizer availability is genuinely global in scale, massively increasing the potential of food production and saving roughly 2.7 billion lives; a number equivalent to 37% of currently living humans [5, 6].

The Haber-Bosch process is an impressive feat of modern chemical engineering, pro-

ducing 140 million tonnes of ammonia per year (Fig. 1.1) at a thermochemical efficiency of up to 70% [4, 7] at an overall 97% conversion of feed gasses [8]. However, the process also has downsides. The process's scale leads to an energy consumption of 2.5 exajoule per year, accounting for 1% of global energy production being expended on just this one process [9]. Also, the hydrogen feedstock is typically obtained via the methane reforming reaction [10], leading to a carbon footprint of 340 million tonnes of CO_2 equivalent per year. This carbon footprint is the highest of any commodity chemical [7]. Furthermore, the high temperatures ($\sim$700 K) and pressures ($\sim$100 bar) lead to substantial capital and operational costs. The economies of scale for these costs favor large plants and highly centralized production with $<$100 plants worldwide with an average capacity of 2200 tonnes day^{-1} [11, 12]. This concentrated production is in contrast to the dispersed use of ammonia-based fertilizers globally (Fig. 1.2), which results in high transportation costs and additional carbon emissions [13]. These transportation costs are particularly impactful in remote locations such as in sub-Saharan Africa, where soils are often nutrient-limited due to low or no fertilizer access by smallholder or poor resource farmers [14, 15, 16]. As a result Africa has significantly lower fertilizer usage compared to other regions (see Fig. 1.1b). The opposite problem of over fertilization also has a negative environmental impact in more developed regions due to the periodic application of higher rates of concentrated fertilizers. These concentrated fertilizers cause nitrate pollution by leaching into waterways, causing vast ocean "dead zones" [17, 18], and high emissions of gaseous nitrous oxide contribute to climate change. Finally, the intense conditions and reactive nature of concentrated ammonia-based fertilizer lead to safety and national security concerns, as evidenced by explosions at fertilizer plants and the common use of fertilizers in makeshift explosives [19].

1.2 Non-Traditional Nitrogen Fixation

Because of the shortcomings of Haber-Bosch, researchers have sought other, less energy and capital intensive, methods of producing fixed nitrogen for decades. This thesis will

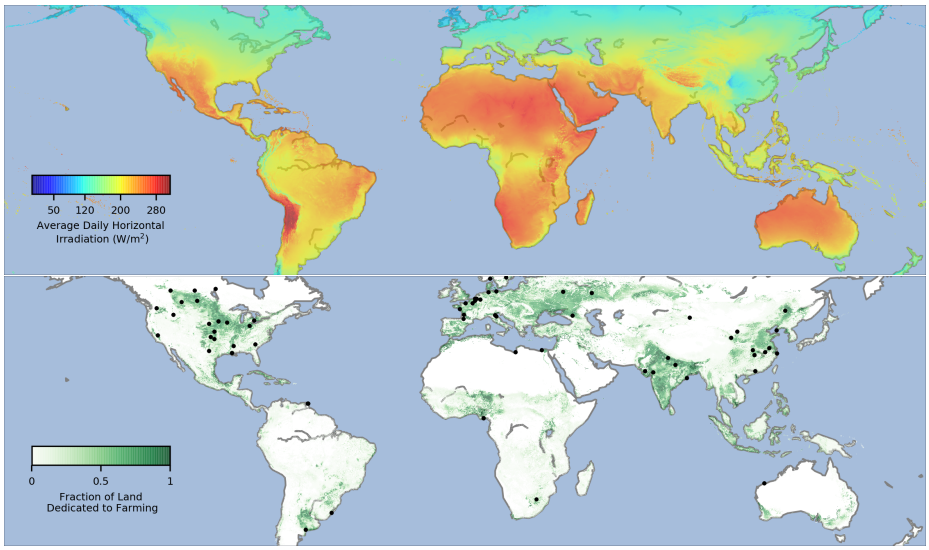

Figure 1.2: (top) Average daily horizontal solar radiation intensity over the surface of the earth (W/m^2). This represents the average flux over a 24 hour period. (bottom) Fraction of land dedicated to crop production (%), dots represent the locations of Haber-Bosch plants. Solar resource data obtained from the Global Solar Atlas, owned by the World Bank Group and provided by Solargis. Cropland data from Ramankutty et al. [20, 21]. Haber-Bosch plant data from McArthur et al.[11] and Africa Fertilizer [22].

primarily focus on photocatalysis but several other non-traditional alternatives are active acreas of researhc. Alternatives under development include electrocatalysis [23], biological catalysis [24], and plasma-enhanced catalysis [25], and thermo-cycling [26].

Electrocatalysis

Recently there has been a surge of interest in photo- and electro-catalytic nitrogen fixation by heterogeneous catalysts [27, 28, 29, 8, 30, 31, 32, 33, 34]. These possibilities are particularly interesting from the perspective of harnessing solar energy since photo(electro)chemical systems interface well with solar energy and can scale relatively easily [27]. photo(electro)chemical systems have also been the subject of considerable research and progress in the solar fuels community, demonstrating the potential for relatively high energy efficiencies exceeding 10% for hydrogen production [35, 36, 37, 38, 39, 40]. However, electrocatalysis suffers from selectivity toward NH_3 production due to the relatively facile reaction producing H_2 gas, known as the selectivity challenge [41]. There has been at least one attempt to commercialize the technology by the startup com-

pany "Atmonia" [42]. However, further work is needed to improve the yield and efficiency of electrochemical nitrogen fixation. Recent developments on the use of creative strategies for electrochemical ammonia synthesis such as "physical catalysis" [43], non-aqueous electrolytes [44], and lithium-mediated nitrogen fixation [45, 46] have led to significant improvements in reported efficiencies, suggesting that this may be a promising route.

Biological Catalysis

Biological catalysis is how most fixed nitrogen is naturally produced, totaling 20 Tg/yr [47]. In biological systems, nitrogen fixation is catalyzed by enzymes and takes place within living cells. The overall reaction is shown in Equation 1.1. In biological systems, ATP is used to drive the reaction via the nitrogenase enzyme, enabling nitrogen fixation at ambient conditions. The enzymes involved in catalyzing the reaction in living cells rely on FeMo co-factors [48]. The cofactor must be successively hydrogenated to allow the N_2 molecule to bind and initiate the reaction [49]. Additionally, Eq. (1.1) shows that some energy is expended to form H_2, indicating that the process is not utilizing some of the input energy. The nitrogenase structure has been found to regulate access to the active metal cofactor by blocking water and oxygen access [8, 24]. Some authors have immobilized the nitrogenase catalyst on glassy carbon. These studies demonstrate electrocatalytic activity toward hydrogen evolution, azide reduction, and nitrate reduction [50].

$$N_2 + 8H^+ + 8e^- + 16ATP \rightarrow 2NH_3 + H_2 + 16ADP + 16PO_4 \tag{1.1}$$

There has been significant work on engineering organisms to perform nitrogen fixation reactions. This work primarily focuses on integrating the genes coding for nitrogenase into plants and other eukaryotes. However, this work has proven exceptionally challenging and has not yet yielded viable technologies [24].

Plasma-Driven

The fixation of nitrogen through electrical arc induced plasmas approximates the natural process of nitrogen fixation via lightning [25]. This process, originally developed as the

Birkeland-Eyde process, predates Haber-Bosch [51] but fell out of favor due to the higher energy efficiency of the Haber-Bosch process at scale. Recently, there has been a resurgence of interest in low-temperature plasma. It has been proposed that plasma-enhanced nitrogen fixation could be one method of circumventing the scaling relations limiting heterogeneous catalysis [52].

Recent work on plasma-enhanced nitrogen fixation has yielded relatively high Faradaic efficiencies (on the order of 40%-60% [25]), indicating that the process can be efficient. Additionally, the competition between H_2 production and NH_3 production heavily favors NH_3 production. Thus, the "selectivity challenge" identified in the electrocatalytic literature [41] may not be present in plasma-enhanced systems. However, current plasma-induced experiments' energy requirements exceed that of Haber-Bosch (see Table 2.1.) Currently, the start-up company "Nitricity" [53] is producing fixed nitrogen based on this technology and has reached the commercialization phase. Due to its relative inefficiency, plasma-induced nitrogen fixation will require work to become a mature technology, but preliminary commercialization efforts are promising [25].

1.3 Reaction Catalysis of Nitrogen Fixation

The chemical conversion of dinitrogen through the breaking of the strong N-N bond is at the heart of nitrogen fixation. This can be done through either a reductive pathway (Equation 1.2) or an oxidative pathway (Equation 1.3.) The challenge of breaking this bond comes from its extremely high dissociation energy (9.79 eV) as well as the unfavorable positions of its highest unoccupied molecular orbital (HOMO) and lowest unoccupied molecular orbital (LUMO) energy levels (-15.6 eV and 7.3eV respectively) [54]. The former causes the direct dissociation of the N-N bond to have an exceedingly high activation barrier ($\sim$ 3.5eV on iron [55]). The latter leads to highly unfavorable electron transfers. These challenges mean that a catalyst is required, especially at benign temperatures. The Haber-Bosch process solves this problem by using high temperatures to speed up the reac-

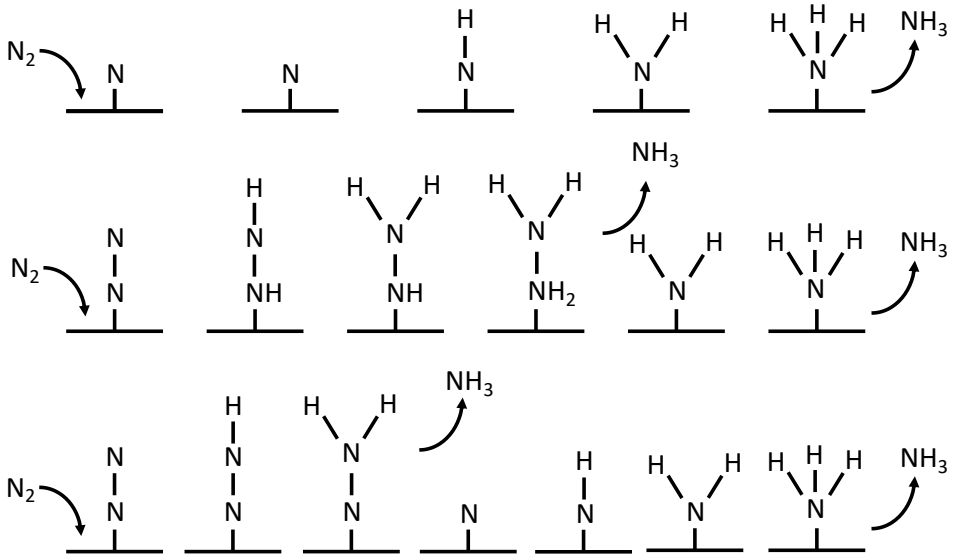

Figure 1.3: A summary of N_2 fixation mechanisms. Top to bottom these are: the direct mechanism, the alternating mechanism, and the distal mechanism

tion kinetics. However, increased temperatures necessitate increased pressure to maintain a thermodynamic driving force for ammonia synthesis [56].

$$\frac{1}{2}N_2 + \frac{3}{2}H_2 \rightarrow NH_3 \tag{1.2}$$

$$\frac{1}{2}N_2 + \frac{x}{2}O_2 \rightarrow NO_x \tag{1.3}$$

Three primary mechanisms must be considered when studying nitrogen reduction to ammonia: the direct mechanism, the alternating mechanism, and the distal mechanism (see Figure 1.3.) Of these, the most kinetically challenging is typically the dissociative mechanism. In this mechanism, the N-N bond is broken in the first reaction step (see Equation 1.4).

$$N_2^* + ^* \rightarrow 2N^* \tag{1.4}$$

While the N-N bond's direct scission may seem infeasible due to its strength, it is the mechanism implicated in most Haber-Bosch catalysts. The reaction is possible through the dissociative pathway due to a combination of the high temperatures and substantial partial pressures of N_2 gas in the reactor. The elevated temperature acts to increase the surface reaction rate constant, which follows an Arrhenius type relationship (Equation 1.6.)

$$-r_{N_2*} = kC_{N_2^*} \tag{1.5}$$

$$k = k_o e^{\frac{E_a}{RT}} \tag{1.6}$$

where $-r_{N_2*}$ is the rate of the surface reaction Equation 1.4, k is the reaction rate constant, $C_{N_2^*}$ is the surface concentration of N_2, k_o is the prefactor, E_a is the activation energy, R is the gas constant, and T is the absolute temperature.

As the temperature increases, the reaction rate constant grows exponentially, allowing for reasonable turnover frequencies even with relatively large barriers. While high temperatures improve reaction rates, they disfavor the thermodynamics of adsorption for N_2 on the surface, as bound surface states have lower entropy than gas-phase states. Elevated pressures combat the decrease in favorability of the N_2 adsorption reaction through Le Chatelier's Principle. As the concentration of the reactant (N_2) grows, the equilibrium is shifted toward the products side (N^*.) The relevant temperatures and pressures for Haber-Bosch are roughly $\sim$700 K and $\sim$100 bar [56].

These elevated temperatures have the side effect of dis-favoring the overall reaction because the total amount of moles decreases across the reaction (see Equation 1.2). Thus the products are lower in entropy, and by extension, are less favored at high temperatures. Higher pressures combat this by increasing the total amount of reactant available, pushing the equilibrium back toward the products side.

The mechanism involved also is affected by temperature. At lower temperatures, the

alternating and distal mechanisms are more feasible (see Figure 1.3). In these reactions, hydrogen is bound to the adsorbed N_2 species, thus weakening the N-N bond and allowing bond breaking. These mechanisms are favored at low temperatures relative to the dissociative mechanism because they involve subsequently attaching atoms to a surface species. These new bonds construct a lower entropy product on the surface. Thus, these are the favored mechanisms for photocatalysis and electrocatalysis, as these are typically performed at lower temperature.

The photo(electro)chemical version of this reaction is known as the nitrogen reduction reaction (NRR) and has been studied extensively. NRR has a redox potential of 0.06 V vs. the reference hydrogen electrode (RHE) and requires an overall applied potential of 1.2 V when coupled with the oxygen evolution reaction based on standard gas-phase thermochemical data [28, 30]. However, the proximity of the redox potential or nitrogen reduction and hydrogen evolution presents a fundamental challenge in nitrogen reduction since the hydrogen evolution reaction is typically faster, resulting in low selectivity [57, 41]. Several novel approaches have achieved high selectivity through creative strategies such as electrochemical looping with molten salts [58] and non-aqueous lithium-mediated electrocatalysis [45, 46]. The field's rapid progress suggests that the selectivity challenge can be overcome, but this will require a more complicated process and more energy input.

Moreover, nitrogen reduction is typically performed under anaerobic conditions to avoid competition with O_2 adsorption or reaction [59], a situation that would require capital-intensive air separation in a practical setting. Another challenge in photo(electro)catalytic nitrogen reduction is the fact that oxygen evolution is typically utilized as a half-reaction. Oxygen evolution catalysts exhibit large overpotentials of $\sim$ 0.4 V, and are often based on rare materials, presenting challenges for process efficiency and scalability [60, 61]. Nonetheless, one of the best-reported catalysts for nitrogen reduction is based on earth-abundant carbon and exhibits an electrical-to-ammonia efficiency of 5% in an aqueous electrolyte [43], suggesting that practical routes to electrochemical nitrogen reduction are

feasible.

A less-explored alternative is direct oxidation of nitrogen to nitrate products (see Equation 1.3). Nitrate production is more thermodynamically favorable than ammonia synthesis. The production of NO is the most thermodynamically challenging step, occuring at a highly oxidizing potential of 1.68 V vs. RHE. However, the reaction requires a modest applied potential of 0.45 V when coupled with the oxygen reduction half-reaction based on standard gas-phase thermodynamic data [30, 28]. Nitrate-based fertilizers are also common, and some crops are able to utilize nitrates more efficiently than ammonium, although nitrates are also more prone to leaching and can be toxic to humans [62, 63, 64, 65]. One key advantage of nitrogen oxidation is that it can occur directly in air, since oxygen is a reactant, and competition with hydrogen evolution is not an issue. Despite these promising advantages, there are considerably fewer reports of photocatalytic nitrate formation [66, 67, 68]. This indicates that catalyst development for nitrogen oxidation will require more effort. This pathway is further discussed in section 4.4.

1.4 Photocatalysis

Photocatalysis relies on the excitation of electrons in the bulk of a semi-conductor to drive reactions at the surface. The process is summarized in Fig. 1.4 [69]. Incident light first enters the bulk of the semi-conductor, interacting with the material. If the light is of sufficient energy, it will excite an electron from the valence band to the conduction band. This process also creates a positive charge, known as a hole. These electrons and holes may have been excited to states above the highest-occupied molecular orbital (HOMO) energy or below the lowest unoccupied molecular orbital (LUMO) and thus will relax to those states. The charges are then able to migrate to the surface and participate in chemical reactions. At the surface positively charged holes drive oxidation reactions, and the excited electrons drive reduction reactions. Honda and Fujishima started the study of solid-state photon-driven reactions in 1972 [70]. They measured water splitting reactions upon illuminating semi-

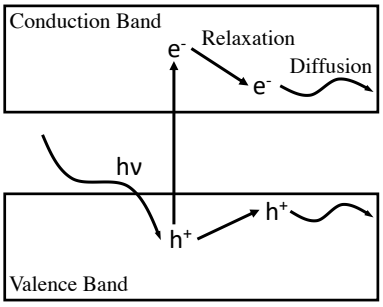

r

Figure 1.4: Generalized schematic of electronic excitation in photocatalysis in a semiconductor, an electron is excited by a photon making it able to move above the band gap and diffuse to the surface along with a positively charged "hole."

conductors. In subsequent years photocatalytic N_2 reduction [71], CO_2 reduction [72], and oxidation of organic wastes [73] was demonstrated as well. Currently, the most common use of photocatalysis is for waste treatment [74].

1.5 Experimental Literature on TiO_2

This thesis will focus on TiO_2 as the primary oxide surface of interest, as it has the most experimental studies dedicated to it [28] and is the earliest material to have been shown to catalyze nitrogen reduction [75, 71]. TiO_2 is often called the most studied oxide material [76, 77]. A review of the surface chemistry by Diebold from 2003 had 783 references and filled 158 pages while still not exhausting the topic [77]. There have been numerous reviews on the photochemistry [78, 79], surface chemical reactions [80] and synthesis [81], some of which will be discussed below. The main reasons for the literature's size are its ease of synthesis and high stability, along with the numerous reactions photocatalyzed by TiO_2. These properties have led TiO_2 to be used as a model photo-catalyst by experimentalists and theorists. While the volume of the literature on TiO_2 material is vast, it suffers from inconsistent results and few attempts to replicate others' results. This inconsistency is especially true in the photocatalysis community, and the photocatalytic N_2 reduction literature in particular [28].

The interaction of titania surfaces with water will play a role in aqueous or humidified

environments relevant to the systems studied in this work. Water adsorption on TiO_2 is a topic of extensive research and debate [82, 83, 84, 80, 85, 86, 87, 88, 89, 90], and there are a great variety of theoretical results regarding the competition between dissociative [87, 90] and molecular adsorption [88, 89, 91] on pristine surfaces, although a clear consensus has not emerged. Analyses including the effects of slab thickness [83] and method [84] support the two modes being nearly degenerate at monolayer coverages, with partial dissociation having slightly higher energy. This viewpoint is consistent with recent experimental studies observing dissociated water on pristine surfaces [92]. Experimental studies from the mid-1990s to the mid-2000s show that on a reduced surface (one containing vacancies at the bridging oxygens), water tends to dissociate to form two hydroxyl groups on the surface, thereby filling the vacancy [93, 89, 94, 95], while on pristine surfaces water adsorbs molecularly at the 5-fold Ti site [96]. As previously noted, there has been one recent report showing partial dissociation of water on the pristine surface [92].

Several other factors have been observed to play an essential role in aqueous TiO_2 photochemistry. The formation of hydroxyl radicals is known to occur in both rutile and anatase [97, 98], and these radicals participate in many oxidation reactions [97]. Furthermore, the influence of both surface and bulk defects, such as oxygen vacancies, can enhance adsorption and influence photocatalytic activity [99]. The field of TiO_2 photocatalysis and surface science is vast, and a thorough review is beyond the scope of this work; the reader is referred to published reports and review articles to gain a complete view [78, 77, 86, 80, 85].

The rutile TiO_2 (110) surface has been well-studied both experimentally [86, 92, 100, 101, 102, 78] and computationally [103, 104, 105, 106]; however, there have been relatively few computational studies of the interactions of rutile TiO_2 surfaces with nitrogen-containing compounds [103, 104, 105, 107, 108]. Two comprehensive computational studies on nitrogen oxides were performed by Stodt et al. [103] and Sorescu et al. [104]. These studies examined N_xO_y compounds on TiO_2 (110) surfaces both experimentally un-

der ultrahigh vacuum (UHV) conditions and theoretically using density functional theory (DFT) at the generalized gradient approximation (GGA) [104] and hybrid [103] levels of theory. This work showed that DFT is able to accurately obtain the vibrational frequencies of intermediates on the surface and is consistent with UHV experiments.

In addition, Cheng et al. [105] examined the adsorption of NH_3 (ammonia), NH_2, and H on clean rutile (110) surfaces using DFT. They concluded that NH_3 and NH_2 adsorb at the 5-fold titanium site, whereas hydrogen could bind at the bridging oxygens or the in-plane oxygen atoms. Several studies have also investigated the binding of ammonia and other nitrogen-containing species on anatase [109, 110, 111, 112, 113] and monoclinic [114] polymorphs of TiO_2. Xie et al. used DFT to calculate the energetics of nitric oxide reduction on TiO_2 [108], and Höskuldsson et al. utilized GGA DFT to screen rutile oxides for electrochemical ammonia synthesis, and found a relatively large limiting potential of 2 V for the (110) surface of rutile TiO_2 [107].

In contrast to the relatively low number of computational studies, there have been many experimental studies of nitrogen compounds on rutile surfaces. Yates and colleagues conducted several studies of NO_x molecules under UHV conditions over rutile TiO_2 (110) [100, 101, 102]. Their early work showed that NO adsorbs and decomposes to form N_2O on reduced surfaces [100]. A follow-up study involved photochemical activation of NO on the surface that resulted in the production of N_2O, even with photon energies below the bandgap [101]. When the surface is dosed with N_2O and exposed to photons at high coverage, N_2O is desorbed from the surface, while at low coverages, N_2 is observed [102]. Much of this was also seen in Kim and colleagues' examination with the additional insight that surface oxygen vacancies play an important role [115, 116]. Furthermore, numerous applied studies focusing on nitrogen-doped titania [81], TiO_2 as an ammonia sensor [117, 118] or in the selective catalytic reduction (SCR) process [119, 120, 121, 122] provide insight into the interaction of titania with nitrogen-containing compounds. Although TiO_2 is typically not considered the active phase for the SCR reaction [123], it is interesting to

note a small body of work on the "photo-SCR." In this literature, anatase TiO_2 has been proposed as an active and selective catalyst [124, 125, 126, 127, 128, 129, 130, 113]. These studies provide useful context for the photocatalytic nitrogen fixation as they involve the interaction of both oxidized and reduced nitrogen species with titania surfaces.

1.6 Experimental Nitrogen Fixation on TiO_2

The first recorded hypothesis of nitrogen fixation via interaction with light was reported by the Indian soil scientist Nil Dhar in 1941 [75]. These experiments indicated that sterilized sands produced higher levels of fixed nitrogen under illumination. He additionally had hypothesized that the oxide materials present in the sands were responsible for the nitrogen fixation activity he observed. However, these experiments are highly questionable, as many other materials were mixed into the sands, probably interfering with the final results. These materials include simple oxygenates such as glucose and other more eclectic substances such as clarified butter and cow dung [75]. Dhar hypothesized that the addition of these substances provided the samples with "chemical energy," though he never outlined a direct mechanism through which the energy was transferred. Because of these issues, it is difficult to conclude that Dhar's results were valid; however, his contribution is worth noting.

More robust reports of experimental photocatalytic nitrogen fixation on TiO_2 appeared in a 1977 report by Schrauzer et al. [71]. Schrauzer and co-workers showed that (sterilized) rutile-laden sands under illumination at room temperature and pressure in humid air produce ammonia. This finding by itself is fascinating considering the harsh conditions needed to produce fixed nitrogen industrially. These experiments were of relatively high quality, including fully off-gassed TiO_2 samples, ^{15}N isotopic labeling, and Argon controls to rule out the possibility of contamination. Despite these efforts, the measured quantity of ammonia was exceedingly small, ranging from 0.74 to 4.98 μmol still making it challenging to rule out contamination, particularly in light of more recent protocols for ammonia quantification [131, 49]. Schrauzer et al. additionally noted that iron contaminates in the

TiO_2 samples tended to promote the reaction (a point examined in Chapter 5), finding that ~ 0.2 wt% iron seemed to be optimal.

Many works since have replicated the experimental results [66, 132, 133, 134, 67, 59, 135]. Augugliaro et al. [132] and Radford et al. [136], among others, showed that ammonia did not appear in control experiments while observing ammonia in experimental runs, bolstering Schrauzer's original findings. One experimental study has been done recently by Hirakawa et al. [59]. Hirakawa et al. performed all experiments in aqueous solution. They tested the effects of bubbling gas rate, bubbling gas composition, pH, and quantified the number of defects. They showed that higher rates of gas bubbling increased the reaction rate, and that bubbling pure N_2 gas was significantly more effective than air. They also reported that the reaction runs optimally at neutral pH and the number of vacancies on the surface scaled linearly with the catalyst activity. Finally, when metals were added to fill the vacancies, it was found that the activity decreased, indicating the vacancies play a key role. However, it lacks theoretical understanding and reaction rates remain low ($\approx 10^{-4}$mol) [28, 59]. The lack of fundamental understanding is surprising, given the promise of photocatalytic nitrogen fixation.

While this literature is intriguing, there has been some controversy, with some authors claiming the reaction does not happen [137, 138, 139, 140]. In addition to this controversy, the actual products of the reaction also vary from study to study. Most experiments show reduced compounds (NH_3 or NH_4^+) as the primary product [132, 133, 134, 59, 135]. However, some show the production of nitrates (NO_3^-) [66, 67], and still others show no reaction at all [137, 138, 139, 140]. This may be in part because of the challenges associated with measuring small amounts of ammonia and contamination from the environment (see Section 1.7). While some patterns emerge from this work, the variation in catalyst particles from doping and synthesis methods makes generalizations difficult.

A significant problem with the current literature is the variance in experimental setups, experimental methods, and reporting standards have varied widely between authors. The

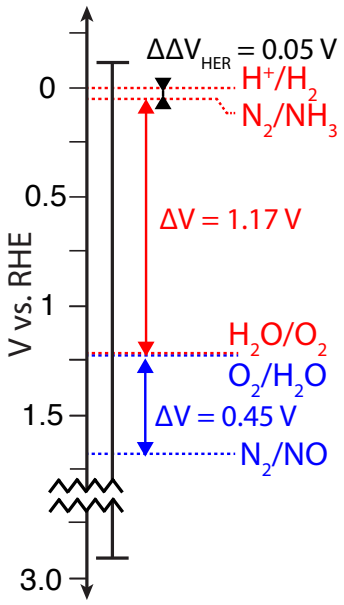

Figure 1.5: The band edges of rutile vs common redox couples. The band edge for reduction is at -0.1V, providing a very small driving force to N_2 reduction whereas the oxidizing band edge is very high, making oxidation comparatively easy. This makes the presence of NH_3 difficult to explain.

first confounding factor is that the field is split between gas-phase [71, 141] and aqueous [67, 132, 59] experiments, with gas-phase typically showing higher rates. A large portion of the literature also uses Xe/Hg lamps [141], while others use solar lamps [59], further confusing exactly how efficient their catalysts are in comparison to others. Many authors also dope their samples to reduce the bandgap but fail to report a measured band gap [141, 73, 142]. These problems highlight the need to set standards for how experiments are to be conducted to avoid a continuation of the literature's scattered state.

The photochemical properties of TiO_2 create another mystery. The -0.1V reducing band edge (see Figure 1.5) only provides $\approx$ 0.15V of overpotential to reduce N_2 to NH_3, an exceedingly small driving force. This small driving force makes the presence of the NH_3 product challenging to explain in the context of standard photo(electro)chemical models [143]. In contrast, the oxidizing potential is considerable, roughly providing 2.9V of potential above the standard hydrogen electrode (SHE) to drive oxidative reactions. The position

of the N_2/NO redox couple means there is 1.3V of overpotential, making the predominance of NH_3 rather than nitrates mysterious. This difference in products could be because the N-N bond breaks through an oxidative pathway rather than a reductive one, and the conversion to NH_3 takes place after. This hypothesis is supported by the observation that the reduction of nitrates appears thermodynamically facile (see Chapter 4). However, reports of nitrates are relatively rare, and it is possible that oxidative driving forces create meta-stable reactive species such as hydroxyl groups or carbon radicals (see Chapter 6).

1.7 Issues With Measurement Interference

One of the most significant challenges in the experimental literature is the issues around contamination in experimental setups and measurement. The photocatalytic and electrocatalytic communities share the same problem. Due to the typically low concentrations measured (0.7-80 μmol/L), there is a significant opportunity for contamination from the synthesis of the samples [144] and the environment [145, 131]. Quantification of ammonia at low concentrations has been identified as a challenge due to issues with contamination and calibration [145, 146, 144, 147, 148], and similar challenges are expected for nitrates or other fixed nitrogen products. Many authors contend that control experiments are as valuable as catalytic experiments due to the high possibility of contamination. In some experiments, it has been seen that 8-40% of the measured ammonia came from contamination [145]. Contamination issues are acute enough that many high profile papers have been retracted due to the measurements being attributed to contamination [149]. The presence of these retractions indicates integrity on the part of the researchers. These retractions help move the field toward a clearer understanding of which catalytic materials warrant further theoretical investigation.

A problem that is primarily found in the photocatalytic literature is the use of sacrificial reagents. Many authors also add sacrificial reagents to their aqueous reaction mixtures as hole scavengers, to increase activity [135, 150, 151, 152]. However, these may inter-

fere with Nessler's reagent, a standard reagent used to measure ammonia content, throwing off measurements by orders of magnitude [146]. Some authors also fail to report calibration curves for their ammonia measurements or report calibration curves measured at much greater concentrations than are measured. These issues cast doubt on whether their experiments measured a catalytic reaction or only contamination from the reagents or the environment given the low concentrations.

Establishing standards for experimental testing conditions and quantification practices will facilitate comparison of results and accelerate the development of photo-electro-catalytic processes for solar fertilizer production. To that end, several authors have laid out standards for measurement and controls [146, 145, 144, 131]. Greenlee et al. [145] and Chorkendorff et al. [131] have outlined a set of standards paraphrased below.

1. All control experiments performed must be reported thoroughly and prominently
2. Quantitatively validate results using $^{15}N_2$ isotopic labeling
3. Ensure all N_2 gas used is cleaned to remove trace NO_x species that is present in commercial gas cylinders
4. Measure the sensitivity of detection methods and ensure appropriate measurement methods are employed

Zhao et al. [144] further contend that at least two measurement techniques should be used and cross verified, prescribing different methods for each pH range and insisting that no sacrificial reagents be used. While these standards are not universally adopted across the field, there is an indication that authors are aware of the problem and strenuously working to overcome it.

Issues of measurement, contamination, and isotopic labeling have become a primary focus of electrocatalytic nitrogen reduction. Authors from many groups [153, 145, 144, 146] recognize the importance of ensuring measurements quantify the amount of fixed nitrogen

being produced catalytically. Additionally, some groups have actively worked to replicate experiments in the literature to bolster the scientific record [153]. While these steps do not guarantee the elimination of the problem in the literature, they provide encouraging signs for the prospects of the field.

CHAPTER 2

TECHNOLOGICAL PROSPECTS FOR PHOTOCATALYTIC NITROGEN FIXATION AND SOLAR FERTILIZERS

The most promising application of photocatalytic nitrogen fixation is for the production of fertilizers using solar energy. These "Solar fertilizers" offer an alternative for local fertilizer production by harnessing solar energy, nitrogen, and water/oxygen from the air to produce low-concentration ammonia- or nitrate-based fertilizers at or near farms where they will be used [27]. This is advantageous since the intermittent solar energy can be directly captured in a storable chemical product that can be utilized near the point of production, avoiding long distance transportation or storage of electrical energy in batteries [154]. This decentralized production will reduce the barrier to adoption of solar fertilizers as compared to solar fuels, since there is no need for retro-fitting the distribution and utilization infrastructure. Solar fertilizers are a special case of "solar chemicals" where the close coupling to agriculture provides unique advantages and the product does not compete directly with current ammonia production, but rather reduces the downstream usage of ammonia and N-fertilizers. The economic advantages arise from inexpensive feedstocks (air, water, sunlight) and the elimination of long haul transportation. There is also a societal benefit since solar fertilizers may improve access to fertilizers in remote regions of developing countries. Additionally, the characteristics of fertilizers with low nutrient concentrations may enable novel strategies of nutrient management that can reduce groundwater and atmospheric pollution due to nutrient losses. These advantages reveal significant potential for reducing downstream fertilizer usage, which is linked to energy usage. A recent estimate revealed that even a 10% reduction in the use of ammonia or urea fertilizers can save around 250 petajoules of energy per year [155]. Furthermore, low-concentration fertilizers produced at ambient conditions are inherently safer from the perspective of both process and product

handling. Although fertilizer products require a range of macronutrients including N, P, and K, here we focus on N production since nitrogen often the most limiting nutrient in agricultural production[156, 16].

Solar fertilizers hold substantial promise as alternative to traditional fertilizer and for sustainable agriculture, but there are also considerable challenges. One critical challenge is in the development of a viable strategy for efficiently using solar energy to break the strong dinitrogen triple bond at ambient conditions. Nitrogen fixation at ambient conditions is a key objective of chemistry and has been the subject of considerable research in homogeneous catalysis, enzyme catalysis, and bioengineering. Yet, no viable strategies have emerged due to issues with low conversion and/or stability under realistic conditions [157, 24, 158, 49].

Solar fertilizers will differ significantly from traditional fertilizers, opening a range of additional agronomic challenges and opportunities. One key difference is that "solar fertilizers" are expected to have considerably lower fixed nitrogen concentration. This is related to the fact that most photo-electro-chemical nitrogen fixation processes will have efficiencies far below the 70% thermochemical efficiency of the Haber-Bosch process [4, 41]. Separating and concentrating the ammonia will require additional steps that add complexity to the process and require additional energy. On the other hand, direct utilization of dilute or low concentration fertilizer will reduce the amount of energy needed for separation/concentration, and may enable more controlled nutrient management in agricultural production[159, 160]. However, this represents a paradigm shift in agricultural practice, and considerable efforts are needed to understand how dilute solar fertilizers can be sustainably and practically integrated into current agricultural systems. These considerations will also inform the development of the photo-electro-catalytic processes for solar fertilizer production, and hence should be considered in parallel.

In this chapter we identify key considerations and performance targets for the photo-electro-chemical production of dilute solar fertilizer from the perspectives of agronomics

and chemical engineering. Some specific advantages and disadvantages of dilute and decentralized fertilizer production are outlined, and the potential agronomic use cases and impacts are examined. The technical requirements for a photo-electro-chemical reaction/separation process for fertilizer production are considered, and a range of possibilities are introduced. These possible designs are used along with back-of-the-envelope calculations to quantify initial performance targets and limiting cases for catalyst reactivity and suggest specific materials properties and tests that will inform process design. We hope that these considerations will serve as a foundation and guide for future research in the development of photo-electro-chemical processes for solar fertilizer production.

2.1 Agronomics of solar fertilizers

Current fertilizer production relies on the Haber-Bosch process, with highly centralized production and fewer than 100 production plants globally [11] to cater to 1.55 billion hectares of arable land and permanent crops (about 12% of total land area) [161] and an estimated 500 million farms [162, 163]. The centralized production is driven primarily by the harsh reaction conditions of the process. The high temperature and particularly the pressure of the process lead to a favorable economy of scale, with a typical capacity scaling exponent of 0.7 [56, 164]. This incentivizes high-volume production with high capital investment, with the most recent 2200 tonne day^{-1} fertilizer plant having a capital cost of $1.5 billion [165]. This leads to long payback periods, and encourages development of production facilities in regions with stable access to feedstock such as natural gas, reliable infrastructure, stable governance, and sophisticated financial systems [11] as indicated by the presence of ammonia production primarily in developed regions (Figure 1.2). The resulting fertilizer products with high nutrient concentration must be transported to globally dispersed agricultural production centers.

Fertilizer use in developing countries has been encouraged due to a significant depletion in soil nutrients. However, for the use of fertilizers to be economically viable and sustain-

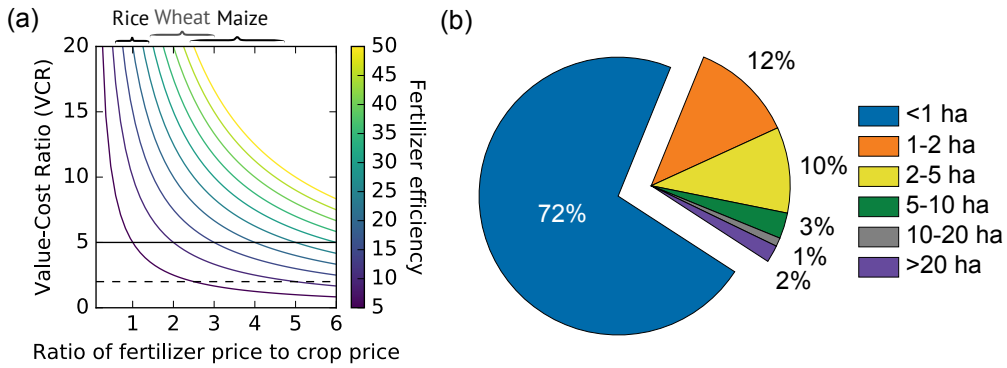

Figure 2.1: (a) Value-cost ratio (VCR) in response to the ratio of unit fertilizer price to unit crop price and fertilizer efficiency (measured as additional unit of crop per unit of fertilizer applied) [166]. Typical fertilizer-to-crop price ratios are denoted for rice, wheat, and maize, and minimum/typical VCR required for investment are shown by dashed/solid horizontal lines. (b) Proportions of farms with various sizes [163].

able, they must produce a significant increase in yield. This is typically quantified by the "value-cost ratio" (VCR), which in this case is the ratio of crop output value to fertilizer input cost. As a rule-of-thumb, farmers will invest and use fertilizer if the VCR is greater than $\sim$2, indicating that for every dollar invested in fertilizer, output revenues will repay the invested dollar plus an additional dollar, for a 100% return on investment. As shown in Figure 2.1 for selected crops the VCR is generally increased as the price of fertilizer decreases [166]; however, the prospect of much lower fertilizer prices or higher fertilizer efficiency would clearly incentivize fertilizer use by increasing the VCR, assuming constant or no downward changes in agricultural output prices. It is important that these economic incentives hold for small ($<$ 1 ha) farms, since $>$70% of farms globally are small (Figure 2.1b), and the proportion is higher in developing countries [163]. This section briefly explores the implications of the centralized Haber-Bosch process on the economics of fertilizer production, and explores the potential impact and challenges of decentralized production of dilute fertilizers in both developed and developing regions.

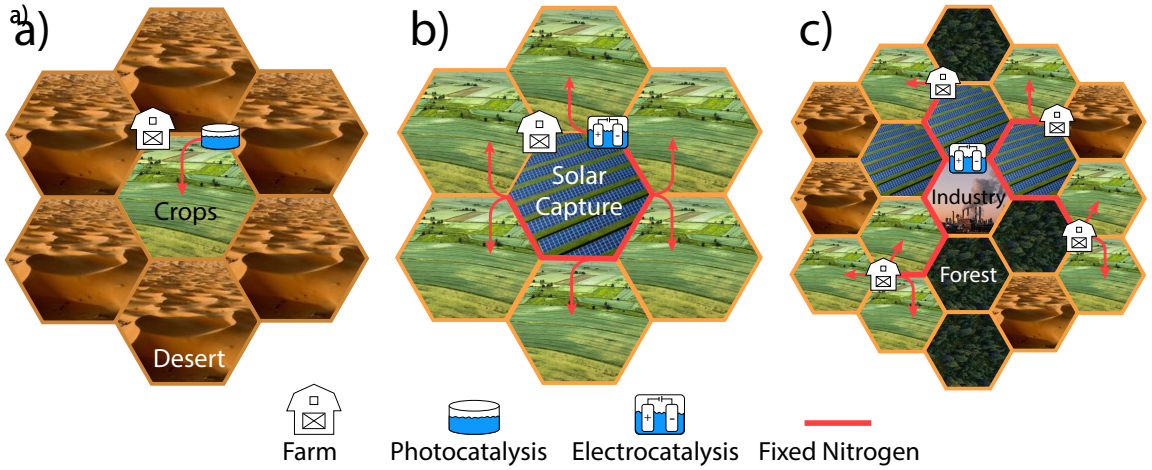

Figure 2.2: The three proposed scenarios for solar fertilizer a) inepensive farm scale production using photocatalysis b) solar fertilizer production integrated with larger farms using electrocatalysis c) high-tech solar fertilization production coupled with distribution infrastructure using electrocatalysis

2.2 Decentralization of Fertilizer Production

There are a continuum of options for moving from the current highly centralized fertilizer production toward smaller-scale distributed production. In this section we briefly explore the general economic factors that favor decentralized production and subsequently consider three possible specific scenarios along the continuum of decentralized fertilizer production. The three scenarios (see Figure 2.2) presented here are (1) inexpensive, robust solar fertilizer production at the scale of small farms in remote and undeveloped regions (2) solar fertilizer production integrated with existing infrastructure on larger farms in developed regions, and (3) high-tech solar fertilizer production coupled with production and distribution infrastructure of existing or emerging agricultural products. These scenarios present exciting opportunities to develop scalable decentralized solar fertilizer technologies with the potential for substantial positive impact on society, energy, and the environment.

From a simplistic and practical perspective the major components of fertilizer retail cost can be broken down into production, transportation, and storage costs. The production cost of fertilizer is controlled primarily by the cost of its feedstock, the natural gas used

as a source of hydrogen for the Haber-Bosch process and hence, varies with geographic, economic, and geopolitical factors [167, 168]. This leads to variable and uncertain cost of fertilizers and presents challenges in agricultural planning [168]. Furthermore, the cost of transportation depends strongly on the location and transport mode available (barge, rail, trucks, pipeline). Barge, pipeline, and rail transport are normally used for long-distance anhydrous ammonia transportation, while trucks are preferred for shorter distances. Distance, location of plant site relative to the agricultural area, availability of transportation equipment, and relative cost of available carriers are the major governing factors for selection of a typical anhydrous ammonia transportation system. International shipping of ammonia between the United States and Western Europe costs on the order of $ 35 per tonne [169]. Typical costs reported in the United States for long distance (greater than 1600 km) by pipeline, barge, and rail transport are $0.0153, $0.0161 and $0.0215 per tonne per kilometer, respectively [169]. Short truck transportation costs are expected to be much higher. For distances of the order of 100 km, typical reported costs are $0.0365 per ton per kilometer [169]. Additionally, storage costs must be considered due to the seasonal consumption of ammonia caused by agriculture's cyclic nature. It has been reported that roughly 75% of the fertilizer production is sold in the spring during the planting season [169]. To reduce storage costs resulting from this cyclic consumption pattern, large refrigerated anhydrous ammonia storage vessels are used, which add another $11-80 per tonne to ammonia cost [170, 169]. Thus, the freight costs can account for more than half of the retail cost of ammonia in some countries. The hazardous nature of ammonia also leads to challenges with transportation and storage, particularly in regions with poor infrastructure [168].

The production, transportation, and storage costs are the main components of fertilizer price, but the overall cost is not directly derived from these categories. For example, as shown in Figure 2.4 the price of fertilizer in Thailand ($ 287 t^{-1}) is roughly half the price of fertilizer in Mali ($ 509 t^{-1}), but this difference cannot be attributed directly to any single category [171]. This discrepancy is largely due to the economies of scale and to other

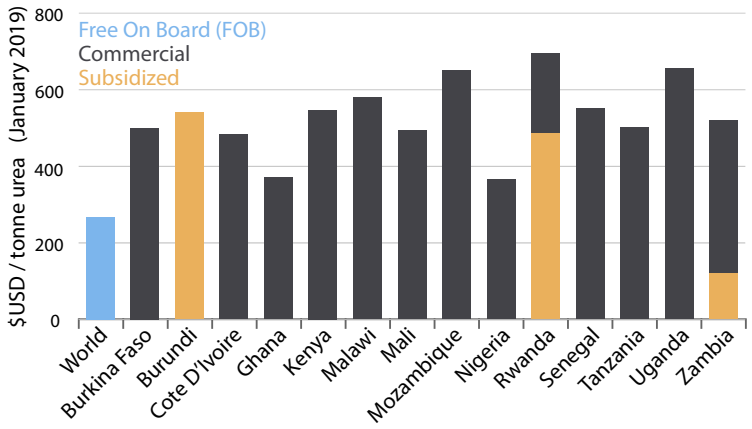

Figure 2.3: Overview of current (2019) commercial and subsidized costs of fertilizers in various African countries compared to the international free on board (FOB) cost [22].

factors that affect the efficiency of fertilizer procurement and distribution. Developing nations in Africa are often purchasing smaller quantities of fertilizer from the international market, limiting their ability to bargain for lower wholesale prices and leading to prices that are generally much higher in African countries (Figure 2.3) [171]. Larger agricultural markets such as in Asia can more effectively negotiate and distribute fixed costs of transportation across more units of fertilizer, reflected in lower prices of fertilizer at retail. This scale-up is not possible in less developed markets for a variety of reasons including port capacity and poor transportation infrastructure [172]. Political instability often compounds this problem by causing existing infrastructure to deteriorate due to lack of investment [173, 174, 175]. Road systems in these regions are often not well maintained or regulated, leading to worse connectivity and excessive wear and tear on transportation equipment. Less developed markets are also subject to more uncertain demand owing to lack of access to finance by smallholder farmers and unpredictable implementation of government subsidies [172, 173, 176, 174, 175]. These subsidies can be critical for making fertilizer more affordable to smallholder and resource poor farmers (Figure 2.3) and removing or reducing subsidies can considerably reduce the amount of fertilizer procured and supplied by private importers. For example, removal of fertilizer subsidies in Ghana in 2014 re-

duced imports by about 50%, and most of the product that was imported was provided to commercial operations rather than smallholder farms [177]. Overall, these factors lead to a perverse situation in which fertilizers are most expensive in the poorest places where the need is greatest. This is a key factor in the distressing fact that despite the tremendous technological developments of the recent decades and ever-increasing ammonia production, world hunger is has stopped declining and is currently increasing (Figure 1.1) with over 800 million people suffering from undernourishment as of 2016 [178]. Notably, many of these economic and geopolitical factors could be alleviated by decentralized production of dilute fertilizers with low capital input from solar/renewable resources. Reducing or eliminating the dependence on natural gas would reduce volatility in fertilizer production costs and prices [168], while producing fertilizer at or near the point of use would reduce transportation costs and perhaps eliminate the cost dependence on economies of scale [170]. Furthermore, local production would improve certainty in fertilizer availability, reduce the influence on price of external factors such as feedstock price volatility and tariffs, and eliminate the needs for subsidies and their burden on governments' budgets. Considering that agricultural production is directly linked to general economic prosperity, local fertilizer manufacturing industries in developing countries could spur substantial economic growth [11].

The most extreme small-scale alternative would be fully decentralized farm-scale fertilizer production (Figure 2.2a), which would have the largest socio-economic and agricultural impact if deployed in low-income countries where access to fertilizer is limited. There is a large range of farm sizes, but most farms in low-income countries are $<$1 ha (Figure 2.1b)[163] . With over 70% of farms being classified as small holdings, a market push toward decentralization could aid a significant portion of the agricultural market. Fertilizer production at the scale of small farms would correspond to roughly 1 fertilizer production facility per ha, an increase of $\sim$ 7 orders of magnitude in the total number of fertilizer production facilities. Naturally, this would correspond to proportional decrease

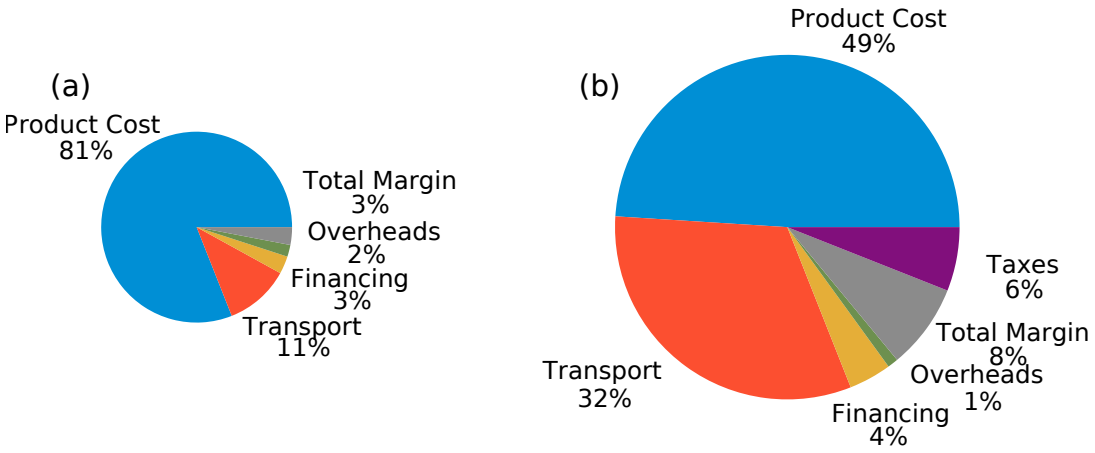

Figure 2.4: The price breakdown for fertilizer in (a) Thailand and (b) Mali for the year 2013. Relative areas reflect the ratio of costs in the two countries ($282 in Thailand and $509 in Mali) [171]

in the scale of production per facility. The required nutrient load varies considerably from about 20 - 200 kg-N per hectare depending on crop and region, but we adopt 100 kg-N per hectare per year as a convenient representative nutrient load [28], which can be used to obtain rough estimates of cost and efficiency. For example, the annual budget for on-site fertilizer production can be estimated based on the cost of fertilizer per country. The estimated average cost of supplying urea at retail point in Ghana under open market conditions during 2018 was $394 per tonne, or $857 per tonne of nutrient N (urea is nutrient 46% N by weight) [179]. This corresponds to an expected annual N nutrient fertilizer budget on the order of $ 86 per hectare per year. This modest number suggests that decentralized fertilizer production at the scale of small farms must have very low capital and operating costs, even in countries where the cost of fertilizer is very high. Furthermore, the process must be sufficiently robust that specialized personnel are not needed for operation or maintenance of production, and additional constraints such as water usage and fertilization infrastructure (e.g. irrigation) must be considered. Strategies of “frugal innovation” [180] can help address these challenges, and the successful development and deployment of solar energy technology to disinfect water through photochemistry and photocatalysis provides

a promising precedent for this approach [181, 182]. This suggests that the development of inexpensive and robust processes for producing solar fertilizer at the scale of small farms in the developing world may be a viable strategy.

An alternative approach to farm-scale production is to target larger farms (larger than 100 ha), particularly those which are already using irrigation systems that can be directly utilized for delivery of dilute aqueous fertilizer (Figure 2.2b). While these very large farms account for less than 2% of farm holdings (Figure 2.1b), they account for over 45% of the agricultural land area, and are more common in developed countries [163]. This scenario presents an economic challenge for decentralized N fertilizer production since they will compete directly with traditional fertilizer. For example, the cost of urea in the United States is approximately $550 per tonne N as of 2018 [183], though there is significant fluctuation. This is compounded by the larger capacity of the farms, and the typically heavier fertilization in developed countries. Assuming a nutrient load of $\sim$ 100 kg of nutrient per hectare per year for a large 100 ha farm leads to an approximate annual fertilizer budget of $\sim$ $5,500 per farm ($55 per ha). This number is relatively modest, but there are additional incentives for larger farms to invest in decentralized fertilization. These larger farms require larger capital investment, and the reduced volatility in price for fertilizers produced on site would improve the predictability of returns. The integration of on-site solar fertilizers with existing irrigation infrastructure may reduce the costs associated with delivering fertilizer to crops, or enable more efficient fertilizer utilization, as discussed further in Sec. 2.3. There are also challenges for scaling solar fertilizers to larger farms. Solar fertilizer production will require a higher level of technological sophistication, particularly if electrochemical technologies are employed. These approaches will require installation, maintenance, and potentially operation by experts. It is unlikely that a full-time employee could be dedicated to fertilizer production, even at very large farms of $\sim$1,000 ha. Nonetheless, periodic access to experts for installation and maintenance is not an issue in developed regions. Numerous industries such as solar capture and heating ventilation and air conditioning (HVAC) oper-

ate on similar business models. This suggests that solar fertilizers are potentially viable for farm-scale production in developed areas as long as they can be operated with only periodic maintenance.

A third scenario is the production of solar fertilizer at a regional, semi-centralized multi-farm scale (Figure 2.2c). The challenge with more centralized production scenarios is competition with the efficient and inexpensive Haber-Bosch process, since both rely on transportation and distribution infrastructure. Nonetheless, semi-centralized production will require shorter transport distances, and can avoid costs and uncertainties associated with international or trans-marine distribution. Moreover, the lack of reliance on natural gas as a feedstock can reduce price volatility, although this can also be mitigated by performing Haber-Bosch with hydrogen generated from electrolysis [184, 185]. Coupling solar fertilizer production with the production of other agricultural products such as phosphorus, potassium, agricultural lime, or biochar can alleviate transportation issues by taking advantage of existing infrastructure. For example, a distributed network of fast pyrolysis facilities for simultaneous production of fuel and agricultural biochar has been suggested as a route to carbon-negative energy production [186, 187, 188]. Coupling these fast pyrolysis plants with photo-electro-chemical nitrogen fixation presents a route to produce nutrient-enriched biochar, as discussed further in Sec. 2.3. According to a technoeconomic analysis of fast pyrolysis these facilities would process on the order of 2000 tonnes of biomass per day, with a yield of $\sim$ 20% biochar [189]. This corresponds to around 150,000 tonne biochar yr^{-1}. The amount of biochar applied to farms varies widely from 0.5 - 50 tonne ha^{-1} [190], but assuming a nitrogen content of 16 mg NH_3 g^{-1} C and a nitrogen loading of 100 kg ha^{-1}, approximately 7.6 tonne ha^{-1} of biochar is required (see Sec. 2.3). This corresponds to $\sim$ 20,000 ha per facility, or 2000 tonne N yr^{-1}. Assuming the price of nitrogen nutrients is similar to that of urea in the developed world ($550 per tonne N) this corresponds to a substantial annual budget of $1.1 million per facility for solar fertilizer production. This would lead to economic viability of more sophisticated solar fertilizer technologies that

require full-time expert operation, such as high-temperature operation and/or large-scale solar concentrators. For example, recent work by Bicer and Dincer on molten salt ammonia reactors coupled with solar-generated hydrogen indicate this strategy may fit into this semi-centralized approach. Their work found that such a system could deliver ammonia at a cost of $840 per tonne at the scale of 176 kg day^{-1} [191, 192]. These semi-centralized approaches carry the largest infrastructural burden, and will face substantial challenges in implementation. However, approaches such as enriched biochar production as a byproduct of biofuel present exciting opportunities for simultaneously improving the sustainability of the agricultural and energy sectors through coupled infrastructural developments.

There are many other possible scenarios for solar fertilizer production, and the qualitative analysis above is far from complete. Yet, the order-of-magnitude estimates suggest that there are many routes through which solar fertilizers can potentially compete with the established Haber-Bosch process by utilizing the advantages of decentralized production offered by photo-electro-chemical processes. We also note that these estimates do not take into consideration the inherent social cost of nitrogen to the environment. Social costs are still not widely understood, but may range from $0.001-10 per kg N depending on the location. [193]. If appropriate policies and regulations are put in place to account for these social costs, the economics of decentralized fertilizer production will be improved. Other niche applications, such as space exploration [194], may also present economic routes to develop solar fertilizer technologies, but are likely to be smaller in scale and are beyond the scope of this work.

2.3 Considerations for Dilute Fertilizers

The centralized production of fertilizers along with the high purity of Haber-Bosch ammonia has driven the development of solid fertilizers with high weight percent nitrogen (35-85%) to reduce transportation and storage costs. Utilization of solar energy is expected to produce fertilizers with nutrient concentrations substantially lower than the traditional

Haber-Bosch process, owing to the lower density of solar energy [154] and the challenges with low efficiency and selectivity in photo-electro-chemical nitrogen fixation [57, 41]. This is similar to the biological fixation of nitrogen that occurs in the root system of the plants and results in relatively low local concentrations of fixed N in the soil, estimated at 20 kg-N ha^{-1} yr^{-1} on average [47, 195] though some estimates put it as high as 45.4 kg-N ha^{-1} yr^{-1} [196]. As we discuss in section 2.5 the required solar-to-ammonia efficiencies and nutrient concentrations are in principle surprisingly low ($<1\%$); however, these low-concentration fertilizer products differ substantially from existing fertilizers and come with both advantages and disadvantages. Here we consider two varieties of dilute fertilizers: liquid fertilizers in aqueous solutions and solid fertilizers based on carbonaceous materials. These fertilizers have the potential to integrate well with solar fertilizer production and existing agricultural infrastructure, but will also require changes to conventional fertilization practices.

Aqueous fertilizers are advantageous since plants require water as well as nutrients. The process of simultaneously applying fertilizer and water is known as fertigation [160, 197]. Fertigation has formidable potential when coupled with solar fertilizer production since fertigation systems can deliver nutrients at a slow rate over time. This leads to a lower overall nutrient concentration relative to solid urea fertilizer, where much of it is lost through leaching and gaseous emissions. High leaching loss is particularly pronounced in areas with high rainfall and sandy soils such as the State of Florida [198]. In tests fertigation has proven to be more effective than both traditional fertilizers in producing growth in citrus trees [199], garlic [200], and potatoes [201], among others [159, 160] and leads to higher NO_3^- concentrations in the top 15cm of soil [202]. Tests in peach orchards showed improved fruit sizes with drip fertigation compared to conventional methods [203]. Additionally, these practices may lower the amount of nitrogen fertilizer needed to achieve the same results as conventional methods by nearly an order of magnitude [198]. Recommended concentrations of nitrogen in fertigation systems range from 50-350 ppm on a

mass basis for most crops [204, 205]. This contrasts with typical solid urea fertilizers that are 46 wt%-N. This stark difference ($\sim$ 4 orders of magnitude) in nutrient concentration by weight indicates that aqueous dilute fertilizers cannot be economically transported, meaning that aqueous dilute fertilizers are only viable at farm-scale production or for use within very short distances within a country region (see Sec. 2.2). This fact leads to additional challenges with dilute fertilizer related to storage, since the solar flux may not always align with crop nutrient needs. This would necessitate on-site storage tanks that would increase the footprint of the fertilizer production system, or electrochemical systems that can operate from the electricity grid or on-site batteries to produce dilute fertilizers on demand. Another challenge is that fertigation relies on irrigation infrastructure nutrient delivery. This may present a particular challenge for many smallholder farms in sub-Saharan Africa, where only around 6% of farms are equipped with irrigation [206]. Nonetheless, these farms present a sizable initial market, and the prospect of combined fertilization/irrigation systems may be economically viable in already-irrigated farms in the developed world (Sec. 2.2), or incentivize investment in irrigation systems in the developing world.

Another approach to dilute fertilizers is to embed the nutrients with a carrier solid. In most current practical applications, the form of nitrogen in fertilizer is urea, which comes as a solid that is dispersed over croplands. Solar fertilizer production could be coupled with adsorbents to uptake and concentrate the products, leading to a solid dilute fertilizer product. In this scenario the ammonia or nitrate products from the photo-electro-chemical reactions could be separated using a solid adsorbent such as activated carbon or biochar [207] (see Sec. 2.4.2). This approach is advantageous since application of carbonaceous materials is already practiced in organic farming in the form of composting [208], and adding adsorbent carbon to soil has been shown to provide many benefits for croplands including water retention, hydraulic conductivity, and resistance to soil erosion [209]. These changes are manifested in the form of improved crop production [188], although the magnitude of the improvements depend on the particulars of crop and soil type. Nonetheless, increases

of 30% in seed germination rate and 13% in biomass production have been observed in woody plants [210]. However, implementation of biochar fertilizers may be challenging, since the ability of biochar to adsorb nitrogen is not well established. The highest reported ammonia loading for biochar is 16 mg/g of NH_3 [207]. This is comparable to the nutrient content of manures, which are commonly used as fertilizers and have nutrient contents that can range $\sim$ 5-50 mg/g [211]. A drawback of this approach is that producing high-surface-area carbon requires furnace temperatures above 400 °C [186], which may present an engineering challenge in a low-resource setting. However, in some developed counties biochar facilities have been built and proven profitable [212], and in others would be profitable with a moderate carbon tax [190]. However, if biochar resources are not managed properly, this strategy could have a negative environmental impact by depleting natural resources, highlighting the importance of good resource management and forestry practices to realize the environmental benefits. This suggests that integration of solar fertilizer facilities with production facilities for carbonaceous soil additives may be a promising strategy, although considerable research is required to determine the efficacy of carbonaceous dilute fertilizers in real agricultural settings.

One enticing possibility for both aqueous and carbonaceous dilute fertilizers is the prospect of improved nutrient management. Currently, the fixed nitrogen in fertilizers is not utilized efficiently, with $\sim$ 20% being lost to leaching or vaporization [47, 213]. Leached fertilizer then enters waterways, leading to hypoxic regions in oceans (called dead zones), eutrophication in lakes and rivers, and groundwater contamination [17, 214, 215]. Pollution of this kind is acute in the Gulf of Mexico and the North Sea, due to the upstream intensive agricultural practices [17, 214]. The vaporization of nitrogen fertilizers can also have deleterious effects on the environment by releasing NH_3 and NO_x compounds that cause global warming and damage the protective ozone layer [216]. The highly concentrated fertilizers responsible for this pollution release nutrients too rapidly for plant uptake, with researchers estimating they are only used at an efficiency of 20-35% [213]. This can

have negative effects on the plants themselves, damaging root systems and seedlings in areas of high nutrient concentration [199]. The most common strategy for mitigation of these effects is the development of coatings that aid in controlled release of nutrients and enhance uptake efficiency [213]. Other effective strategies include deep placement of fertilizer products, and balanced nutrition with micronutrients [217]. While these slow-release fertilizers improve performance, the use of dilute fertilizers offers a different approach in which nutrients are delivered at a controlled rate, and in smaller amounts [198, 218]. This would enable matching N supply with crop demand. However, substantial additional research into agronomics and plant nutrition is required to determine the potential of this strategy and identify the optimal nutrient concentration and application rates. If dilute fertilizers are applied through fertigation, there is an opportunity to fertilize crops each time they are irrigated, controlling exactly the timing of nitrogen addition. Nitrogen-saturated biochar also holds promise, as these could release nitrogen slowly over the crop growing cycle, more effectively resisting leaching than solid urea with the added benefit of improved retention of P and K based fertilizers in the soil through higher ion exchange capacity [188]. If the nitrogen content was well known it would also provide an advantage over manures where quantification of nitrogen content presents a challenge for nutrient management [211]. In addition to improved nutrient management, dilute fertilizers are inherently safer since they will be less corrosive and more difficult to convert into explosives. These factors suggest that further research into the utility and effectiveness of dilute fertilizers is relevant to the field of solar fertilizers.

2.4 Solar Fertilizer Production Processes

The prospect of solar fertilizers shares much with the well-studied approaches to solar hydrogen and solar fuel production. For example, both require photon absorption, catalysts for the reaction, efficient transfer of energy from the absorber to the catalyst, and materials that are stable under operating conditions. However, there are also some key differences

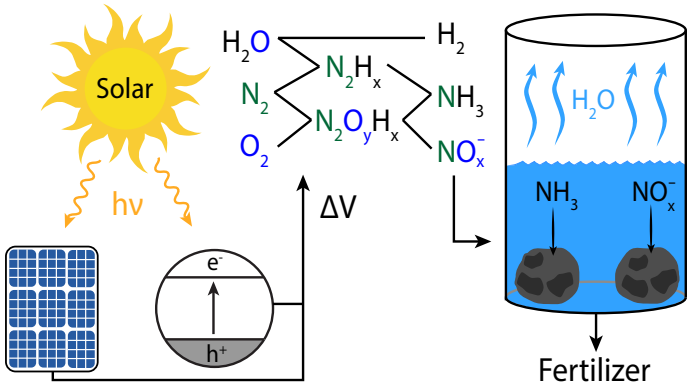

Figure 2.5: Solar energy is captured via solar panels and/or photocatalytic particles, generating an electrical driving force ΔV. This drives a (photo)electrochemical reaction converting molecular dinitrogen to fixed nitrogen products including ammonia and nitrates in aqueous solution. Fertilizer can be produced by separating the fixed nitrogen products by adsorption onto solid carbon or concentrating via passive evaporation.

since solar fertilizers must integrate with agricultural infrastructure, and the products are different in their chemistry and application. In this section we examine three key aspects of solar fertilizer process design: solar capture, reaction and catalysis, and separations, depicted schematically in Figure 2.5. We focus primarily on aspects unique to solar fertilizers, and refer to numerous reviews on solar fuels and solar chemicals for additional considerations [219, 36, 220, 38, 40].

2.4.1 Solar Capture

The solar fuels community has identified two basic strategies for conversion of solar to chemical energy: direct capture of photons through photochemistry (photocatalysis), or indirect capture through photovoltaics coupled to electrochemistry (PV-electrolysis)[219, 220]. Photoelectrochemistry, whereby electrical bias is applied during solar capture represents a third hybrid (indirect+direct) approach for solar-fuel production. There has been considerable debate and analysis regarding the efficiency of each approach for fuel production [40, 221, 39, 222], and while there is no clear consensus, indirect capture has received considerable attention for the production of hydrogen. This has largely been driven by the goal of maximizing solar-to-hydrogen efficiency, and the target of 20% efficiency has been

achieved by multiple systems [223, 224]. Solar fuels technologies are typically envisioned to operate at large scales in relatively centralized industrial production facilities [38]. Yet, in the case of solar fertilizers there is a strong motivation for technologies that operate in decentralized locations or at an agricultural site as discussed in Sec. 2.2. Indirect solar capture requires a relatively high level of technological sophistication since solar capture arrays, electrochemical reactors, and associated electrical connections and controls must be maintained, and the resulting fixed nitrogen products must be separated from the electrolyte. Furthermore the low areal energy density of photovoltaics [154] coupled with the need for separate solar capture, fertilizer synthesis, and separations facilities will lead to a relatively large footprint for indirect capture. This suggests that PV-electrolysis approaches are best suited to semi-centralized solar fertilizer production, or on-site production at large farms in developed regions (see Sec. 2.2). Nonetheless, photovoltaic technology is well-established, and efficiencies of 10-20 % are typical. This leads to a required electrical-to-ammonia efficiency of $\sim 1\%$ (see Sec. 2.5), which is relatively low and has been reported at the lab scale for state-of-the-art ammonia electrocatalysts [225, 226, 43, 227, 33]. Further, electrochemical fertilizer production can be integrated with an electrical grid (though the fertilizers resulting from grid-based electricity cannot technically be considered "solar fertilizers") or battery system, providing reliable yields even in periods of no sunlight. The use of high current densities can also enable the production of higher concentrations of fixed nitrogen. In addition, electrochemical technologies have been demonstrated at scale, including the chloroalkali process, water hydrolysis, and hydrogen fuel cells [228, 229, 230], and many of these technological developments could be applied to semi-centralized solar fertilizer production processes.

The alternative approach of direct capture and photocatalytic conversion through a single material or integrated device has also been explored for solar fuel production [40, 39, 36], and some technoeconomic analyses suggest that particle bed photocatalytic systems will lead to the lowest costs, although the potentially explosive product mixtures present

technical challenges [36]. In the case of solar fertilizers this safety concern is alleviated since low-concentration products are expected (see Sec. 2.3). Direct solar capture systems contain few if any moving parts, driving down the expected costs of maintenance and installation and making them better suited for decentralized fertilizer production at small scale farms in developing regions. However, production rates in direct capture are directly proportional to the solar flux, leading to uncertainty in production capacity. This uncertainty can potentially be mitigated through storage, though this will increase the footprint of the solar fertilizer production process, and/or by identifying regions where the solar flux is high such as sub-Saharan Africa or India (see Figure 1.2). Another challenge is that the highest reported efficiencies for direct photocatalysis are relatively low (0.1 %, see Figure 2.6). In general, the materials constraints for direct capture are more stringent since the same material must act as an absorber and a catalyst, or the interfaces between the two materials must be carefully engineered [40]. The constraints are even more severe when cost is considered, since materials containing rare elements or requiring expensive processing are unlikely to be viable in a low-cost design. However, many reported catalysts are based on earth-abundant materials such as TiO_2, or Fe_2O_3 [70, 231, 28], and required efficiencies are expected to be $< 1\%$ (see Sec. 2.5), indicating that inexpensive, low-efficiency photochemical reactors similar to those used in air purification may be viable [232, 233, 234].

In the case of direct solar energy capture, the band gap and band edge alignment of the material must be optimized along with the catalytic performance. The optimal band alignment will depend on the absorber configuration (single vs. dual) and the over-potential required for the oxidative and reductive half-reactions. Substantial effort has been dedicated to the question of optimal band configuration for solar fuel production, resulting in several modeling frameworks [235, 236]. These tools can be easily adapted to optimize band configuration and identify performance limits for solar fertilizers [28]; however, knowledge of the half-reactions and catalytic over-potentials is required. There are still open questions

regarding the relevant half-reactions and catalytic mechanism for photocatalytic nitrogen fixation (see Chaptes 4 and 6) [140, 28]. Resolving these fundamental questions is of critical importance for the practical optimization of solar fertilizer technology.

2.4.2 Separations

The chemical separations required to generate reactants and convert the effluent of a reaction to a fertilizer are also of critical importance to advance solar fertilizer technology. In the case of solar fuels this is less critical, since many fuels like hydrogen are gaseous and easily separable. Some work has also reported the production of gas-phase ammonia [237, 238, 29], but many electrochemical techniques use aqueous electrolytes. Ammonia, nitrates, and urea are all highly water soluble, creating a challenge in separating or concentrating the product. Further, if the process is not resistant to oxygen or other common environmental contaminants then an air separation or purification unit will be necessary. In addition to the chemical separation it may also be necessary to separate the catalyst from the solution, for example in the case of slurry photoreactors. These separations are a critical consideration for decentralized fertilizer production since high capital investment and expert operation may be required, which would not be feasible at the scale of a small or even a relatively large farm (see Sec. 2.2). We briefly discuss the key separations challenges for solar fertilizers: separation of nitrogen from air, upgrading the concentration of products, separation of products from the electrolyte, and separation of the catalyst from the electrolyte. The possible application of absorption, distillation, and/or membrane separation technologies are considered for each case.

Many photo- and electrochemical processes for nitrogen fixation are based on a pure nitrogen feedstock. For example, oxygen has been shown to inhibit photocatalytic nitrogen fixation over the commonly-used TiO_2 catalysts [59], and high-purity nitrogen is typically used in electrochemical tests [43, 238, 239]. The need for air separation presents a critical challenge for farm-scale fertilizer production. The most common air separation processes

are based on cryogenic distillation, which is energy intensive (6.9 kJ mol-N_2^{-1}) [240] and requires significant scales ($>$ 230 kg-N h^{-1}) [241]. Cryogenic separation units typically account for up to 25% of the capital for a Haber-Bosch ammonia synthesis facility [12], and would not be economically feasible, even at the scale of a large farm, suggesting that semi-centralized production is the most viable production scenario if high-purity nitrogen is required. Other air separation technologies such as pressure-swing adsorption and membrane separations are more viable at smaller scales, but the purity of the resulting nitrogen is typically lower [242]. The need for air separation will likely be the limiting factor for decentralizing solar fertilizer production. Hence, the development of processes that are directly compatible with air or low-purity nitrogen is an important but relatively unexplored research direction.

The concentration of fixed nitrogen in the product stream may also need to be upgraded to produce viable fertilizer products. Solar fertilizer products are generally expected to be more dilute, as discussed in Sec. 2.3. Nonetheless, strategies to separate or concentrate the fixed nitrogen product may be required even for dilute fertilizers, particularly if production is semi-centralized. Separation of aqueous ammonia is challenging due to the strong hydrogen bond between water and ammonia, and is complicated by the effect of pH since ammonia is more soluble in acidic solutions [243]. Most research in separating ammonia from water has been in the field of wastewater treatment where steam stripping from basic solutions has been shown to efficiently remove trace ammonia, with some research being done on membrane separation systems [244, 245, 246]. However, these processes are optimized to reduce ammonia concentration rather than increase it, and are capital and energy intensive. One possibility to concentrate ammonia is to capture energy from the infrared region of the solar spectrum and use the resulting heat for passive distillation. This would be inexpensive, but the resulting nitrogen content would likely remain relatively low. Another possibility is the production of gas-phase ammonia or use of a carrier gas. Capture of ammonia from the gas-phase can be achieved with acidic liquids both at the lab scale

[243] and at the industrial scale [245]. These processes have their drawbacks, with lab scale acid traps using dilute acids and being specialized for holding small amounts of ammonia, emitting 20-30% of ammonia passing through them[243]. At industrial scales, 98% sulfuric acid is used to absorb ammonia from carrier gases, producing a solution that is 30% ammonia. These processes are well-established, but would introduce the requirement of removing the ammonia from the sulfuric acid, introducing additional unit operations and increasing the cost of the process. [245] Further investigation of these systems is needed to assess their viability in solar fertilizer processes. An alternative approach is the use of adsorption for separation, which may be viable for either gas-phase or aqueous ammonia. This is particularly promising if the adsorbent itself acts as a part of the fertilizer, for example if biochar is used as an adsorbent as discussed in Sec. 2.3. This removes the need for an energy-intensive desorption cycle, although it is critical that the absorbent release nutrients when placed in the soil. Ideally, the need for upgrading can be mitigated by discovery of catalysts that are both active and selective for nitrogen fixation, and through design of processes that result in effluents with high concentrations of ammonia or nitrates.

Another consideration is that photo-electro-chemical processes often require electrolytes to provide electrical conductivity and control the pH. For example, some of the highest reported electrochemical ammonia formation rates are based on Li-based electrolytes [43]. While the effect of electrolytes on plant growth is unknown, the role salinity plays in soil science is well documented and suggests salinity of fertilizers should be minimized [247]. Furthermore, electrolytes that contain metals such as Li are costly, indicating that separation of electrolytes may be required. This could potentially be achieved relatively efficiently via precipitation or membrane-based separation processes, though electrolyte recovery has not been studied in this context. An alternative approach is to seek electrolytes that are abundant and non-toxic, such as NaCl, or utilize electrolytes such as KOH and $Na_2H_2PO_4$ that provide an additional source of P and K nutrients, although this would require that these compounds are available which may present a challenge. Research into the role of elec-

trolytes and pH on soil fertility and plant nutrition can identify optimal or acceptable ranges for dilute aqueous fertilizers. This will enable design of photo-electro-chemical processes where electrolyte selection minimizes or removes the need for additional separations.

The final role of separation is extraction of the catalyst from the electrolyte. This is only required in the case of particle slurry photocatalytic reactors, or homogeneous photo-electro-catalysts. Membranes or sieves present an efficient opportunity for removing catalyst particles, since the size of particles will be substantially larger than the molecules in the electrolyte, reactants, or products. Another possibility is to separate the fixed nitrogen products directly from the electrolyte via adsorption, effectively immobilizing the products on the absorbent. In the case of homogeneous catalysts, the removal of the catalyst is substantially more challenging. Separation of homogeneous catalytic complexes has been the subject of research in many other contexts. These separations are particularly challenging due to the temperature sensitivity of homogenous catalyst complexes, meaning distillation is not a feasible option [248]. Thus, they generally require sophisticated processes that are specific to a particular catalyst such as adsorption columns, liquid-liquid extraction, and nano-filtration [249]. The need for this separation can be mitigated by reactor designs with supported catalysts, and the use of solid catalyst materials.

2.5 Preliminary Performance Targets

There has been a substantial recent increase in photo-electro-chemical nitrogen fixation research, yet there are no clear targets for how efficient these processes need to be to enable practical impact for fertilizer production. Further, the metrics typically used to assess the performance of catalytic materials are not standardized or clearly linked to solar fertilizer yield. Substantial effort was devoted to identifying standardized tests and benchmarking procedures for photo-electro-catalytic water splitting [250, 251, 252, 253, 254, 255], many of which are relevant for solar fertilizers. In this section we propose several metrics that capture the photon absorption, reaction, and separation performance: solar-to-chemical

conversion efficiency, nitrogen fixation rate, energy per nitrogen fixation, energy per utilizable nitrogen, and time required to establish a 100 ppm solution. Performance targets for these metrics are identified, and relevant testing conditions such as solar spectrum, operating current density, oxygen content, and nutrient concentration are discussed. These targets are not meant to be authoritative, but rather provide guidelines for catalyst development and fertilizer testing. While the targets are identified with photo-electro-chemical processes in mind, some may also be applicable to other alternative approaches for nitrogen fixation such as chemical looping, plasma catalysis, or bio-engineering.

Assessing the photon absorption performance in the case of direct absorption and photocatalytic conversion is best assessed by the efficiency of converting solar energy to the chemical energy of the nitrogen nutrients in the fertilizer. The chemical energy of nutrients varies between ammonia, nitrates, and urea, and the required nutrient load also varies depending on the crop and agricultural region, making it difficult to identify an exact target for solar-to-chemical conversion efficiency. An order-of-magnitude estimate for the areal energy density required for fertilization is obtained by assuming the average nutrient density of 100 kg-N ha^{-1} yr^{-1} is provided by ammonia-based fertilizers:

$$100\frac{\mathrm{kg_N}}{\mathrm{ha.yr}} \times \frac{10^3}{14}\frac{\mathrm{mol_{NH_3}}}{\mathrm{kg_N}} \times \frac{667}{2}\frac{\mathrm{kJ}}{\mathrm{mol_{NH_3}}} \times \frac{1}{10^4}\frac{\mathrm{ha}}{\mathrm{m^2}} \times \frac{1}{3.15\mathrm{e}7}\frac{\mathrm{yr}}{\mathrm{s}} = 7.54\frac{\mathrm{mW}}{\mathrm{m^2}} \tag{2.1}$$

Converting this to efficiency also requires assumptions about the solar flux and amount of arable land dedicated to solar capture. A prior initial estimate of 0.1 % solar-to-ammonia efficiency was obtained assuming 50 kg-N/ha, 8 hours of full sunlight per day at 1000 W m^{-2}, and 1% of arable land dedicated to solar capture [28]. Data on actual average daily solar fluxes reveals that they vary from 120 - 280 W/m^2 depending on latitude [154] (see Figure 1.2), and there is also considerable variability in the nutrient load required, ranging from 15-200 kg-N m^{-2} depending on a myriad of factors including crop and soil type [161]. The amount of land that farmers are able to dedicate to solar capture will also likely

vary depending on region, and has not been studied. Based on these estimates the required solar-to-ammonia efficiency may range from 0.05 - 1.25 % depending on solar flux and required nutrient load. These estimates assume that 1% of arable land is dedicated to solar capture, and will vary linearly with the percentage of land available, as illustrated in Figure 2.6. We propose that 1% is a relatively conservative number, corresponding to 100 m^2 ha^{-1} or roughly 6 typical solar panels per hectare.

The solar-to-chemical conversion efficiency is a critical metric for assessing the viability of solar fertilizer catalysts, but it is not always reported. However, solar-to-ammonia efficiencies as high as 0.1% have been reported for graphitic carbon nitride catalysts without the use of sacrificial reagents [256], suggesting that the target of 100 kg-N/ha can be achieved with <10% of land dedicated to solar capture in regions with high solar flux such as sub-Saharan Africa (Figure 2.6). In the case of photocatalysis the solar-to-chemical conversion efficiency can be computed as:

$$\eta_{\mathrm{SCC}} = \frac{\Delta \mathrm{G_{rxn}} \mathrm{C_{nutrient}} \mathrm{V_{sol}}}{\mathrm{A_{illum}} \int_0^{\mathrm{t_{rxn}}} \phi_{\mathrm{s}}(\mathrm{t}) \mathrm{dt}} \tag{2.2}$$

where η_{SCC} is the solar-to-chemical conversion efficiency for a solar fertilizer cell, ΔG_{rxn} is the reaction free energy to form the nutrient product (typically ammonia), $C_{nutrient}$ is the molar concentration of the nutrient at the end of the experiment, V_{sol} is the volume of solution at the end of the reaction, t_{rxn} is the total time of the experiment, ϕ_s is the solar flux, and A_{illum} is the cross sectional area exposed to light [250]. The solar-to-ammonia efficiency of electrochemical processes is not directly measured, but can be estimated based on the electrical energy conversion efficiency:

$$\eta_{\mathrm{EEC}} = \frac{\Delta \mathrm{G_{rxn}} \times \eta_{\mathrm{F}}}{\mathrm{U_{app}} \times \mathrm{F} \times \mathrm{n_e}} \tag{2.3}$$

where η_F is the Faradaic efficiency, U_{app} is the applied voltage, F is Faraday's constant, and n_e is the number of electrons in the reaction. Based on currently-reported overpoten-

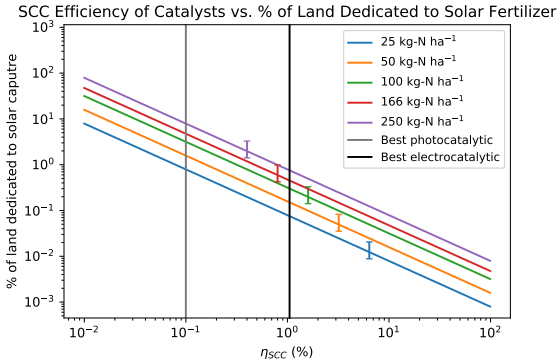

Figure 2.6: The solar-to-chemical conversion (η_{SCC}) efficiency (Eq. 2.2) vs. the percentage of land area required to achieve a target nutrient concentration. The highest reported efficiencies for photochemical [256] and electrochemical [43] systems are plotted for reference. The yearly average solar constant for a 24 hour period was assumed to be 200 W m^{-2}. Error bars show deviations in the average solar constant of $\pm$ 80 W m^{-2}. 50kg-N ha^{-1} is the global average N loading, 100, 166, and 250 kg-N ha^{-1} represent the suggested loading for rice (NE China) [257], potatoes (Mediterranean) [258], and wheat (France) respectively [259]

.

tials for the oxygen evolution reaction, Suryanto et al. propose that $U_{app} = \nu_{NRR} + 1.8\text{V}$ where ν_{NRR} is the overpotential for nitrogen reduction. [148] This metric can be multiplied by the efficiency of solar photovoltaics ($\sim$ 20%) to obtain a solar-to-ammonia efficiency. The highest reported energy-to-ammonia efficiency for an electrocatalytic process is 5.25% [43], corresponding to a solar-to-ammonia efficiency of approximately 1%. Figure 1.2 suggests that in this case $<$1% of land is needed to obtain 100 kg-N/ha. These promising metrics suggest that practically relevant solar-to-chemical conversion efficiencies are likely attainable for both direct and indirect photo-electro-chemical nitrogen fixation.

The rate of nitrogen fixation is related to the efficiency through the current at an applied voltage for electrochemistry, or the formation rate for a given flux of photons for photochemistry. The rate is a commonly reported metric for catalyst performance; however, there are no standards for how the rate is normalized. For electrochemical nitrogen fixation the rate is proportional to the current and Faradaic efficiency toward fixed nitrogen products. In the case of nitrogen reduction, the Faradaic efficiency typically depends on the applied

potential, and decreases at high current densities, such that there is an optimum operating potential. This leads to rates and efficiencies that are reported at different operating potentials for different catalysts, so ammonia yield at the optimum operating potential is a useful metric for comparison. As recently pointed out by Suryanto et al., it is also critical to normalize yield or current to the geometric surface area of the electrode, since this will determine the size of the electrode assembly [148]. A detailed technoeconomic analysis is needed to determine a viable electrode size per hectare, and the results will likely depend on the specific agricultural scenario, as discussed in Sec. 2.2. However, a recent DOE report estimated that a 10 kW hydrogen fuel cell system will have an active electrode surface area of 1.44 m^2 [260]. Assuming a similarly-sized cell stack can be dedicated to a single hectare leads to a target current density of 5 mA/cm^2 ($17 \cdot 10^{-9}$ mol_{NH_3} cm^{-2} s^{-1}), corresponding to 109 kg-N per hectare per year. This represents an optimistic goal, given that the cost of 100 kg of N is approximately $55 in developed countries (see Sec. 2.2). This suggests that the equivalent ammonia synthesis cell stack would need to be much cheaper than the proton exchange membrane cells used for hydrogen conversion. Moreover, the target of 5 mA/cm^2 is substantially higher than most reports where the largest current densities are below 1 mA/cm^2 [43, 23]. This highlights the importance of improving the catalyst performance and engineering low-cost electrochemical cells to make solar-driven electrocatalytic nitrogen fixation viable. However, this estimate is still $\sim$100 times lower than the DOE target rate for fuel applications [23], indicating that fertilizers provide a more attainable goal.

Photochemical rates also suffer from a lack of standardization, and are often reported as mass of ammonia per unit-mass of catalyst. Key quantities such as catalyst loading and illumination area are needed to effectively compare the rates, yet these are not always reported. In the case of photochemical nitrogen fixation, the rate normalized to illumination area is critical, and will be proportional to the solar-to-chemical conversion efficiency. Additionally, photocatalytic experiments should be performed and reported without the use of sacrificial reagents, even if experiments with their use are also reported. Similar to the

case of electrochemical conversion, determining an exact target rate will require a more thorough technoeconomic analysis. However, an order-of-magnitude estimate can be obtained based on the assumption of 1% solar area capture, or 100 m^2 per hectare. The maximum amount of catalyst is estimated as 100 kg/ha, corresponding to a coating thickness of approximately 250 μm for a catalyst with a density of 4 g/cm^3 (similar to titania). This corresponds to a target rate of 1 g-N per g of catalyst per year, or around 8 μmol/g/hr. The common practice of only reporting ammonia concentration vs. time, without unambiguously specifying the reactor volume or amount of catalyst used, makes it difficult to estimate the rate for many reported photocatalysts. The rate corresponding to 0.1 % efficiency is estimated as 2 μmol/g/hr, suggesting that photocatalytic rates and efficiencies are approaching targets that may enable practical implementation.

An alternative approach to comparing catalyst performance across different reactions and photo-electro-chemical approaches is quantification of the energy input required to produce one mole of fixed nitrogen product. This metric is more appropriate for solar fertilizers since, unlike fuels, the energy content of the resulting product is not related to its performance as a fertilizer. In the case of solar fertilizers the molar energy density is closely related to the efficiency:

$$\rho_{\mathrm{E}} = \frac{\Delta \mathrm{G_N}}{\eta_{\mathrm{SCC}}} \tag{2.4}$$

where ρ_E is the molar energy density and ΔG_N is the free energy of reaction for the fixed nitrogen product (e.g. ammonia). This metric can be directly compared between various fixed nitrogen products such as ammonia, nitrates, urea, or others. The metric also permits comparison between different approaches to nitrogen fixation such as thermochemical looping or plasma-induced nitrogen fixation. For example, the energy requirement for Haber-Bosch with hydrogen from water electrolysis is 566 kJ mol^{-1} [184]. For ambient conditions with aqueous electrolytes, the best reported electrocatalytic, photocatalytic, and plasma-induced molar energy densities are 6460 kJ mol^{-1} [43], 3.39 $\cdot 10^5$ kJ mol^{-1} [256],

Table 2.1: Summary of energy density required for nitrogen fixation by various methods, assuming water as a hydrogen source.

Process	Lowest energy density (kJ/mol-N)	Reference
Electrocatalytic	$6.46 \cdot 10^3$	[43]
Photocatalytic	$3.39 \cdot 10^5$	[256]
Plasma	$1.39 \cdot 10^5$	[25]
Haber-Bosch	$5.66 \cdot 10^2$	[184]

and $1.39 \cdot 10^5$ kJ mol^{-1} [25] respectively (see Table 2.1). Recently, it has been suggested that the molar energy density of a solar fertilizer should be competitive with the molar energy density of the Haber-Bosch process for solar fertilizers to be viable [148]. This assumes that the energy costs are similar in both cases, and that the ultimate price of fertilizer is primarily determined by the energy costs. However, the goal of solar fertilizers is to capture latent solar energy that has no inherent cost, and the analysis in Sec. 2.2 highlights the importance of transportation costs for fertilizer prices. Processes with higher molar energy density will certainly have higher capital costs, and this will likely become prohibitive for indirect approaches, where both photovoltaics and electrochemical cell stacks must be purchased. However, direct photocatalytic processes can be far simpler. For example, in the case of a batch process similar to solar water disinfection [181], the primary cost would be directly related to the catalyst material. If the catalyst is an earth-abundant material the cost may be extremely low, and processes with substantially higher molar energy densities than Haber-Bosch may be viable. In this best-case-scenario, the target can be estimated based on the necessary nutrient density and solar flux. A preliminary target corresponding to 100 kg-N ha^{-1}yr^{-1} at 200 W m^{-2} illumination and a 1% solar capture footprint is 8.83 $\cdot 10^4$ kJ mol^{-1}.

The prior analysis indicates that the best-reported electrocatalytic efficiency meets the target for solar fertilizers, which suggests that energy efficiency for the chemical transformation of atmospheric nitrogen may not be the limiting factor. However, this only covers the efficiency of the photon capture and reaction steps (see Sec. 2.4). The rate and yield must also be considered to determine capital investment, as discussed in previous para-

graphs. Moreover, the high-efficiency processes reported use pure nitrogen as a feedstock, and the effluent of the electrochemical system contains a lithium-based electrolyte, meaning that they are unlikely to be economically viable for solar fertilizer production. It is important to consider the energy required for both upstream and downstream separations needed to generate feedstocks and convert the effluent of the process into a usable fertilizer, as well as any energy inputs into the process itself (e.g. heating for high temperature processes). This energy will vary considerably based on the details of the process, and has not been reported for any photo-electro-chemical process. We propose the metric of "energy per utilizable nitrogen" as highly relevant for assessing a solar fertilizer process, particularly if all of the energy is expected to come from solar capture. The molar energy density per fixed nitrogen represents a lower limit of the energy per utilizable nitrogen, and the energy per utilizable nitrogen is an upper limit on the amount of energy required from solar sources. Hence, these two metrics together provide significant insight into the viability of a solar fertilizer process. Based on the preceeding analysis an energy of $8.83 \cdot 10^4$ kJ mol^{-1} should be considered a target for energy per utilizable nitrogen, rather than a target for molar energy density. In practice, precise estimates of energy per utilizable nitrogen may be very difficult to obtain due to the complexity and uncertainty in upstream and downstream processes. Nonetheless, researchers in the field can use the concept along with order-of-magnitude estimates to assess the potential viability of a photo-electro-catalytic process for solar fertilizer production.

Another practical consideration is the time required to generate the solar fertilizer product. This is typically quantified by the chemical engineering concepts of residence time or space velocity. These quantities are related to the rate and efficiency, but will also provide a measure of catalyst stability and activity under realistic operating conditions where the nutrient concentration is high. Based on prior fertigation studies, we propose that 100 ppm of fixed nitrogen is an appropriate initial target for ammonia concentration in aqueous fertilizer solutions [204]. Keeping the nutrient concentration target of 100 kg-N per hectare

per year corresponds to a volumetric flux of around 150 liters of aqueous fertilzer solution per hour for one hectare of arable land:

$$100\frac{\mathrm{kg_N}}{\mathrm{ha.yr}} \times \frac{10^3}{14}\frac{\mathrm{mol_N}}{\mathrm{kg_N}} \times \frac{1}{8760}\frac{\mathrm{yr}}{\mathrm{hr}} \times \frac{10^6}{100}\frac{\mathrm{mol_{H_2O}}}{\mathrm{mol_N}} \times \frac{1}{55.4}\frac{\mathrm{L}}{\mathrm{mol_{H_2O}}} = 147\frac{\mathrm{L}}{\mathrm{hr.ha}} \tag{2.5}$$

Converting this volumetric flux to a space-time requires the volume of the reactor. In the case of photocatalysis the reactor area is given roughly by the solar capture area, which will be 100 m^2 ha^{-1} assuming 1% of land is dedicated to solar capture. The reactor height will be determined by the optical penetration, which depends on the catalyst loading and scattering properties. However, a depth of 1-10 cm is reasonable, yielding a reactor volume of 1000 - 10,000 L ha^{-1} and a residence time of around 7 - 70 hours. In the case of electrochemical conversion the reactor volume will be independent of solar capture area, and will likely be smaller in general. Given the dependence of residence time on reactor design, the volumetric flux per illumination area provides a better metric for comparing process performance. Assuming that 1% of land will be used for solar capture and converting the volumetric flux from 147 L hr^{-1} ha^{-1} to more convenient lab-scale units yields a target volumetric flux per illumination area of 150 μL cm_{illum}^{-2} hr^{-1}. The volumetric flux per illumination area measured from experiment can be computed with the following formula:

$$\mathrm{Q_{fertilizer}} = \frac{\mathrm{V_{fertilizer}}}{\mathrm{t_{rxn}A_{illum}}} \tag{2.6}$$

where $Q_{fertilizer}$ is the volumetric flux per illumination area, $V_{fertilizer}$ is the volume of the effluent with sufficient nutrient concentration to be a fertilizer after the experiment (suggested initial target is 100 ppm), and all other variables are defined in Eq. 2.2. While this equation only applies directly to photocatalysis it can also be adapted to electrocatalysis by estimating the area of conventional photovoltaics needed to provide the electrical energy and substituting this as A_{illum}. This will depend on the overpotentials of both half-

reactions, as well as the area of the electrode and Faradaic efficiency:

$$\tilde{A}_{illum} = \frac{i_{NH_3} \times (V_{applied})}{\eta_{PV} \times \eta_F \times J_{solar}} \tag{2.7}$$

where $\tilde{A}_{illum}$ is the effective illumination area, i_{NH_3} is the current producing ammonia, $V_{applied}$ is the applied potential (including both reductive and oxidative overpotentials), η_{PV} is the photovoltaic cell efficiency (typically 20%), η_F is the Faradaic efficiency toward ammonia, and J_{solar} is the solar flux (typically 300 W m^{-2}). For example, assuming the target current density of 5 mA cm^{-2}, a Faradaic efficiency of 10% at an overpotential of 1.15 V for nitrogen reduction [43] and 0.45 V for OER yields an effective illumination area of 23 $cm^2_{illum} cm^{-2}_{electrode}$.

The volumetric flux is not currently reported for any photo-electro-catalytic nitrogen fixation experiments, and cannot be calculated since reactor volumes are not typically reported. It is expected that the relatively large reactor volumes used in most experiments prevents the concentration from ever reaching the target of 100 ppm, and most reported concentration are in the μmolar regime [59, 28]. However, specialized reactor designs with higher surface area to volume ratios may enable experiments where the volumetric flux can be measured; a similar strategy enabled measurement of minor products for electrochemical CO_2 reduction [261]. Another advantage of this type of experiment is that the relatively large resulting ammonia concentration will overcome the many issues with ammonia quantification [145, 146, 144, 147, 148], and should even be qualitatively detectable by odor. Demonstrating the production of a prototype solar fertilizer, even at a very small scale, represents an important step toward solar fertilizer development.

Finally, we note that it is also important to report and control the conditions under which the metrics are measured. Some key variables are the type of illumination, the atmosphere or reactants used, the properties of the electrolyte or solution used. For photo-electrocatalysis solar efficiency should be measured with an AM1.5 solar simulator rather than

xenon or mercury lamps with high UV content [262], which is standard in the photovoltaics community. We also propose a "standard atmospheric" test for photocatalysis where the reaction is run in air with distilled water. This standard test will provide an important control experiment, can act as a common reference for comparing the performance of various photocatalysts, and will provide an estimate of the "energy per utilizable nitrogen" since no upstream or downstream processing would be required. In the case of electrochemistry it is more difficult to prescribe a standard test since electrolytes are always required and have been shown to have a considerable effect on nitrogen fixation activity [43, 263, 264, 147]. However, it is still useful to consider the robustness of the process to air, and we recommend reporting the activity with air as a feedstock to assess the need for upstream air separations. Assessing stability and measuring turnover number has also been identified as an important metric that will help establish how robust catalysts are under operation [148]. Another critically important consideration is the standardization of how nutrient concentrations are measured.

2.6 Conclusions

Solar fertilizers present an exciting opportunity to directly capture diffuse solar energy and convert it to chemical energy that can be applied at or near the point of production. The technology falls at the complex nexus of energy and agriculture. Substantial additional research is needed to establish the most promising approaches and to demonstrate the technology. This work grapples with some initial considerations from the perspective of agronomics and photo-electro-chemistry and identifies some preliminary strategies that will aid in the development and deployment of solar fertilizer technologies. Several scenarios for decentralized fertilizer production are presented and the potential social, economic, and technical advantages and disadvantages are discussed. The key technical needs for solar fertilizer production are identified as solar capture, reaction, and separation, and some possible strategies and considerations are presented. Specific metrics and testing conditions

are identified, along with targets that may enable solar fertilizer technology. The metrics and considerations presented draw on a range of expertise in the diverse fields of agronomics, photo-electro-catalysis, chemical separations, and process systems engineering, and provide a starting point for further development of solar fertilizer technologies. There are many possible routes forward for this nascent field, and identifying the most promising will require a diverse range of technical, social, and economic considerations. However, the vast potential impact of solar fertilizers on the growing problem of world hunger makes this challenging endeavor worthwhile.

CHAPTER 3
OVERVIEW OF THEORETICAL METHODS

Atomic level study using computational chemistry methods will allow us to isolate surface environments and test hypotheses at the molecular scale. This can help clear up the ambiguity of the experimental literature. However, there are significant challenges to modeling the geometric and electronic structure of TiO_2, as well as treating the excited states inherent in photocatalysis. Among the most difficult of these is the wide range of different catalyst phases and surfaces. Most studies utilize a mixed phase of two polymorphs of TiO_2: anatase and rutile. Studies often use powders rather than pure crystal faces, with dopants which alter their electronic band properties, further convoluting the process. This massively increases the complexity of understanding the surface chemistry. In general, computational catalysis relies on modeling ideal crystal faces, occasionally examining step sites and defects, so these complex phases present a serious impediment. Nonetheless, insight can be gained from studying the pure crystal phases and lower index surfaces, but non-ideal systems must also be considered. Even with the correct active site model, TiO_2 is also quite difficult to treat in electronic structure calculations, with results depending heavily on the methods used [84]. Thus methods must be employed to quanitfy the uncertainty in our calculations based on methodology.

3.1 Density Functional Theory

To gain a theoretical understanding of the system, we will employ density functional theory (DFT). DFT is an approximate method based on the first and second Hohenberg-Kohn theorems and implemented with the Kohn-Sham equations [265, 266]. DFT can provide an atomistic view on the surface intermediates and activation barriers that ultimately control the rate of reaction. It has been shown to yield adsorption energies with an average ap-

proximate error of $\sim$0.2eV [267]. We will primarily use theory at the generalized gradient approximation (GGA) level of theory, and more specifically we will use the Bayesian error estimation functional (BEEF-vdw). The reason for this choice of method is its speed relative to higher level methods. BEEF-vdw has many advantages over the more commonly used Perdew–Burke-Ernzerhof functional [268] (PBE). Chief among them is its ability to produce an ensemble of values for the electronic energy based on an ensemble of functionals. The ensemble is designed to recreate the error in the experimental energy values on which the functional was fit. The error bars throughout this proposal represent one standard deviation of these ensembles. These error bars can also be thought of as the range of values you would expect to get from different GGA functionals. This will allow us to deal with the difficulty of modeling the electronic structure of TiO_2 as it will give us an idea of how sensitive our results are to changing our methods. Calculations will be performed in the plane wave code Quantum Espresso [269], along with a periodically repeating slab model.

3.2 Surface Phase Diagrams

Error estimation was also implemented in the phase diagrams in Section 4.1 and Section 6.3. The probability of a species existing on the surface was calculated using the following equation:

$$P_i = \frac{1}{N}\sum_{l}^{N}\frac{\exp(\frac{-G_i^l}{kT})}{\sum_j^M \exp(\frac{-G_j^l}{kT})} \tag{3.1}$$

where P_i is the probability of species i on the surface given DFT uncertainty, G_i^l is the free energy of species i computed from energy l of the BEEF-vdW ensemble, M is the number of total species considered, and N is the total number of energies in the BEEF-vdW ensemble (2000). This is equivalent to the average surface coverage from a ensemble of phase diagrams generated from the energies of the BEEF-vdW ensemble.

3.3 Thermodynamic Corrections

Since DFT implicitly calculates energies at 0K in a perfect vacuum, we must add thermal corrections and zero point energy (ZPE). For all structures we will perform a vibrational frequency calculation using a finite difference method implemented in the Atomic Simulation Environment (ASE) [270]. The vibrational frequencies will be used to add ZPE and statistical mechanics to add the effects of elevated temperature and pressure. We will use the ideal gas approximation for gas phase species and harmonic oscillator for surface species. We enforce a low frequency cutoff for 33 cm^{-1}, setting all all frequencies lower to the cutoff value. This is to account for the translational modes of the adsorbates on the surface and avoid diverging entropies due to the harmonic approximation.

3.4 Photoelectrochemistry

In addition to modeling the electronic structure and thermal behavior of the system, we must model the photoexcited electrons and holes. This cannot be done easily within the framework of DFT; requiring formalisms like time dependent DFT which are prohibitively expensive. To avoid this, we will assume that charge transport is independent of surface kinetics, and that electric field effects are negligible. Nørskov et al.[271, 143] provides a model for implementing these assumptions to which we adhere, commonly called the computational hydrogen electrode model (CHE). This model has been used extensively in the water splitting [272] and CO_2 reduction [273] and N_2 reduction literature [57]. The CHE model, originally designed to treat electrochemisty, sets the free energy of hydrogen splitting, reaction 3.2, to zero at a potential of zero. Additionally, the energy of each state involving the addition of an electron is varied by an energy of eU, where e is the fundamental change and U is the potential relative to this zero point (Equation 3.3). The potentials of excited electrons and holes are evaluated at the band edge potentials of the given material as reported in the literature [274]. The CHE model sets zero volts to the same value as the

reference hydrogen electrode (RHE), and thus conceptually equivalent to RHE [273]. We also neglect solvent effects, restricting our analysis primarily to gas phase systems. Given that DFT is best suited for treating gas phase systems, this is an obvious starting point. While these assumptions do not capture the full complexity of photocatalytic systems, they allow us to tractably work around the main difficulties and provide insight that is valid in well-defined limits.

$$\frac{1}{2}H_2 \rightarrow H^+ + e^- \tag{3.2}$$

$$\Delta G = \Delta G + eU \tag{3.3}$$

CHAPTER 4

ANALYSIS OF MECHANISM ON RUTILE (110)

To understand the mechanism of N_2 reduction on the rutile TiO_2 surface, we must closely examine the thermodynamics of adsorbed states. In this chapter we utilize simple models to establish the feasibility of various hypotheses. The study of photocatalytic nitrogen fixation on TiO_2 is carried out using DFT calculations to provide molecular-scale insight into the thermochemistry of adsorbed intermediate states. Computational investigations of photocatalysis on TiO_2 are difficult due to the complex nature of photocatalytic interfaces [275, 143] and the electronic structure of TiO_2 [276, 77]. The energetics of adsorbed species are computed under ideal gas-phase conditions (e.g. solvent effects, electric field effects, and coverage effects are neglected) and it is assumed that excitation and charge transport are decoupled from the electrochemical reactions, enabling the use of the CHE approach [272, 273, 143, 275]; all voltages are relative to the computational hydrogen electrode (CHE) unless otherwise stated. It should be noted that potentals relative to CHE are conceptually equivalent to those referenced to the reference hydrogen electrode (RHE.) To treat the electronic structure the generalized gradient approximation (GGA) with van der Waals (vdW) level of theory is used. The use of the Bayesian error estimation functional [267] (BEEF-vdW) provides error estimates that quantify uncertainty in order to assess the sensitivity of conclusions to the error due to the GGA approximation; more details are provided in Chapter 3. This approach is used to test four hypotheses, as discussed in the following sections: i) photocatalytic nitrogen fixation rates are greater in the gas phase than the aqueous phase ii) rutile (110) is an active surface for nitrogen reduction iii) oxygen vacancies or Fe substititions on rutile (110) are active sites for nitrogen reduction iv) rutile (110) is an active surface for nitrogen oxidation and subsequent NO reduction.

4.1 Nitrogen Adsorption Under Gas and Aqueous Environments

The literature contains examples of experiments done in aqueous solution[132, 59] and humidified air [71, 141]. Of these, humidified air generally has a higher rate [134]. To better understand the difference in performance under aqueous and gas-phase conditions ab-initio thermodynamics [277] have been used to compute surface phase diagrams for rutile (110) as a function of water and nitrogen chemical potentials. Figure 4.1a shows the surface free energy (top) and surface coverage (middle) of the reactants available at ambient gas-phase conditions (H_2O, N_2, O_2, OH). The results show that the bare TiO_2 surface is dominant at gas-phase conditions. The ensemble of energies from the BEEF-vdW functional can be exploited to evaluate the sensitivity of these coverages to DFT error. The probability analysis (Fig 4.1a, bottom) suggests that there is a very low probability of having appreciable N_2 coverage at 100% RH, but under dry conditions there is a probability of $\approx 10\%$ of having a N_2 coverage > 0.25 ML. This suggests that arid environments may favor N_2 adsorption, though it is noted that water also acts as a proton source so nitrogen reduction cannot occur if the humidity is too low. One interpretation of the surface coverage probability is that the BEEF-vdW functional is not sufficiently accurate to precisely determine the surface coverage, though the bare surface is the most likely. Another perspective is to view this as a sensitivity analysis of coverage with respect to binding energies of competing surface species. From this view, the results indicate that adsorption sites with slightly higher relative N_2 adsorption are likely to have a significant N_2 coverage under gas-phase conditions. This could include defect sites or other facets, although the site must have both stronger absolute binding energies and stronger relative adsorption of N_2 vs. H_2O. There are likely sites that satisfy this criterion, but their prevalence must also be considered. Regardless of the interpretation, the conclusion is that nitrogen coverages are expected to be relatively low on rutile TiO_2 (110) which is unsurprising given the inert nature of N_2.

The surface phase diagrams under aqueous conditions (4.1b) indicate that water will be

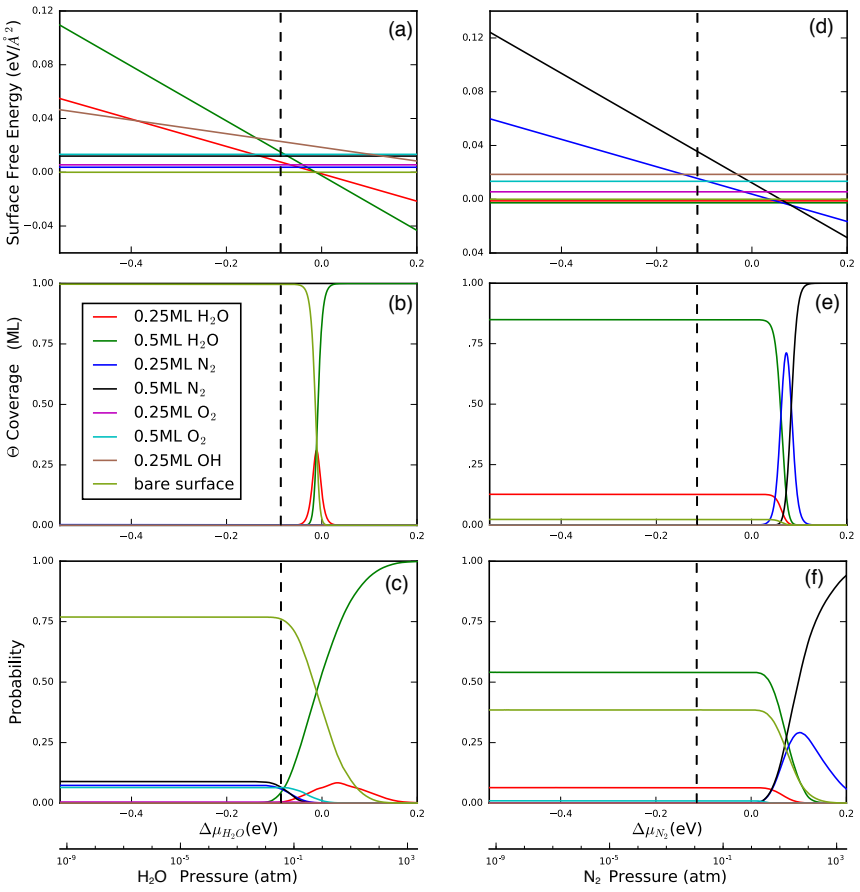

Figure 4.1: Surface free energy (a,d), coverage (b,e), and coverage probability (c,f) for H_2O, N_2, O_2, and OH as a function of H_2O (a-c) and N_2 (d-f) chemical potentials. The relevant water potential under gas-phase conditions (0.035 atm) and nitrogen potential under aqueous conditions (0.012 atm) are shown by dashed lines in (a-c) and (d-f) respectively. Graphs a-c use constant N_2 chemical potential set at atmospheric pressure of N_2 (0.8 atm) and d-f use constant water chemical potential set at 100% relative humidity of H_2O. Nitrogen pressure at aqueous conditions is estimated using Henry's law. The probability of various coverages (c,f) given the uncertainty in the BEEF-vdW functional is calculated using Eq. 3.1.

the dominant surface species for a wide range of N_2 pressures, with adsorbed N_2 becoming dominant at approximately 100 atm. In this case the probability analysis indicates that although the surface coverage of water/hydroxyl is not well-determined by the BEEF-vdW functional, the probability of a significant N_2 coverage is negligible at aqueous conditions. Interestingly, several reports have shown appreciable nitrogen fixation rates under aqueous conditions [132, 59]. The fact that competitive nitrogen adsorption is not favored under aqueous conditions indicates that highly reactive surface groups or defect sites with higher N_2 binding energy but low stability may play a role. The finding that nitrogen adsorption is more favorable in the gas phase suggests that the enhanced photocatalytic activity under gas phase conditions is due to the improved ability to adsorb N_2 in the absence of water. This intuitive result corroborates previous findings indicating that a key challenge in photocatalytic nitrogen fixation is getting N_2 to adsorb [278, 279, 134], and qualitatively explains the correlation between N_2 pressure and photocatalytic nitrogen reduction activity [134, 280]. The issue of nitrogen adsorption must be addressed in any photo(electro)catalytic system regardless of reaction mechanism, and will be a fundamental problem for low pressure nitrogen fixation processes.

4.2 Thermochemistry of Nitrogen Reduction

The electrochemical nitrogen reduction reaction converts nitrogen to ammonia and occurs at an equilibrium potential of 0.05 V vs. RHE (Figure 1.5). The proximity of this redox couple to the hydrogen evolution reaction (H^+/H_2 at 0 V) makes selective reduction of nitrogen to ammonia challenging [57, 281, 41]. Furthermore, the alignment of the rutile TiO_2 conduction band edge (Figure 1.5) indicates that the available overpotential for nitrogen reduction under photocatalytic conditions is relatively low ($<$0.15 V). Nonetheless, selective nitrogen reduction has been observed on TiO_2 photocatalysts [71, 141, 134, 132], indicating that TiO_2 is capable of dissociating the strong N-N bond more easily than the much weaker H-H bond. This suggests that identification of the active site for photocatalytic

nitrogen reduction may enable the development of improved nitrogen reduction electrocatalysts. In this section we hypothesize that the active site is stoichiometric rutile (110), and examine the binding free energies of intermediates for the dissociative and associative nitrogen reduction pathways.

The mechanism for thermocatalytic nitrogen reduction (i.e. Haber-Bosch catalysis) is established as a dissociative mechanism in which the first step is scission of the N-N bond, followed by hydrogenation of adsorbed mono-nitrogen [282, 283, 284, 285]; the electrochemical equivalent is shown in equations 4.1 - 4.6. Calculations of N-N scission on rutile oxides shows that they follow "ideal" scaling, suggesting that the activation barrier for nitrogen dissociation may be low [286], hence we first investigate the dissociative mechanism. Figure 4.2 shows the free energy diagram for the dissociative mechanism at standard temperature and pressure at the equilibrium potential. The dissociation energy of N_2 is remarkably high ($>$8.5 eV), indicating that this route is not remotely thermodynamically feasible on rutile (110). This extreme barrier is not sensitive to the BEEF-vdW exchange-correlation approximation, and is expected to be prohibitively large even in the presence of solvent stabilization since each adsorbed N* would need to be stabilized by $>$3 eV, significantly more than typical solvent stabilization values [287, 288, 143]. Furthermore, this step is not electrochemically driven, so even the application of large overpotentials will not enable direct N-N scission. This provides strong evidence against direct dissociation of the N-N bond on the stoichiometric rutile TiO_2 surface. The same stabilization would be required for NH* species, effectively eliminating any pathway involving NH* (e.g. dissociation of NNH). Adsorbed NH_2 species are somewhat more stable, and may exist under solvated conditions, opening the possibility of mechanisms involving dissociation of $N_2H_{x>2}$ species, similar to the associative mechanism that will be discussed subsequently.

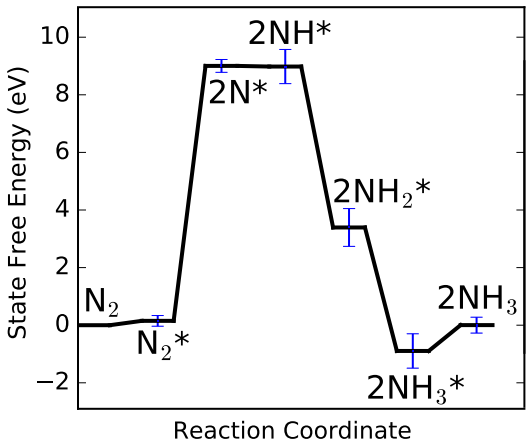

Figure 4.2: Free energy diagram for dissociative nitrogen reduction at the equilibrium potential computed from DFT (0.008 V, compared to 0.05 V from experiment). The blue error bars represent one standard deviation of the BEEF-vdW energy ensemble. Adsorbed states are labeled, and the full reaction mechanism is listed in equations 4.1 - 4.6.

$$N_2(g) + * \rightarrow N_2^* \tag{4.1}$$

$$N_2^* + * \rightarrow 2N^* \tag{4.2}$$

$$2N^* + 2(H^+ + e^-) \rightarrow 2NH^* \tag{4.3}$$

$$2NH^* + 2(H^+ + e^-) \rightarrow 2NH_2^* \tag{4.4}$$

$$2NH_2^* + 2(H^+ + e^-) \rightarrow 2NH_3^* \tag{4.5}$$

$$NH_3^* \rightarrow NH_3(g) + * \tag{4.6}$$

The associative nitrogen reduction mechanism proceeds via diazene (N_2H_2) and hydrazine (N_2H_4), as shown in equations 4.7 - 4.14. This mechanism has been proposed to be most relevant for electrochemical nitrogen reduction [107, 57, 289], and the fact that hydrazine has been observed as a photoreduction product on TiO_2 [134] suggests that it may be the relevant photocatalytic nitrogen reduction mechanism. The free energy diagram for the associative mechanism at the equilibrium potential is shown in Figure 4.3a, while the free energy diagram at the conduction band edge energy for rutile is shown in

Figure 4.3b. Under photocatalytic conditions the conduction band edge is the relevant potential, corresponding to an overpotential of 0.15 V. However, examination of the free energy diagram reveals a thermodynamic limiting potential of 2.5 V due to the unstable NNH* adsorbed intermediate, which is consistent with previous work [107]. This barrier is significantly higher than the conduction band potential, making the route improbable unless the adsorbates are stabilized significantly ($\approx$ 2 eV) by solvent/dipole effects. The rate-limiting hydrogenation of N_2 is consistent with studies of electrochemical nitrogen reduction on metals [57], nitrides [290], and oxides [107] indicating a general trend for photo- and electrochemical nitrogen reduction.

$$N_2(g) + {}^* \rightarrow N_2^* \tag{4.7}$$

$$N_2^* + H^+ + e^- \rightarrow NNH^* \tag{4.8}$$

$$NNH^* + H^+ + e^- \rightarrow HNNH^* \tag{4.9}$$

$$HNNH^* + H^+ + e^- \rightarrow HNNH_2^* \tag{4.10}$$

$$HNNH_2^* + H^+ + e^- \rightarrow H_2NNH_2^* \tag{4.11}$$

$$H_2NNH_2^* + {}^* + H^+ + e^- \rightarrow NH_2^* + NH_3^* \tag{4.12}$$

$$NH_2^* + NH_3^* + H^+ + e^- \rightarrow 2NH_3^* \tag{4.13}$$

$$2NH_3^* \rightarrow 2NH_3(g) + 2^* \tag{4.14}$$

The results indicate a prohibitively high barrier for both dissociative and associative nitrogen reduction on stoichiometric rutile TiO_2 (110), although the associative pathway is significantly more favorable than the dissociative pathway. These findings are robust to the error of the exchange-correlation approximation employed, and the energetic barriers are significantly larger than the typical magnitude of electrochemical interface effects that have been neglected (solvent, electric field). This evidence refutes the hypothesis that rutile (110) is the active site for photocatalytic nitrogen reduction on TiO_2, necessitating

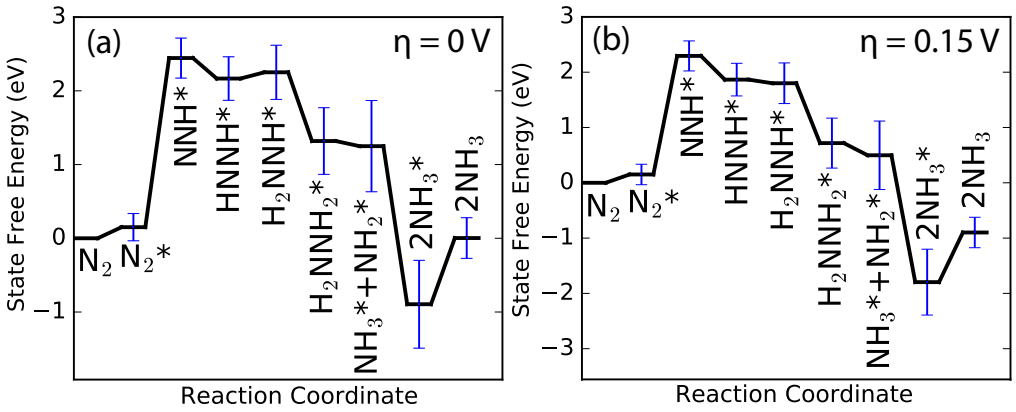

Figure 4.3: Free energy diagram for associative nitrogen reduction at an overpotential (η) of zero (a) and at the overpotential due to the conduction band edge ($\eta = 0.15$ V) (b). The equilibrium potential ($\eta = 0$) is computed to be 0.008 V (0.05 V experimentally). The blue error bars represent one standard deviation of the BEEF-vdW energy ensemble. Adsorbed states are labeled, and the full reaction mechanism is listed in equations 4.7 - 4.14.

the development and testing of alternative hypotheses.

4.3 Nitrogen Reduction at Oxygen Vacancies

Surface defects are known to play a key role in many types of heterogeneous catalysis [291], and oxygen vacancies in particular have been shown to participate in numerous catalytic reactions on oxides [292] including TiO_2 [115, 116, 77, 80, 85]. Oxygen vacancies are typically highly reactive, leading to binding energies that are often substantially stronger than binding at the stoichiometric surface. The unstable nature of N_2H on stoichiometric rutile (110) (Figure 4.3) indicates that defect sites may enable nitrogen reduction by enhancing the stability of N_2H and other high-energy intermediates. Bridging oxygen (O-br) vacancies are known to occur commonly on rutile (110) surfaces [77, 80, 85], and a recent analysis of nitrogen reduction over titania has shown that the reaction rate is proportional to the measured number of oxygen defects [59]. Due to these considerations the O-br vacancy is a natural starting point for evaluating the effect of surface defects, although it is noted that other intrinsic defects, such as Ti vacancies in the surface or sub-surface may also play a role [293].

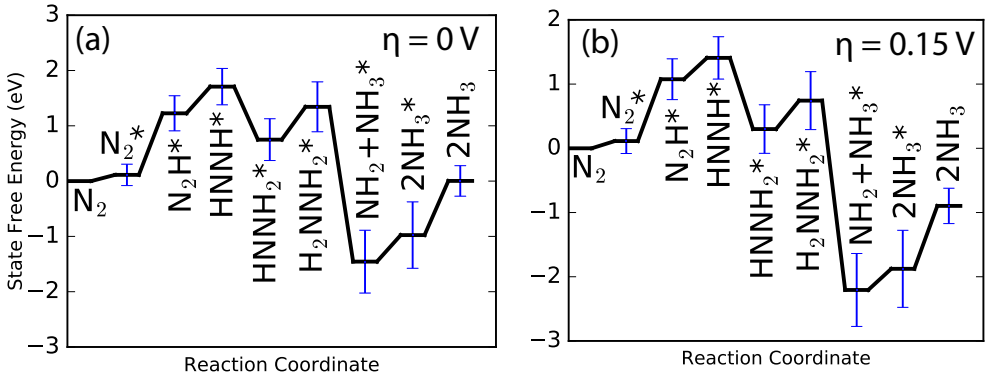

Figure 4.4: Free energy diagram for associative nitrogen reduction at an O-br vacancy site at an overpotential (η) of zero (a) and at the overpotential due to the conduction band edge ($\eta = 0.15$ V) (b). The equilibrium potential ($\eta = 0$) is computed to be 0.008 V (0.05 V experimentally). The blue error bars represent one standard deviation of the BEEF-vdW energy ensemble. Adsorbed states are labeled.

The energetics of the associative nitrogen reduction pathway at the rutile (110) O-br defect site are shown in Figure 4.4. Comparison to the energetics of the stoichiometric surface (Figure 4.5a) reveals a significant stabilization of the N_2H intermediate, corresponding to a thermodynamic limiting potential of 1.21 V. However, examination of the energy diagram at the conduction band potential of rutile TiO_2 (Figure 4.4b) indicates that the N_2H and N_2H_2 intermediates are still too unstable to explain the photocatalytic reduction observed, although it is plausible that the thermodynamic barrier of 1.39 eV (energy of N_2H_2 at the conduction band edge) may be overcome by stabilization if solvent or dipole effects for N_2H and N_2H_2 are considerably larger than typical amounts of $\approx$0.6 eV [287, 288, 143]. Furthermore, other defects such as sub-surface O or Ti vacancies may increase the reactivity of the surface, although as defects become less stable they will also become less prevalent on the surface. This tradeoff between stability and reactivity has been noted previously for amorphous oxides [294], and suggests that more reactive (unstable) defects will have a limited impact due to low prevalence. The O-br defect considered here has a formation free energy of 1.54 eV at 0V SHE referenced against water, indicating that it will occur with an relatively low probability on thermodynamically equilibrated surfaces. Mor-

phological (e.g. particle edges) and kinetic (e.g. trapped bulk defects) effects will increase the prevalence of vacancies or other defects in real catalysts [99]; these effects are difficult to control and characterize, and may be the source of some discrepancies in the nitrogen photofixation literature [28].

An alternative possibility is a mixed mechanism proceeding through dissociaton of partially hydrogenated species, since the NH_x species are stable at the O-br vacancy; however, this would still necessitate the formation of the potential-limiting HNNH* species from the associative mechanism and would be thermodynamically (though not kinetically) equivalent. Furthermore, we note that the free energy diagram in Figure 4.5b requires two O-br vacancies, since each N* (or NH_x) is adsorbed at a vacancy. The relatively high metal substitution energy of O-br vacancies suggests that this is improbable, and the experimental investigation of Hirakawa et. al. [59] shows a linear dependence on oxygen vacancies, rather than the quadratic dependence that would be indicative of direct N-N (or HN-NH) scission by two vacancy sites. This finding strongly refutes the proposed hypothesis that direct N-N scission by O-br vacancies is the mechanism of photocatalytic nitrogen fixation on TiO_2. However, the fact that the O-br vacancy significantly stabilizes NH_x species, making NH_x binding close to exothermic suggests that it can promote nitrogen reduction and ammonia formation after the N-N bond has been cleaved.

4.4 Nitrogen Oxidation and Indirect Reduction

The majority of experimental investigations of photocatalytic nitrogen fixation on TiO_2 catalysts have identified reduced products of ammonia or ammonium. However, several reports have observed nitrates as the main product [66, 67], and examination of the standard redox potentials and TiO_2 band edges (Figure 1.5) indicates that the band alignment for nitrogen oxidation to NO is significantly more favorable on TiO_2 than the band alignment for nitrogen reduction. The band alignment provides $\approx$ 1.25 V overpotential for both the oxygen reduction half-reaction and the oxidation of nitrogen for NO. Based on this we

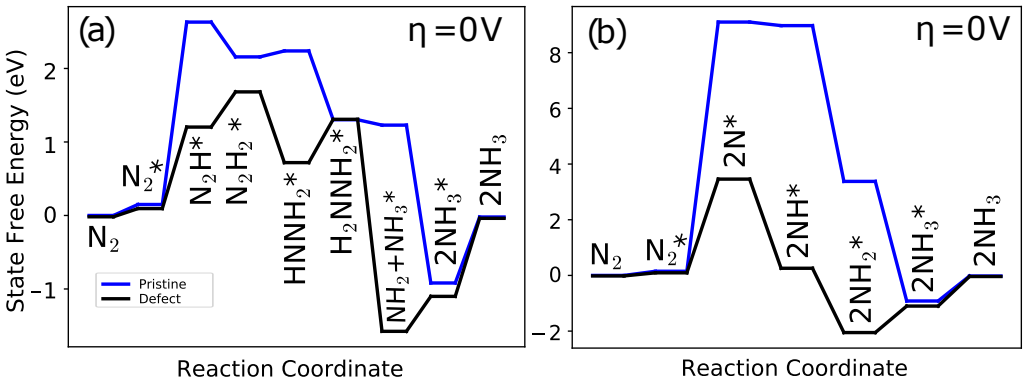

Figure 4.5: Comparison of free energy pathways over stoichiometric (blue) and oxygen-vacant (black) for the associative (a) and dissociative (b) nitrogen reduction pathways at the equilibrium potential. All details are consistent with Figs. 4.2a - 5.6a. Error bars are omitted for clarity.

hypothesize that the scission of the N-N bond on rutile (110) proceeds via the oxidation of nitrogen to NO, which is subsequently oxidized or reduced depending on the details of the catalyst and reaction conditions.

The thermodynamics of nitrogen oxidation intermediates on rutile (110) are shown in Figure 4.6 the energy of the TiO_2 valence band edge. Figure 4.6 reveals that the thermodynamic limiting potential is 0.72 V (surface oxygen formation is the potential-limiting step), considerably lower than the case of nitrogen reduction. In addition, the direct adsorption of N_2 to this reactive surface oxygen is endergonic by 0.15 eV, indicating that adsorption of N_2 is challenging on oxygen-rich surfaces. When the significant driving force provided by the photo-excited hole (1.22 V overpotential) is taken into account (Figure 4.6b) the oxidative path becomes extremely favorable, with all photoelectrochemical steps being exergonic with the exception of N_2O_2 dissociation which is very slightly (< 0.1eV) uphill. However, when kinetic barriers are considered the reaction looks significantly less feasible. Computed barriers to the two oxygen coupling steps are in excess of 2eV, showing highly unfavorable surface reactions. This result suggests that the key challenge of photochemical nitrogen oxidation is the kinetics of coupling oxygen to the N_2 and N_2O molecules. However, solvent effects have been neglected from this analysis. The stablizing effects of

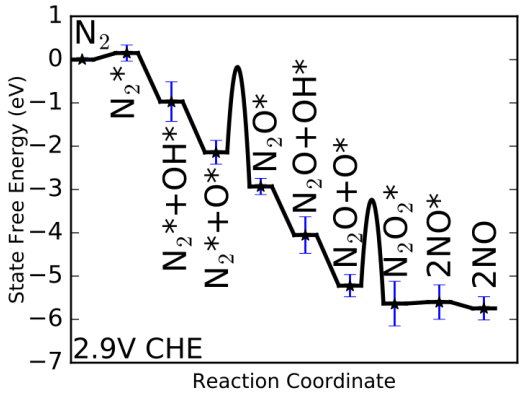

Figure 4.6: Free energy diagram for nitrogen oxidation to NO at an overpotential (η) of zero (a) and at the overpotential due to the valence band edge ($\eta = 1.22$ V) (b). The equilibrium potential ($\eta = 0$) is computed to be 1.465 V (1.68 V experimentally). The blue error bars represent one standard deviation of the BEEF-vdW energy ensemble. Adsorbed states are labeled.

solvents may lower these kinetic barriers or an alternative pathway may exist that had not been considered.

The computational results provide strong evidence that nitrogen oxidation is thermodynamically feasible on the rutile (110) active site, while N_2 reduction is thermodynamically challenging. This is at odds with the experimental observation of reduced products on TiO_2 [71, 141, 132, 133, 134, 59]. One possible explanation is that nitrogen is first oxidized to NO and subsequently reduced to ammonia. The conversion of NO to NH_3 is a 5 electron process with a redox potential at 0.71 V vs. RHE, well below the band gap of TiO_2[28], and has been reported experimentally [295] and studied theoretically [108]. The thermodynamic feasibility of this pathway on rutile (110) has been computed and the most thermodynamically favorable path is shown in Figure 4.7. The mechanism and energetics are consistent with prior work [108], and indicate that this is indeed thermodynamically feasible. However, reduction of nitrogen oxides is a complex process that can also form partially reduced species such as N_2O or N_2. In particular, the reaction of NO to N_2O and the reaction of N_2O to N_2 has been observed under UHV conditions by Yates and colleagues [101, 102]. Fully understanding the selectivity of photocatalytic NO reduction on

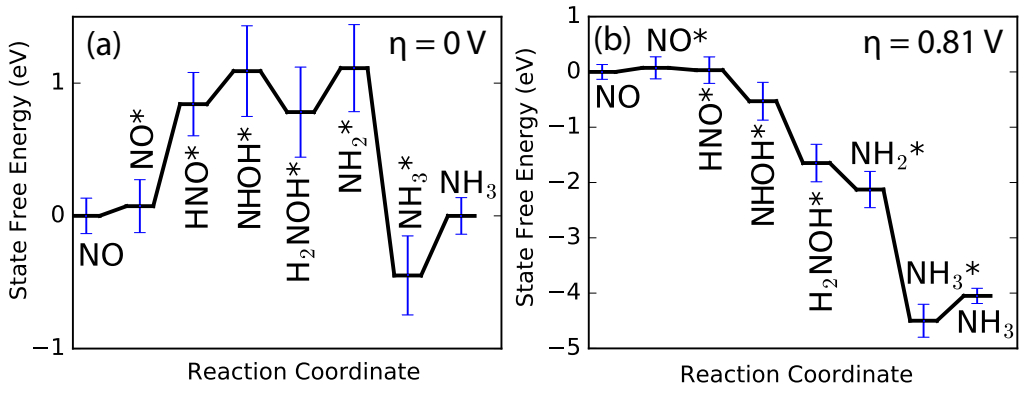

Figure 4.7: Free energy diagram for NO reduction to NH_3 at an overpotential (η) of zero (a) and at the overpotential due to the valence band edge ($\eta = 0.81$ V) (b). The equilibrium potential ($\eta = 0$) is computed to be 0.59 V (0.71 V experimentally). The blue error bars represent one standard deviation of the BEEF-vdW energy ensemble. Adsorbed states are labeled

TiO_2 is beyond the scope of this work, but selectivity should be considered in future studies of NO reduction.

Experimentally, titania photocatalysts have been reported to reduce nitrates under aqueous conditions, although selectivity to dinitrogen vs. ammonia varies widely based on preparation conditions and metal dopants [296, 297, 295, 298, 108, 299]. Contrarily, oxidation of ammonia has also been reported for TiO_2 photocatalysts [300, 301, 302], as well as simultaneous reduction of nitrate and oxidation of ammonium to N_2 [302]. Furthermore, the observation of hydrazine as a product from TiO_2 nitrogen photofixation is not explained by this mechanism [134]. These conflicting results suggest that other hypotheses should also be considered. In particular, the formation of hydrazine should be examined more closely to determine if hydrazine could be formed through recombination of NH_x species (consistent with the oxidative pathway) or if it is formed associatively (consistent with the reductive pathway). Isotopic scrambling experiments [303] and use of photoelectrochemical applied bias experiments may provide insight into this outstanding question.

4.5 Conclusions

The hypothesis that any of the sites on stoichiometric rutile (110) are the active site for nitrogen reduction was shown to be false based on the results of BEEF-vdW DFT calculations for both the associative and dissociative mechanism, although the associative mechanism was found to be considerably more thermodynamically favorable. The revised hypothesis that oxygen vacancies are active sites was shown to be more plausible, and a significant stabilization of NH_x by O-br vacancies was found. Yet, the predicted thermodynamic barriers are considerably higher than the conduction band edge, and the defects are not predicted to be thermodynamically stable under operating conditions, leading to the conclusion that this hypothesis is also improbable. However, the results indicate that N-N bond cleavage is thermodynamically facile on rutile (110) through an oxidative pathway, particularly with the strong oxidative driving force provided by photogenerated holes. Based on this finding, the hypothesis of an oxidized NO* intermediate in nitrogen reduction is introduced as a possible mechanism for photocatalytic nitrogen fixation on rutile (110). This chapter provides initial molecular-scale insight into the mechanisms that underly photocatalytic nitrogen fixation on TiO_2 by conclusively eliminating several possible explanations for this important process and identifying a novel hypothesis of indirect reduction through an oxidized intermediate.

CHAPTER 5

DOPANTS FOR THE PROMOTION OF N_2 FIXATION ON RUTILE (110)

One of the greatest problems for researchers studying this catalyst is the state of the literature. The literature on nitrogen photofixation on TiO_2 is enormously inconsistent in terms of synthesis methods, and observed products. Various dopants added to TiO_2 to improve its activity, among them are C [304], N [81], Fe [71], and V [305]. The presence of the rutile crystal phase and iron dopants were found to be critical for enhancing nitrogen reduction activity by some authors, while most do not attempt to detect them [71, 141, 132, 133]. These iron dopants have been proposed to promote the formation of rutile domains [71], and/or enhance separation of charge carriers by acting as an electron sink [133]. While the exact role is not known, the prevailing hypothesis is that Fe is not part of the active site based on the observation that excess Fe content reduces catalytic activity [133].

In this Chapter, we examine the role of metal doping in the promotion of N_2 fixation on TiO_2. Rutile TiO_2 (110) is chosen as a model surface based on the experimentally observed correlation between rutile content and reaction rates for photocatalytic nitrogen fixation [71]. Additionally, there is a rich literature on the surface science of rutile (110) [77, 291, 100, 92], and recent surface-science experiments and DFT calculations indicate that carbon substitution defects on the rutile (110) surface are active for photocatalytic nitrogen reduction. From this model surface, slabs containing metal dopants at the surface formally in the 2+ and 4+ oxidation states are generated for each dopant metal. It should be noted that these oxidation states may not represent the true oxidation state of each site, but rather represent the oxidation state the site would take on if all Ti metal atoms retained the 4+ oxidation state. In total, all d-block transition-metals, except Mn (23 total), are screened for their surface metal substitution energy and activity for nitrogen reduction. The binding energies of N_2H and NH_2 have been identified as descriptors for activity in the literature as

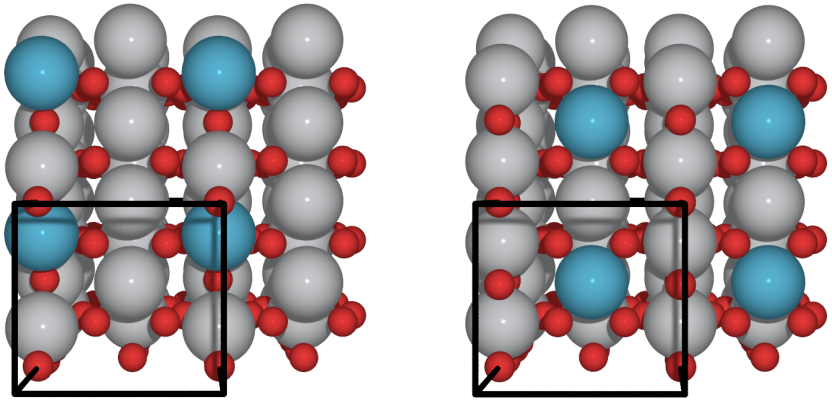

Figure 5.1: An example of the screened 2+ (left) and 4+ (right) slabs. For 2+ sites the substituent metal has replaced a 6 fold Ti atom (seen in blue) and a bridging oxygen vacancy has been formed to allow the metal to enter the 2+ oxidation state. For 4+ sites the substituent metal has replaced a 5 fold Ti atom (seen in blue) resulting in a 4+ formal oxidation state.

they are typically involved in the rate-limiting steps [107, 281]. Thus, these energies have been calculated to assess the activity of generated surfaces. Full details of the calculation methodology are in the Methods section (Sec. 3).

5.1 Trends In Active Site Formation Energies

The stability of substituted metal surface sites is examined with respect to the position of their *d*-band center. In Figure 5.2a, the metal substitution energy of the studied active sites has been plotted against the location of the *d*-band center of the corresponding transition-metal. The pure metallic form is the reference for the metal substitution energy of each metal substituted site. The *d*-band centers are calculated from the metallic bulk state rather than the single atom [306]. The plot indicates there is a strong correlation between the *d*-band center and metal substitution energy of the metal substitution (R^2 = 0.91 and 0.79 for 4+ and 2+ respectively.) It should be noted that the use of the d-band center as a descriptor is not meant to imply the anything about the band structure of the studied materials. We the speculate that the observed correlation is related to the *d*-band model of chemical bonding

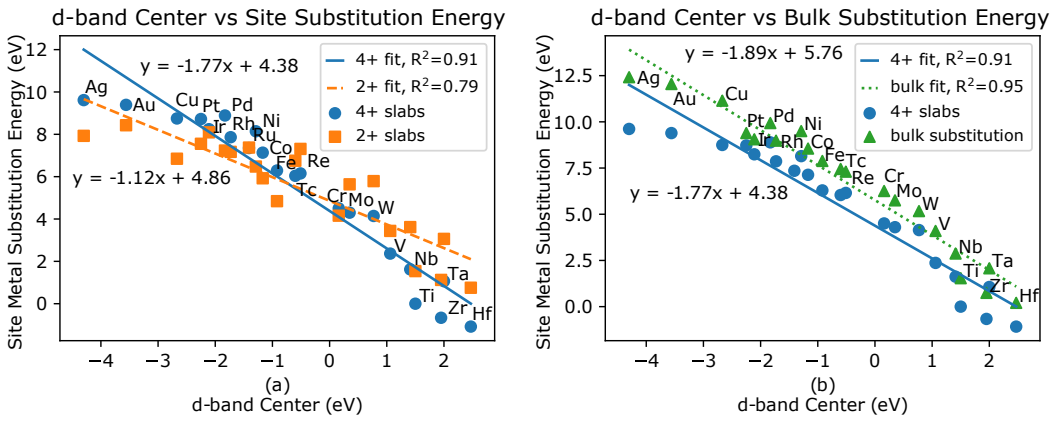

Figure 5.2: (a) The metal substitution energy of 4+ surface sites (blue) and 2+ surface sites (orange) with respect to their bulk metallic state vs. the metallic *d*-band center (b) The metal substitution energy of 4+ surface sites (blue) and bulk substitutions (green) with respect to their bulk metallic state vs. the metallic *d*-band center. *d*-band centers were obtained from Ref. 306. Only metals whose *d*-band center was previously reported in Ref. 306 are included.

[307, 308] summarized in Equation 5.1 below:

$$\Delta E_d = \int^{E_F} E(\rho'(E) - \rho(E))dE \tag{5.1}$$

where ΔE_d is the binding energy associated with interaction with the *d*-band, E_F is the Fermi level energy, $\rho(E)$ is the *d*-band density of states before adsorption, and $\rho'(E)$ is the density of states after adsorption. The interaction between adsorbates and the metal *s*-states are assumed to be approximately constant for all metals, such that variations in binding energies are controlled primarily through bonding interactions with the *d*-band. Interaction with the *d*-band causes the orbitals of the adsorbate to separate into bonding and anti-bonding orbitals. As the *d*-band center approaches the Fermi-level, the anti-bonding orbitals increasingly fill, leading to a weaker bond.

Our system involves a metal atom interacting with an oxide surface rather than an adsorbate binding to the metal surface. We hypothesize that the *d*-orbitals of the integrated metal atom interact with the *p*-orbitals of oxygen atoms in the surface similar to the way a metal surface interacts with adsorbing oxygen atoms. This explanation is consistent with the ob-

servation that the interaction weakens from left to right on the periodic table, as predicted in the literature [309]. This trend implies that the metals most able to integrate into a surface are those with the most favorable interaction with oxygen. A similar relationship has been reported previously for doped rutile oxides [310] and oxide-supported single-atom catalysts [311]. Other reports suggest that the electronegativity of the substituted metal is the relevant descriptor predicting stability [312]. The electronegativity is also correlated with the metal substitution energy (R^2=0.81 and 0.62 for 2+ and 4+ respectively, see Fig. 5.3), but not as strong as the correlation with the *d*-band center of the metal (R^2=0.79 and 0.91, see Figure 5.2). The fact that both of these quantities correlate with the metal substitution energy is not surprising, as a lower energy *d*-center indicates a more favorable addition of electrons, which is similar to the concept of electronegativity. The main exceptions to this trend are Ti, Zr, Hf, and Ag. The first three can be rationalized easily since all three lie in the same column of the periodic table, which is the same as the host metal, Ti. The improved stability of substituent metals within the group lines up with the chemical intuition since these elements have the same number of valence *d* electrons. This chemical similarity affords approximately 1.5 eV of improved stability relative to the trend. The final outlier, Ag, is more difficult to explain. However, the *d*-band center of Ag is itself an outlier for its position on the periodic table. This deviation may indicate that more complex bonding interactions are involved that are not easily described by the *d*-band model.

These results have implications for the relative stability of single-atom sites over surface metal clusters or bulk substitutions in TiO_2, and will relate to the feasibility of synthesizing metal-doped surfaces experimentally. We note that many of the metal substitution energies are exceedingly high (up to 10 eV) indicating that many of these surface sites are unlikely to be synthesized experimentally. Some elements (Y, Sc, Zr, Hf) favor integration into the surface structure rather than the formation of surface metal clusters (see Table 7.2 and 7.2). Conversely, noble metals such as Rh and Pt do not integrate into the surface favorably and will tend to form surface nano-clusters. This result agrees with TEM measurements

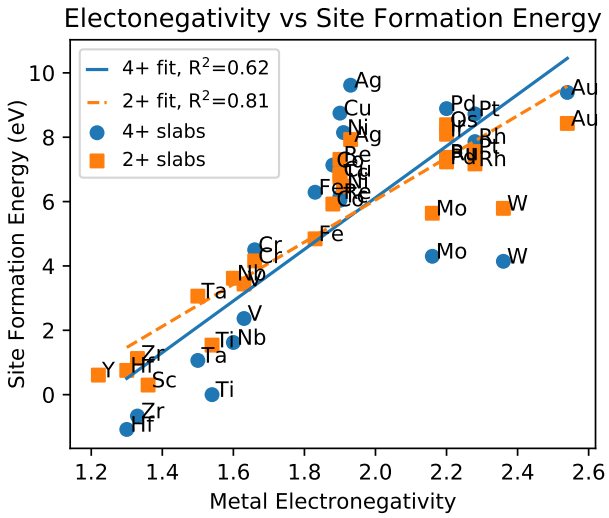

Figure 5.3: Electronegativity vs metal substitution energy of 2+ dopant site

in the experimental literature, indicating that clusters of metals such as platinum, silver, gold, nickel, rhodium form on a TiO_2 surface [313, 314, 315, 316] and rutile's reputation as a support [317]. A metal's ability to form surface sites is also dependent on the relative stability of bulk substitution, since a dopant that is more stable in the bulk than the surface will tend to segregate into the bulk rather than forming surface sites. Figure 5.2b shows that the 4+ surface sites are more stable than the bulk substitutions for all metals studied. The relative stability of surface sites relative to bulk integration suggests that bulk synthesis techniques such as co-precipitation should lead to a concentration of surface sites that exceeds the concentration of bulk sites for all metals considered. The correlation between the bulk formation energies of dopant metals and their corresponding 4+ surface sites (Figure 5.2b) is also striking, indicating that bulk and surface integration are controlled by similar electronic structure interactions.

Figure 5.2a also indicates that the oxidation state of the surface site that forms is dependent on the energy of the substituent metal's *d*-band center. Elements with more negative *d*-band centers tend to favor forming 2+ surface sites, whereas more positive *d*-band centers favor 4+ sites, with the cross-over point being approximately 0.8eV below the Fermi-level. This trend makes intuitive sense, as a more negative *d*-band center implies that the addition

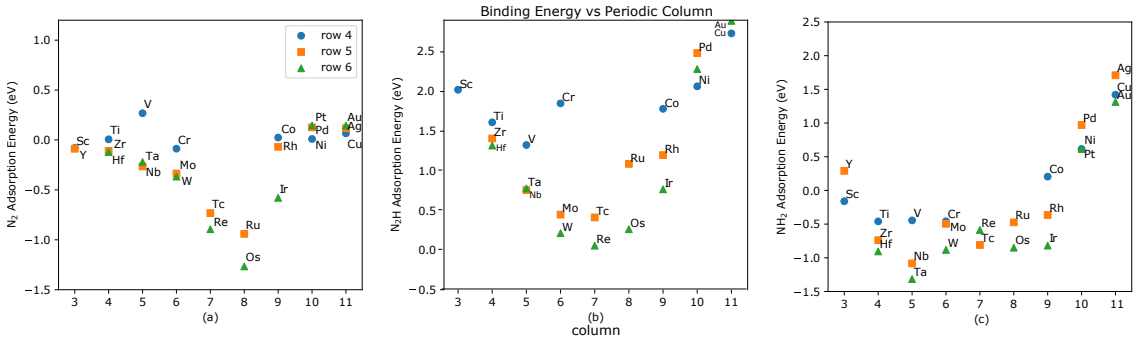

Figure 5.4: The binding energies of (a) N_2, (b) N_2H and (c) NH_2 plotted against the periodic column for 2+ metal substituent sites

of electrons is more favorable, making the more negative oxidation state more stable. For most metals studied, the 2+ site is either more stable or nearly as stable, suggesting that the 2+ substitutions are generally more favorable. An alternative interpretation is that the inclusion of metal dopants favors the formation of surface oxygen vacancies, since the 2+ site involves an oxygen vacancy. The reactivity of oxygen vacancies is typically greater than the pristine surface, so promoting oxygen vacancy formation may be yet another indirect mechanism through which metal dopants affect catalytic activity.

5.2 Trends In Nitrogen Adsorption and Cohesive Energies

The adsorption of the inert N_2 molecule is required for nitrogen fixation, and the first hydrogenation to N_2H is known to be the potential-limiting step on pure TiO_2. In addition, the $NH_2 \rightarrow NH_3$ reaction has been identified as potential limiting on some materials [107]. This suggests that the trends in N_2, N_2H, and NH_2 binding will provide an indication of a metal's ability to promote nitrogen reduction. The N_2 and N_2H energies are calculated for both 2+ and 4+ slabs to screen the surface's ability to reduce N_2. The N_2H binding energy is $>$1.5eV for all 4+ sites (see Table 7.2), therefore the subsequent analysis focuses exclusively on 2+ sites.

The results for N_2, N_2H, and NH_2 adsorption on 2+ sites as a function of periodic table group are shown in Figure 5.4. The results differ from the typical linear correlation that

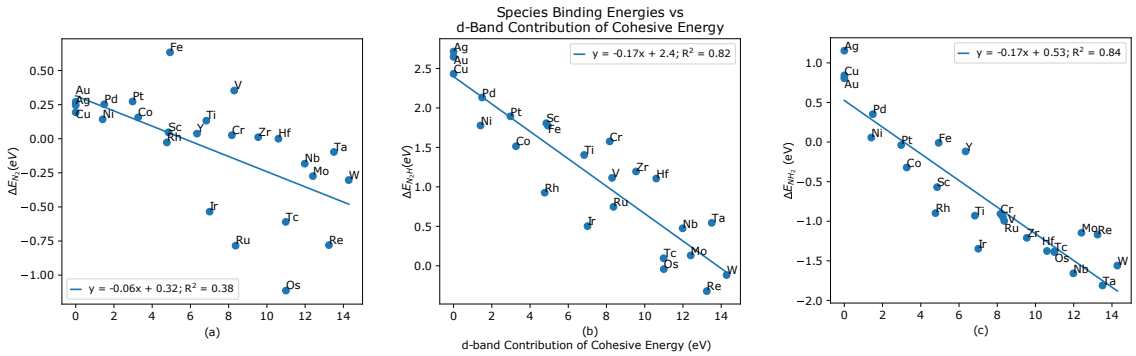

Figure 5.5: The *d*-band contribution to cohesive energies vs. the binding energies of (a) N_2, (b) N_2H, (c) NH_2 for 2+ metal substituent sites. The *d*-band cohesive energy contributions obtained from Turchanin and Agraval [318]

we expect from the *d*-band model [308], and instead, show relatively quadratic behavior with a maximum near the middle of the *d*-block at Os and Re for N_2 and N_2H respectively. Similar results are found for NH_2 adsorption (Figure 5.4c), though the magnitude of the adsorption energy varies, and there is small upward trend near the middle of the *d*-block.

While the N_2, N_2H, and NH_2 binding observed deviates from the near-linear correlation expected from the *d*-band model, we find a linear correlation between the binding energies and the *d*-band contributions of the cohesive energies of the corresponding bulk systems (Figure 5.5) although the correlation is relatively weak in the case of N_2. Cohesive energy is defined as the change in energy associated with isolated, neutrally charged atoms being brought together to form a bulk material [319]. A metal's cohesive energy is made up of a *d* contribution and a *s* contribution (Eq. 5.2). Cohesive energies have generally been a measure of the "bulk-nobleness" of a metal [307], with higher cohesive energies correlating to a more noble character. The metals with the highest "bulk-nobleness" are in the center of the *d*-block and resist corrosion due to the difficulty of breaking their strong metal-metal bonds. In our case, the inverse is true: the stronger the metal-metal bonds of the bulk material, the stronger the interaction between the metal and a given nitrogen species.

$$E_{coh} = \epsilon_d + \epsilon_s \tag{5.2}$$

where E_{coh} is the total cohesive energy, ϵ_d is the *d* contribution and ϵ_s is the *s* contribution.

The correlation between *d*-band contribution to cohesive energy and binding is the strongest for N_2H and NH_2 (Figure 5.5b-c). These two species show a relatively strong quadratic dependence (Figure 5.4b-c) suggesting that the bonding of nitrogen species to these substituent metals is similar to that of forming metal-metal bonds of the original bulk material. Thus, we hypothesize that the physics of nitrogen bonding to these substituent sites is similar to the bonding between single metal atoms and a bulk metal. A similar quadratic trend is seen for N_2 adsorption in Figure 5.5a, though there are several outliers near the middle of the *d*-block (Tc, Ru, Re, Os, Ir) that bind N_2 substantially stronger than predicted by the cohesive energy descriptor. The origin of this anomalously-high reactivity toward N_2 is not clear, though we note that the bonding mechanism changes between physisorption for early/late metals and chemisorption for more reactive metals, indicating that the quadratic trend may still hold for chemisorption.

The trends observed for site metal substitution energy (Figure 5.2) and nitrogen compound adsorption energy (Figure 5.5) differ qualitatively from trends observed in bulk metals. For single transition-metal dopant atoms, the *d*-band center controls metal substitution energy, while the cohesive energy controls adsorption energy. In bulk metals the inverse is true: the d-band center controls a material's ability to bind gas-phase species, whereas the cohesive energy controls how stable the material is [307]. This suggests that the origins of scaling relations for single-atom catalysts or dopant sites may differ from the case of bulk metals. However, the trend does not seem to hold in the case of 4+ sites (see Table 7.2), and prior work suggests that adsorption energy oxygen is correlated to the *d*-band center [309], so the trend is not general. The implication of different factors controlling the scaling relations of different adsorbates is that these adsorbates will also not scale with each other. This suggests that single metal atoms or dopants may be able to "break" the scaling relations between adsorbates and reach more active regions of the catalytic phase space [320, 321].

5.3 The Role of Iron Dopants

Many experimental studies have noted that iron dopants significantly increase the nitrogen photofixation rates [71, 141, 132, 133]. Iron dopants may affect catalyst activity through effects in the bulk or on the surface chemistry. In the bulk, iron has been shown to improve charge separation, reducing recombination of electron-hole pairs. This charge separation enhancement has been suggested to be the dominant effect of iron dopants for photocatalytic nitrogen fixation on titania [133]. Alternatively, an iron substitution at the surface may stabilize the states along the reductive pathway, directly improving the energetics of the process. The latter hypothesis was tested by computing the energetics of the associative mechanism on a slab with an iron substitution defect. Two defects were considered, an Fe^{4+} defect arising from direct substitution of the 5-fold Ti atom, and an Fe^{2+} defect formed by substitution of a Ti atom beneath a bridging O and removal of the bridging O, effectively forming a O-br defect and Fe substitution (see Fig. 5.1). The Fe^{2+} defect was found to be more stable, and Figure 5.6 shows the energetics of the associative pathway with an iron-substituted rutile (110) surface . This mechanism is very similar to the mechanism on the pristine and O-br vacancies, with the slight difference that N-NH_2 is more stable than HNNH on the Fe defect. The limiting potential of 2.2 eV is comparable to that of the defected surface in Figure 4.4 (1.7 eV), but is slightly higher due to the stronger adsorption of N_2. The energetics of the associative pathway on Fe-substitution defects are compared directly to O-br defects and pristine rutile (110) in Figure 4.5a, illustrating that the Fe-substitution defect has a similar effect to the O-br vacancy. The energy required to form this defect was calculated to be 1.1 eV relative to bulk rutile and BCC iron. This moderate metal substitution energy is lower than that of the O-br defect, and N_2 adsorbs with a relatively strong binding energy of -0.5 eV. This suggests that Fe surface defects promote the formation of O-br vacancies and adsorption of N_2. Nonetheless, the high limiting potential of 2.2 V indicates that the Fe-substitution defect is not active for photocatalytic

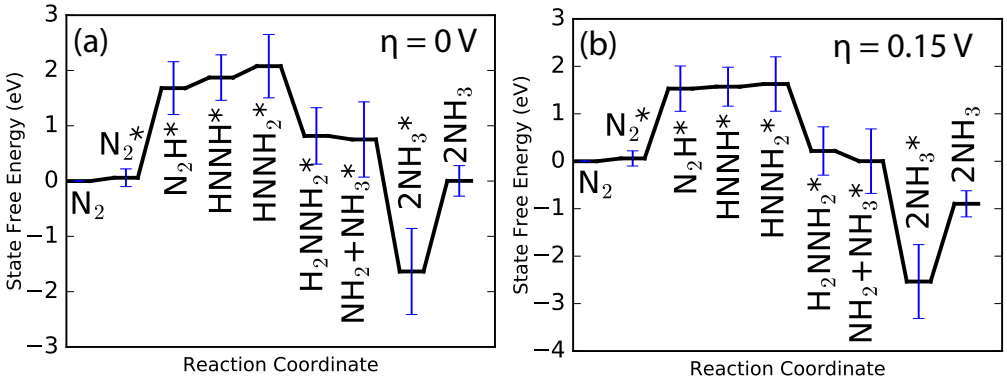

Figure 5.6: Free energy diagram for associative nitrogen reduction at an iron substitution site at an overpotential (η) of zero (a) and at the overpotential due to the conduction band edge ($\eta = 0.15$ V) (b). The equilibrium potential ($\eta = 0$) is computed to be 0.008 V (0.05 V experimentally). The blue error bars represent one standard deviation of the BEEF-vdW energy ensemble. Adsorbed states are labeled.

nitrogen reduction.

It has been noted in the literature that iron contaminates tend to promote nitrogen fixation [141]. Thus, we have closely examined the role of iron on the rutile 110 surface. Iron catalysts are known to activate the N-N bond in the Haber-Bosch process [282, 285], suggesting that the Fe site may play a role, and Hirakawa et al. [59] have hypothesized that direct N-N bond scission at O-br vacancies is the mechanism for photocatalytic nitrogen fixation. The energetics of the dissociative pathway for both Fe-substitution and O-br vacancy defects are compared with the energetics of the pristine surface in Figure 4.5b. The results show that the Fe-substitution has a relatively small effect on the thermodynamics of N-N bond scission, although a more pronounced effect is seen for NH* intermediates that are stabilized by $>$1 eV. The O-br vacancies have a much larger effect on N-N bond scission, stabilizing adsorbed N* by $>$2 eV per adsorbate. However, the thermodynamic barrier of $\approx$ 4 eV is still prohibitive at ambient conditions, and significantly higher than the 1.21 V thermodynamic limiting potential needed for the associative mechanism at the O-br vacancy.

5.4 Trends in Catalytic Activity for Nitrogen Reduction

The photocatalytic activity of doped TiO_2 surfaces can be assessed by computing the maximum thermodynamic barrier with electrons at the conduction band edge potential, while the electrocatalytic activity of doped TiO_2 surfaces can be assessed by computing the thermodynamic limiting potential [272, 312]. The computational hydrogen electrode (CHE) provides a route to computing the thermochemical potential of electrons at the TiO_2 surface (Sec. 3.4), and the resulting analysis provides only a thermodynamic picture of the reaction pathway. This analysis establishes a lower bound on the kinetics and correlates well with experimental trends in the literature [61].

Computing the maximum barrier or limiting potential requires the free energies of each state along a given reaction pathway. The full thermodynamics of the N_2 reduction reaction pathways on all 2+ sites were calculated, allowing the generation of free energy diagrams for all possible reaction pathways . Höskuldsson et al. [107] also previously found strong scaling relations between the binding of nitrogen compounds and the N_2H binding energy for rutile metal oxides. The binding energies of all species are fit to linear scaling relations with N_2H and NH_2 as descriptors to assess the scaling relations for this system (Figure 5.7). The scaling relations have a root mean squared error on the order of 0.2 eV, consistent with general scaling relations for other reactions [322]. The N_2H and NH_2 were also used to fit scaling relationships for all electrochemical steps, yielding similar accuracy to scaling relations for individual species (Figure 5.8). These scaling relations directly predicting reaction energies are used for subsequent analyses.

A primary consideration when assessing the electrocatalytic activity of a surface is the largest thermochemical barrier. Thermochemical steps do not involve electron transfers, so they are not considered when computing the limiting potential. However, they may still present a substantial barrier that will affect the overall rate. The largest thermochemical barriers for each surface can be seen in Table A5. The three steps with significant thermo-

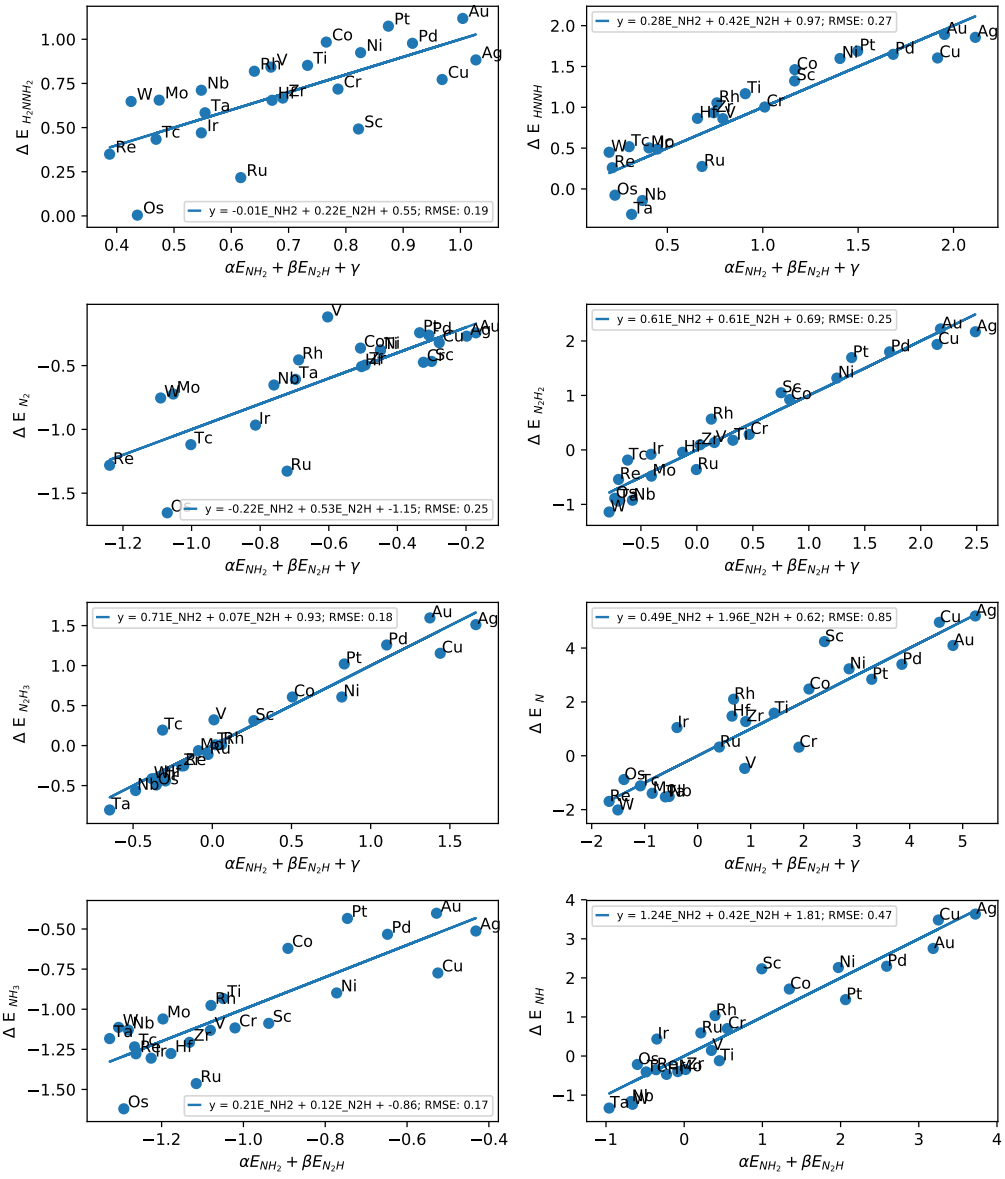

Figure 5.7: The calculated scaling relations between the binding energies of various species and the binding energies of N_2H and NH_2 on 2+ dopant sites

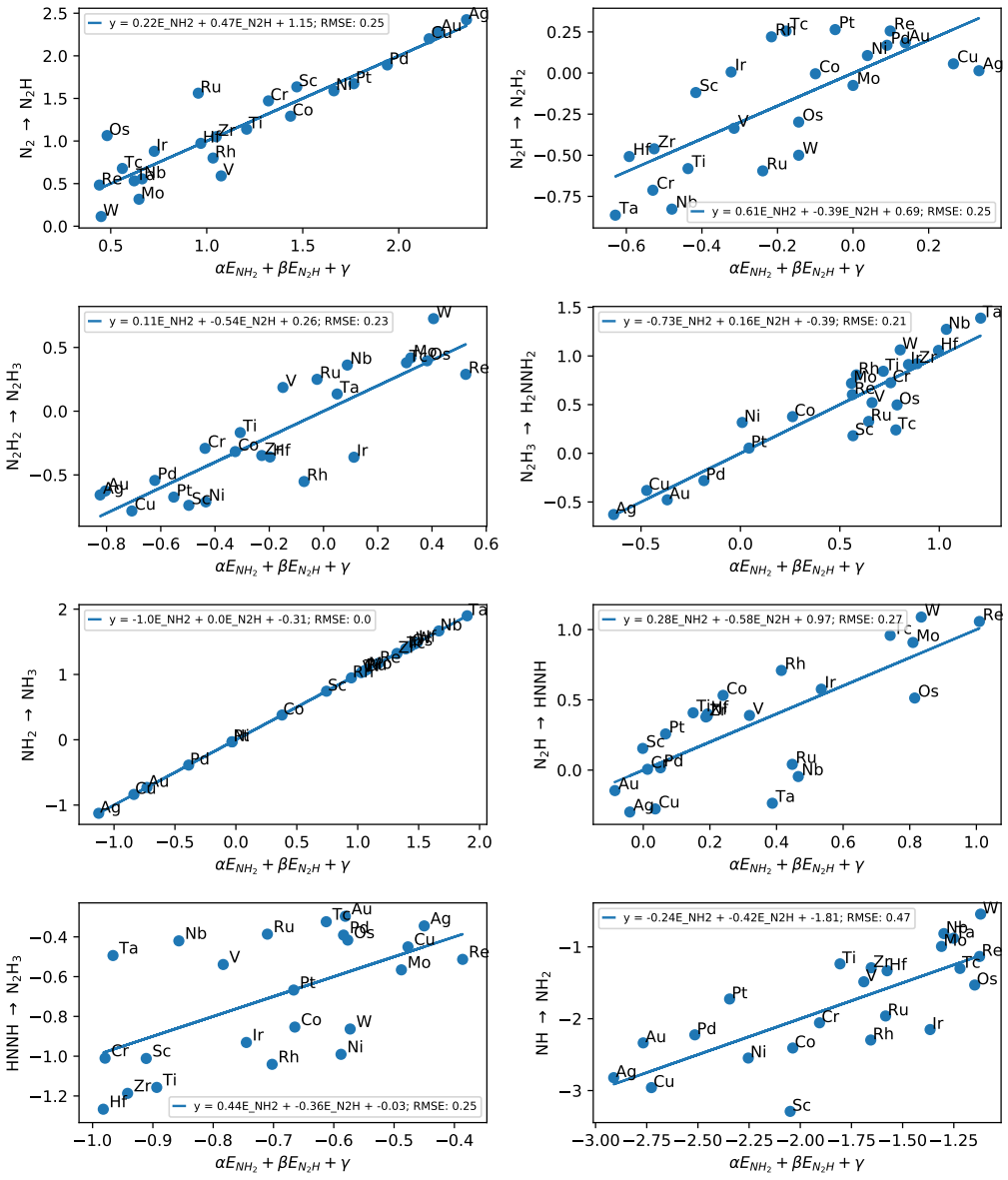

Figure 5.8: The calculated scaling relations between the reaction energies energies of all electrochemical reations and the binding energies of N_2H and NH_2 on 2+ dopant sites

chemical barriers are N_2 adsorption, NH_2-NH_2 scission, and NH_3 desorption. For the case of the most promising dopant, Mo, the adsorption of N_2 is exergonic by -0.27 eV, which is large enough to yield reasonable to N_2* coverages. However, competitive adsorption with H_2O and O_2 have not been considered. Moreover, there is a substantial thermochemical barrier of 0.83 eV for NH_3 desorption. Desorption of NH_3 is the thermochemical limiting step for most dopants, suggesting that NH_3 may exist at high coverages or even poison the surface. However, solvation effects have been neglected, and the free energy is computed at a chemical potential of NH_3 equivalent to 1 bar, suggesting that NH_3 desorption may not be limiting in aqueous solutions with low NH_3 concentrations. Some of the noble dopants (Pd, Ag, Au, and Cu) also show substantial thermochemical barriers of 0.5-1.5 eV for NH_2-NH_2 scission, indicating that rates for these metals will be low even at the limiting potential. A more detailed kinetic analysis of both electrochemical and thermochemical activation energies is required to predict the electrocatalytic rate for any dopant, but this thermochemical analysis provides lower bound for the kinetic barrier.

We assess the ability of dopant metals to improve photocatalytic nitrogen reduction. This is calculated based on the largest thermodynamic barrier at a reductive potential equal to the conduction band edge of TiO_2 (approximately -0.15 V vs. RHE [274]). This approach assumes that the conduction band edge of TiO_2 is not significantly affected by the presence of the dopant, and neglects improvements in other photochemical properties such as introduction of defect levels, charge separation or carrier lifetime. Nonetheless, it provides a good starting point for assessing the impact of dopant metals on the surface catalytic properties. The highest thermodynamic barrier for the best reaction pathway is plotted vs. the NH_2* binding energy in Figure 5.9. The results are qualitatively similar to the electrochemical limiting potentials in Figure 5.10, but there are some deviations that occur for two reasons. The first is that the photochemical analysis includes both thermochemical and electrochemical steps. The desorption of NH_3* is a thermochemical step that becomes rate-limiting for reactive surfaces. For less reactive surfaces the electrochemical step of N_2

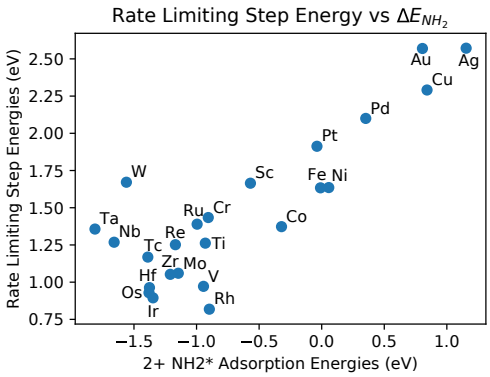

Figure 5.9: The highest barrier observed vs the NH_2 binding energy with the potential set to band edge of rutile. The data for this plot can be seen in Table S5. Any surface for which a full path was not available has been excluded.

hydrogenation is rate-limiting, which becomes slightly more favorable under the applied bias, effectively shifting the right side of the volcano downward. The second reason for deviation is that multi-electron transfers are less sensitive to small potentials, so dopants such as Re which have relatively unstable $N_2H_{x>2}$ states are not as favorable under photocatalytic conditions. Overall, the results predict minimum thermodynamic barriers of 1.06 eV, 0.97 eV, 0.96 eV, 0.90 eV, 0.82 eV, for Mo, V, Hf, Ir, and Rh, respectively. This represents a substantial improvement over the 1.26 eV limiting potential for pure Ti, indicating that these metals may act as surface promoters for photocatalytic nitrogen reduction if kinetic barriers are low.

The electrochemical limiting potential is calculated for all surfaces to assess their ability to reduce N_2 under applied bias. The results are plotted against the NH_2 binding energy in Figure 5.10a. This plot reveals a clear volcano relationship between the NH_2 binding energy and the limiting potential. In contrast to prior work by Höskuldsson et al. [107] and Montoya et al. [281], we find that the NH_2 binding energy is a slightly more reliable descriptor than N_2H binding; however these quantities are linked by scaling relations, indicating that either descriptor will provide consistent trends. In this case, the limiting step shifts from NH_2 desorption on the left to N_2 hydrogenation on the right, with most dopants being limited by NH_2 desorption. This means that NH_2 adsorption energy directly controls

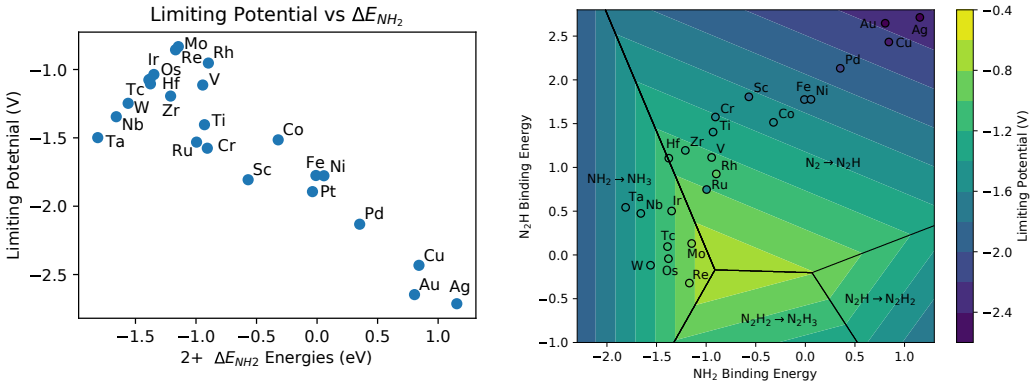

Figure 5.10: (a)The limting potential vs the NH_2 binding energy. (b) A two dimensional volcano plot for electrochemical limiting potential using N_2H and NH_2 as descriptors for the studied systems. Note that points are colored in with the limiting potential calculated from DFT, whereas they are positioned based on their predicted activity from scaling relations. Any surface for which a full path was not available has been excluded.

the reactive side of the volcano, and explains why it is an accurate descriptor in this case.

To better understand the relationship between the descriptors, limiting potential, and limiting steps, the fits of the scaling relations (see Figure 5.8) were used to generate a two dimensional volcano plot (Figure 5.10b). It should be noted that the points on this plot are filled in with their calculated limiting potential from DFT, but placed based on their predicted limiting potential from the scaling relations. As with the scaling relations, the root mean squared error of the predicted limiting potential in Figure 5.10b is roughly 0.2V. The results confirm the findings from Figure 5.10a, but provide additional insight into the limiting steps. The results also show that the optimal limiting potential is still relatively large ($\sim$-0.8 V), and that Mo is near-optimal. There are also a few dopants that deviate from the trend. Notably, Os, Ir, and Hf are on the reactive side of the volcano, but the potential limiting step is N_2H formation [107]. Nonetheless, these elements fortuitously fall close to the trend predicted by the volcano plot.

Overall, the results suggest that several dopants are capable of improving the performance over pure TiO_2. The elements that show significant improvement are Mo, Rh, and Re. Mo is relatively inexpensive and abundant, whereas Re and Rh are relatively scarce

[323]. Moreover, synthesis may be a challenge since the metal substitution energy of the surface sites is generally positive relative to the bulk metals (Figure 5.2). Nonetheless, the results indicate that Mo is the most promising dopant for reducing the thermodynamic limiting potential of ammonia synthesis on TiO_2. This is also interesting since Mo is known to play a role in biological nitrogen fixation [324], and Mo-based transition-metal complexes are known to reduce nitrogen in homogeneous catalysis [325].

Experimental observations can provide further insight into the computational predictions. Several prior reports have investigated transition-metal dopants for enhancing photocatalytic ammonia production on TiO_2 [71, 326, 59]. Interestingly, Schrauzer et al. report increases in ammonia yield in the presence of Mo dopants [71], though this report comes from the early literature and rigorous controls [145] or isotopic labeling studies [131] were not included. Moreover, the same report revealed enhanced rates for Fe and Ni, so the confirmation of the prediction regarding the former two should be treated with caution. The rate enhancement for noble metals such as Ru, Rh, and Pd is conflicting even in the early literature, with Schrauzer and Guth reporting no enhancement [71]. However, Ranjit et al. reported enhancement for all noble metals with the most significant improvement for Ru [326]. In all of these systems, the metal dopants were incorporated via co-precipitation, and catalysts were polycrystalline TiO_2, indicating that the metals may also enhance yields via charge separation, mediation of crystallization, or other mechanisms [28]. Hirakawa et al. added Ru, Pt, and Pd to pre-synthesized TiO_2 particles and reported no significant improvement in the reaction rates [59]. These experiments are more consistent with the computational model system used in this study since only surface properties are affected, and the results are consistent with the prediction that these noble metals will not improve the rate. However, further systematic and well-controlled experiments that characterize the state of the metal incorporation in the TiO_2 surface are required to validate the predicted trends.

5.5 Conclusions

The stability of metal dopant surface sites and their effects on the reaction thermodynamics of N_2 reduction on rutile (110) are studied using DFT. We find that the metal substitution energy of these doped surface states is strongly related to the location of the *d*-band center of the substituted metal, with a trend consistent with the *d*-band model. We also find a correlation between the cohesive energy of metals and their N_2H and NH_2 binding energy on the surface, suggesting that the bonding of nitrogen species is similar to that of bulk metals. Finally, we investigate the effects of dopant sites on the full reaction pathways for 2+ sites on all studied metals. We find a clear volcano relationship between NH_2 binding and both the electrochemical limiting potential and the highest thermodynamic barrier for photocatalytic reactions. The formation of Rh 2+ sites is proposed to yield a slight improvement of reaction rates in both electrocatalysis and photocatalysis. Other metals commonly used in catalysis, such as Pt and Pd are predicted to have a limited or detrimental effect on the surface catalytic properties of TiO_2 for nitrogen reduction. This suggests that the role of metal dopants in photocatalytic ammonia synthesis by TiO_2 is likely related to modifications of bulk properties in most cases. However, the existence of clear trends in the metal substitution energy and reactivity of single metal atom dopants toward nitrogen intermediates suggests that computational design of metal-doped oxide materials is a promising strategy for other oxide systems and/or other nitrogen conversion reactions.

CHAPTER 6

THE POSSIBLE ROLE OF ADVENTITIOUS CARBON

The prevailing hypothesis is that oxygen defects are the active sites for nitrogen fixation [59, 135, 327], based primarily on an observed correlation between oxygen defect density and ammonia yields [59, 135]. However, the alignment of the conduction band edge relative to the N_2/NH_3 redox couple provides a relatively small driving force equivalent to an overpotential of only 0.15 V. DFT calculations have shown that the bridging oxygen (O-br) vacancy of rutile (110) exhibits weak N_2 adsorption energy (0.2 eV uphill) and requires substantially larger overpotentials (>1.2 V) [107]. One alternative hypothesis is that oxidative processes drive nitrogen fixation due to the substantially larger electrochemical driving force from photo-generated holes [67]. However, adsorption of N_2 is still required, and nitrate products have rarely been reported [67]. This indicates that other mechanisms are likely involved. In this chapter we examine the role of adventitious surface carbon in photocatalytic nitrogen reduction. We use both near-ambient-pressure XPS (AP-XPS) and DFT calculations to demonstrate a plausible of role surface carbon in catalyzing this chemical reaction[1].

6.1 Near-Ambient-Pressure XPS

Direct insight into the nature of the active state of titania is obtained using AP-XPS experiments. A rutile (110) model surface is chosen based on the observation that ammonia yields correlate with the amount of rutile [134]. The experiments are conducted in the absence of light and with in situ illumination (Figure 6.2-6.1) with ultraviolet/visible light at a temperature of 200°C. The sample is exposed to 300 mTorr of N_2 both with and without

[1]The experiments in this chapter were performed by Yu-Hsuan Liu, Marm B. Dixit, Kelsey B. Hatzell, Yifan Ye, Ethan J. Crumlin, and Marta C. Hatzell

illumination. All X-ray photoelectron spectroscopy (XPS) experiments were performed at beamline 9.3.2 at the Advanced Light Source (ALS) at Lawrence Berkeley National Lab. The AP-XPS experiments were led by Dr. Marta Hatzell and her team. The sample TiO_2 rutile (110) (Princeton Scientific Corp. - Easton, Pa) was mounted using tantalum clips onto a ceramic button heater. Type K thermocouple wires were placed next to the sample to monitor the surface temperature. The spectra were collected (survey, C1, N1s, O1s, Ti2P and the valance band) at a photon energy of 630 eV. Surfaces were cleaned through slowly introducing oxygen (100 mTorr) into the chamber and annealing at 500°C for approximately 1-2 hours (time includes a ramping phase). Cleanliness was monitored through the C1s spectra. Samples were then cooled to a desired temperature (200 or 30°C). Cleaning was conducted for shorter periods of time when adventitious carbon was intentionally probed. The desired partial pressure of gas phase species (e.g. N_2 (300 mT), H_2O (100 mT), oxygen (100 mT) and/or CO_2 (100mT)) were introduced into the main chamber using leak valves, and equilibrated over a 15 minute period. For in situ illumination an Asahi Spectra (Torrance, CA) 300 W broadband light source was fixed to the viewing window. Initial experiments were conducted only in the presence of 300 mT N_2 (Figure 6.2). In these tests, light and dark conditions at various temperatures were probed. The C1s and N1s peaks with and without illumination for as-prepared samples are shown in Figure 6.4. The arbitrary units for the XPS are all incrementing by 20000 counts, and thus changes in peak height reflect the change in intensity of each peak. The N1s peak was between 3-5 at% of the survey scans.

The results for the as-prepared rutile (110) crystal (Figure 6.1a-b) indicate the emergence of a peak at 398 eV in the N1s spectrum upon illumination (Figure 6.1b). This value has previously been attributed to reduced nitrogen N_{red} (NH_3=398.8 eV) [328, 329, 330]. No changes in the binding energy of $Ti2P_{3/2}$ or $Ti2P_{1/2}$ are observed with the addition of N_{red} (Table A6-A9), indicating that the reduced nitrogen on the surface does not change the titania crystal structure through surface nitride formation [329]. Furthermore, repeated

experiments at lower temperatures of 35°C and 100°C (Figure 6.3) reveal that reduced nitrogen species remain on the surface in the dark at low temperatures, indicating that they are adsorbed.

The AP-XPS results also indicate that adventitious carbon is present on the sample (Figure 6.1a), a result typical for titania [331, 332]. However, oxygen vacancies are not detected, as evidenced by the sharp the Ti $2p_{3/2}$ peak (Figure 6.2) that indicates all Ti^{4+} sites are well-coordinated [333]. The adventitious carbon is removed from the sample by annealing at 500 °C in 100 mTorr O_2 for 90 minutes, resulting in a substantial reduction in the C1s peak intensity and likely oxidation of surface hydrocarbons. After this cleaning procedure the N1s peak is no longer detected upon illumination. To confirm that the disappearance of the photo-induced N1s peak is not due to annealing of oxygen defects. These results provide strong direct evidence of a photo-induced interaction between the titania surface and nitrogen.

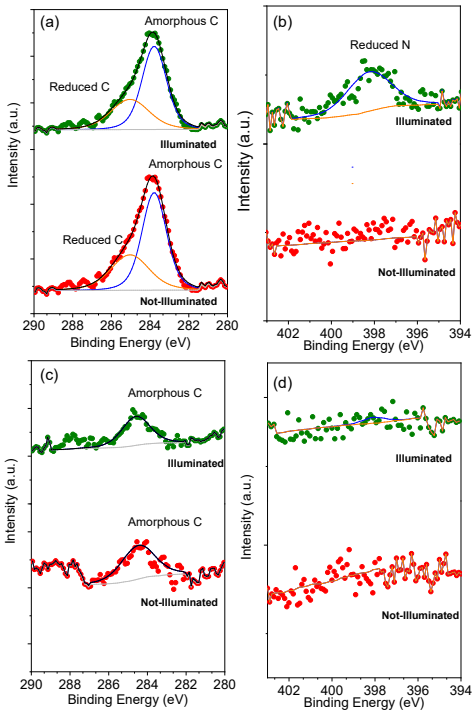

Figure 6.1: Results of in situ AP-XPS on rutile (110) single crystal with C1s (a,c) and N1s (b,d) peaks for the as-received (a-b) and cleaned (c-d) surfaces in the dark (red) and under visible illumination (green) when exposed to 300 mTorr nitrogen.

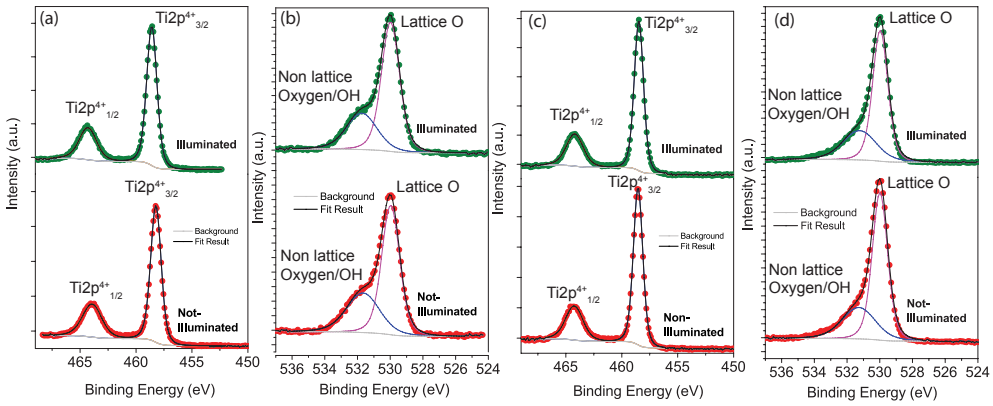

Figure 6.2: Results of in situ AP-XPS on rutile (110) single crystal with Ti2P (a,c) and O1s (b,d) peaks for the as-received (a-b) and cleaned (c-d) surfaces in the dark (red) and under visible illumination (green).

In a second set of experiments the effect of adventitious carbon and oxygen vacancies were probed. Initially an as-received single crystal was probed in 300 mT N_2 under illumination for an hour (Figure 6.3a). The sample was then pulled into a prep chamber, where oxygen vacancies were introduced through Ar+ sputtering in a preparation chamber, prior to being transferred into the main chamber (Figure 6.3b). Sputtering is also commonly used as an approach to clean the crystal surface. The sputtering did result in a decrease in amount of surface carbon (C1s); however, the presence of reduced nitrogen remained. This is likely due the strong binding of ammonia to the surfaces at low temperatures (near ambient). Typically, elevated temperatures and dilute acids are required to remove adsorbed ammonia. Oxygen vacancies can be noted through the presence of Ti^{3+} in the Ti2p region. Ti^{3+} are undercoordinated, due to the presence of the oxygen vacancy. In the presence of oxygen vacancies and less carbon, the resulting N_{red} peak was smaller than without oxygen vacancies. To add carbon back to the sample, the sample was exposed to 100 mT CO_2 for an hour, with the C1s peak monitored. Finally the addition of 100 mT H_2O healed the oxygen vacancies. Peak areas were quantified using Shirley background correction, which were fitted using a combined Gaussian/Lorentzian line shape.

In this second set of experiments sputtering the sample simultaneously removed a por-

tion of the adventitious carbon. The presence of oxygen vacancies is confirmed by the appearance a shoulder in the Ti2p spectra; however, the introduction of oxygen vacancies does not result in a greater reduced nitrogen peak (Figure 6.3). The addition of CO_2 resulted in increased C1s and N_{red} peaks (Figure 6.3), providing additional evidence of the interaction between surface carbon and nitrogen. This finding also indicates that oxygen vacancies may play an indirect role by favoring formation of surface carbon.

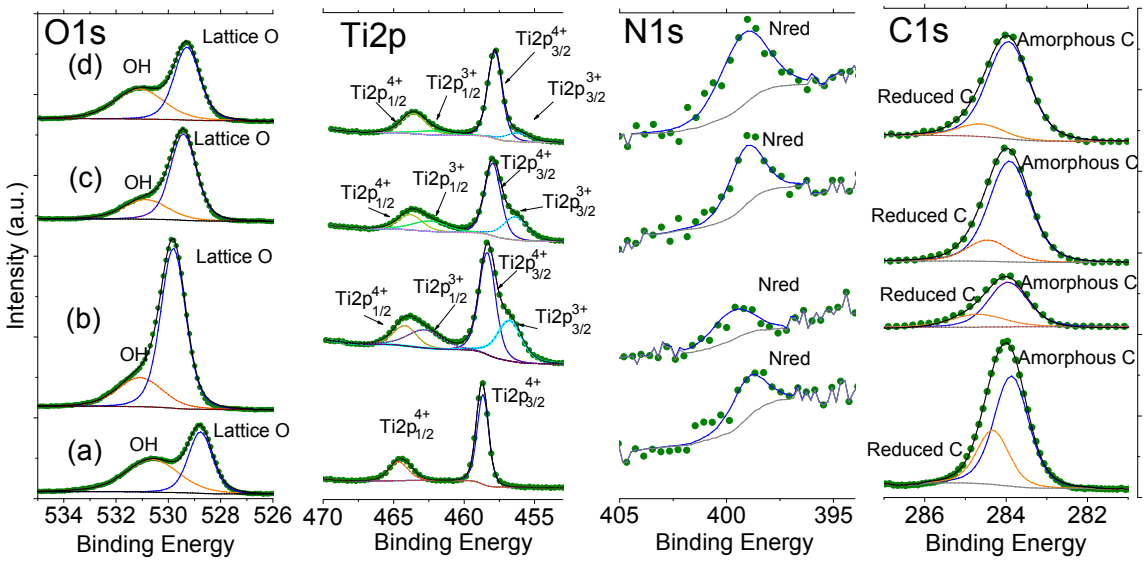

Figure 6.3: Results of in situ AP-XPS (O1s, Ti2P, N1s, C1s) on rutile (110) single crystal with adventitious carbon after 1 hr exposure to gas mixtures and light. Titania when exposed to 300 mT N_2 only (no oxygen vacancies) (a), Ar^+ sputtered titania with Ti^{3+} sites indicating the presence of oxygen vacancies and a reduction in adventitious carbon (b). Sputtered titania exposed to 100 mT CO_2 (increasing carbon) and 300 mT N_2 (c). Sputtered titania exposed to 100 mT CO_2, 100 mT H_2O and 300 mT N_2 (d).

6.2 Atomistic Modeling of Potential Carbon Active Sites

The atomic-scale structure of adventitious surface carbon is not well-defined [334], and an ensemble of active-site structures are likely to contribute. To address this challenge the N_2 binding energy and surface energy of a large swath of active sites are calculated using DFT with the BEEF-vdW functional. These sites include a range of oxygen/titanium defects and carbon additions/substitutions on the rutile TiO_2 (110) surface. The results, shown

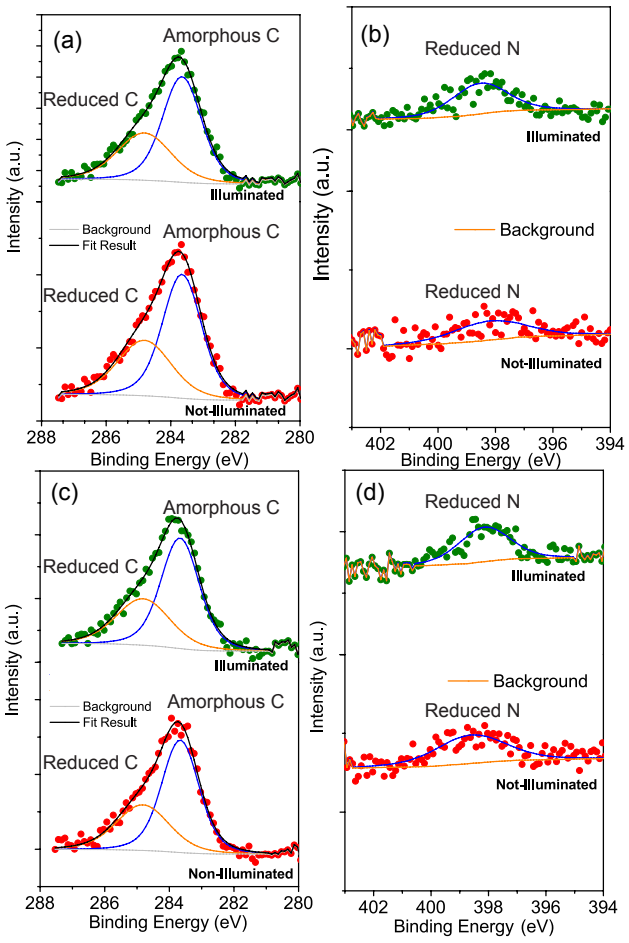

Figure 6.4: Results of in situ AP-XPS on rutile (110) single crystal with C1s (a,c) and N1s (b,d) peaks for the 100 °C (a-b) and 35 °C (c-d) surfaces in the dark (red) and under visible illumination (green).

in Figure 6.5, illustrate a tradeoff of reactivity and stability, where the most relevant sites exhibit maximum stability for a given N_2 adsorption energy [294].

There are several carbon-based active sites that exhibit remarkable N_2 adsorption free energies of $\sim$2 eV, providing further theoretical support for the hypothesis that adventitious carbon enables interaction between TiO_2 and N_2. In addition to strong binding, it is necessary that N_2 adsorption be selective against other reactants, that active sites are sufficiently stable to exist under reaction conditions, and that a catalytic mechanism for N-N bond scission exists. We select a single representative active site, a carbon substitution at a bridging oxygen (C*), as a model to investigate these issues.

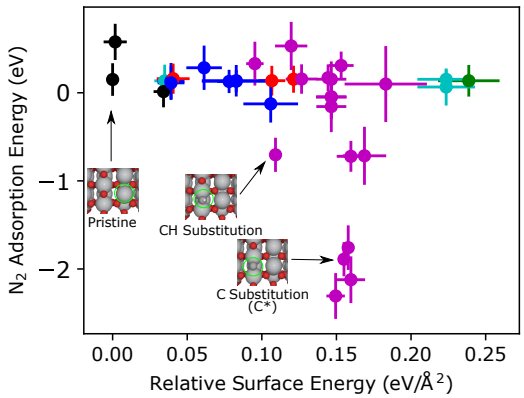

Figure 6.5: The surface formation energy of various surface models vs the adsorption energy of N_2 evaluated at 0V RHE relative to pristine rutile (110), bulk TiO_2, and graphite. Site classes include stoichiometric TiO_2 (black), O vacancies (blue), carbon additions (red), Ti additions (green), Ti addition and carbon (cyan) and O vacancies with carbon (magenta).

6.3 Competitve Binding of O_2 and N_2 on the C* Site

The C* site has a remarkably strong N_2 binding free energy of -1.89 eV, equivalent to the gas-phase analog of the reaction ($C+N_2 \rightarrow CN_2$). This equivalence indicates that the C* site acts as a surface-bound carbon radical, which is corroborated by 2 unpaired electrons in surface slab and a magnetic dipole of 1.56 μ_B on the C atom from bader spin analysis [335]. This reactive carbon radical can also interact with other species under reaction conditions. The presence of H_2O is required for proton formation via oxygen evolution, and O_2 is also present in many studies. The adsorption selectivity toward N_2 is assessed by computing the free energy of adsorption for H_2O and O_2 as a function of O_2 chemical potential at ambient temperature and pressure (300 K, 1 bar) and 100% humidity (Figure 6.6); the BEEF-vdW ensemble is used to propagate DFT error and compute surface coverage probabilities (see Equation 3.1). The results illustrate that N_2 adsorption is competitive within the error of DFT, and that N_2 adsorption will be favored by decreasing O_2 pressure. This is consistent with the observation that anaerobic conditions increase reaction rates [59]. These results support the hypothesis that C* and other carbon-based sites enable selective adsorption of N_2 at ambient conditions.

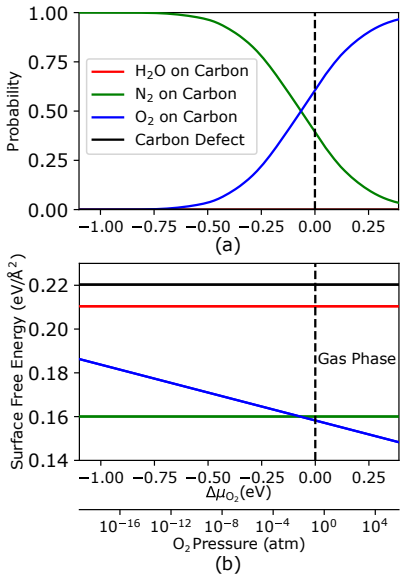

Figure 6.6: (a) The probability of each reactant species being dominant on the C* site based on uncertainty propagation from BEEF-vdW DFT calculations and (b) the surface energy of each reactant species at different O_2 chemical potentials. All chemical potentials are evaluated at 300K. The reference chemical potential (0 eV) corresponds to 0.2 atm of O_2, 0.8 atm of N_2, and 0.035 atm of H_2O (100 % RH).

6.4 Thermodynamics of N_2 Fixation on C* Sites

The carbon-based active sites show a clear trend toward strong N_2 adsorption, but are also relatively unstable (Figure 6.5), raising the question of whether they exist in a real system. The surface energies shown in Figure 6.5 are computed relative to graphite, one of the most stable forms of carbon. Adventitious surface carbon will be less stable, and likely consists of a variety of short-chain hydrocarbons and carbon oxides [334]. The photocatalyic activity of TiO_2 for hydrocarbon oxidation and CO_2 reduction is well-established [336, 337], suggesting that the carbon site may be formed by a photo-oxidation/reduction. Adventitious carbon has also been reported to play a role in photocatalytic CO_2 reduction [332], and hydrocarbon-based sacrificial reagents have been shown to increase ammonia yields [152, 338, 339]. We model the hydrocarbon influence by selecting CH_4 as a model hydrocarbon. Any alcohol or short-chain hydrocarbon on the surface will be thermodynamically easier to oxidize. The photochemical oxidation is modeled using the CHE [143], and an O-

br vacancy is used as the active site such that the adsorbed C* is equivalent to the bridging carbon substitution. The results show that photo-oxidation of CH_4 to the C* site is highly exothermic (Figure 6.7a) owing to the strong oxidative potential of photo-generated holes. This is clear from the band alignment of TiO_2 where there is a thermodynamic driving force of >1 eV even for the formation of gas-phase C atoms from CH_4. This is also consistent with experimental observation of CH_x surface species on including radicals on titania [340, 341, 342]. These findings provide strong evidence that the formation of metastable carbon active sites on titania is feasible under photocatalytic conditions.

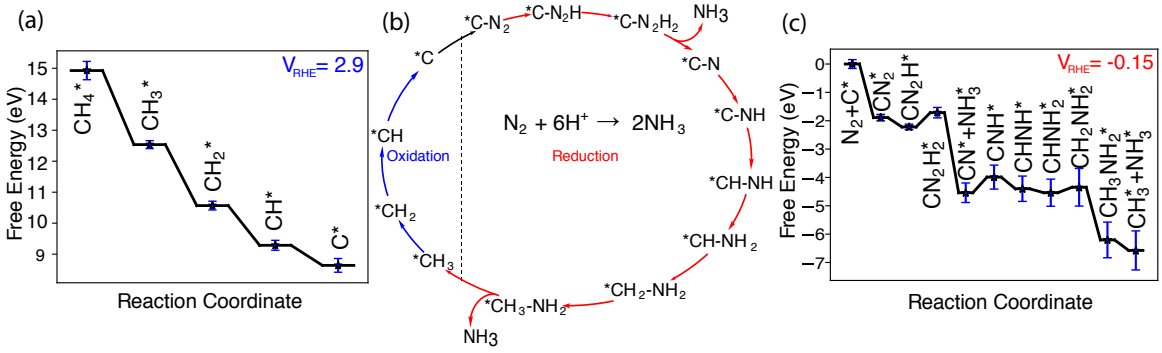

Figure 6.7: (a) The free energy diagram of the oxidative active site regeneration. The potential is set to that of oxidizing holes at the band edge of rutile TiO_2 (b) The thermodynamic cycle of N_2 reduction on a carbon substitution at a bridging oxygen (C*) on TiO_2. The path consists of a reductive portion (red) and an oxidative active site regeneration portion (blue). (c) The free energy diagram of the reductive ammonia production portion of the thermodynamic cycle. The potential is set to that of reducing electrons at the band edge of rutile TiO_2

Even after accounting for the relatively unstable nature of the carbon substitution site the N_2 adsorption free energy of -1.89 eV is remarkable, indicated by the fact that numerous other unstable carbon-based sites have considerably lower N_2 adsorption energies (Figure 6.5). The 1.56 μ_B magnetic dipole is quenched upon adsorption of N_2, similar to the mechanism reported for an FeN_3 active site on Fe-doped graphene [343]. This is also consistent with prior reports of carbon radicals at graphene edges interacting strongly with nitrogen under ball-milling conditions [344], and numerous reports of carbon-based catalysts for photocatalytic nitrogen fixation [28]. This indicates that the TiO_2 surface plays

an indirect role by forming and stabilizing radical carbon species. This mechanism may also be relevant for the wide range of other wide-band-gap semiconductors that have been reported as nitrogen fixation photocatalysts [28].

Finally, adsorption of N_2 is only the first step in the formation of ammonia; the challenge of dissociating the N-N bond still remains. The feasibility of the ammonia synthesis half-reaction on the C* site was mapped out following a range of possible reaction mechanisms (see SI). The CHE approximation is used, and only thermodynamics of intermediate states are considered. The most favorable route follows the distal mechanism of N-N bond scission [289], and exhibits a low thermodynamic barrier of 0.55 ± 0.12 eV with the potential-limiting step being the hydrogenation of CN* (Figure 6.7c). The formation of the second NH_3 requires hydrogenation of both the C and N in order to weaken the C-N bond (Figure A2-A3) resulting in a surface CH_3*, which must be regenerated via photo-oxidation in order to close the catalytic cycle (Figure 6.7b). While kinetic limitations have been neglected, the results show that carbon-based active sites provide a thermodynamically feasible route to photocatalytic nitrogen fixation on titania catalysts.

The proposed mechanism explains how photocatalytic reduction of nitrogen to ammonia can occur despite the relatively small reductive driving force from the TiO_2 conduction band edge. The oxidative potential of photo-generated holes is captured by the formation of meta-stable reactive carbon species that promote strong N_2 bonding and subsequent reduction via surface-bound CN_2H_x species. This is similar to the well-known role of photo-generated O_2^- and $OH^\cdot$ radicals in TiO_2 photo-oxidation [345].

The proposed hypothesis also explains numerous prior experimental observations and inconsistencies: rates correlate with oxygen vacancies because they promote the formation of reactive carbon sites, the rate of ammonia formation decreases with oxygen concentration due to poisoning of N_2 adsorption sites, and the wide range of experimentally-observed rates is due to the lack of effort to control or characterize carbon-based impurities on the catalyst surface or reaction environment.

6.5 Conclusions

In conclusion, a combination of AP-XPS experiments and DFT studies provide strong experimental and theoretical support for the hypothesis that adventitious surface carbon promotes photo-induced adsorption of N_2 at TiO_2 through the formation of meta-stable active sites by photo-oxidation of hydrocarbon species. The DFT results indicate that carbon-based sites interact strongly with N_2, and that subsequent reductive hydrogenation of CN_2 is a thermodynamically-feasible route to produce ammonia and regenerate the surface hydrocarbon. This hypothesis is consistent with prior reports of carbon radical formation [340, 341, 342], the role of surface carbon contaminants in photocatalysis [332], spin-mediated N_2 adsorption [343], and strong interactions between nitrogen and graphene edges [344]. The hypothesis is also consistent with a number of key observations in the nitrogen photofixation literature including the correlation of rate with oxygen vacancies [59, 135] and sacrificial reagents [152, 338, 339], the detrimental effect of gas-phase oxygen [59], and the large variations and inconsistencies in measured rates for catalysts that are nominally identical [140, 28, 59]. The findings indicate that careful characterization and control of surface carbon is critical to ensure reproducibility in photocatalytic nitrogen fixation on titania and other semiconductors, and suggest that engineering carbon-based active sites is a promising strategy for enhancing photocatalytic nitrogen fixation.

CHAPTER 7
CONCLUSIONS AND FUTURE WORK

7.1 Overview

Photocatalytic nitrogen fixation is a technology that can provide fertilizer to many communities where it is currently expensive or unavailable. In this thesis, we reviewed the literature on the surface chemistry of TiO_2, photocatalytic nitrogen fixation, and more recent literature on measurement and contamination effects in photoelectrochemical ammonia synthesis. We find that process has a long history but suffers from poor experimental design and issues with ammonia contamination and measurement. We have shown that the process of photocatalytic nitrogen fixation can be feasible technologically. We have demonstrated that such a technology could generate nitrogen-based fertilizer in a distributed way. While this technology is unlikely to replace Haber-Bosch entirely, it can have applications in areas with poor infrastructure and high levels of solar radiation. Additionally, we have proposed several possible forms of the technology, showing that remarkably low solar-to-chemical efficiencies are practical if separations are not required. Notably, the application of aerobic photocatalytic nitrogen fixation to produce fertigation water could provide a low capital cost solution to delivering fertilizer, removing costly separations.

In addition to laying out the technological prospects for photocatalytic nitrogen fixation, we have performed a theoretical analysis of the surface reaction on rutile TiO_2 (110). Utilizing the computation hydrogen electrode (CHE) approximation to simulate the contribution of photo-excited electrons and holes, we have shown that the pristine and oxygen vacant surfaces are not capable of catalyzing nitrogen reduction. On these surfaces, the reaction cannot proceed through the dissociative mechanism (see Figure 1.3), having barriers above 3 eV for all studied systems. Additionally, these surfaces cannot catalyze the reaction

through an associative mechanism, with the first hydrogenation reaction being rate-limiting and having a barrier over 1eV. We have also demonstrated that while nitrogen oxidation is thermodynamically feasible, the kinetic barriers may make the reaction untenable on pristine rutile (110). Thus, the rutile (110) surface appears to be inactive for nitrogen fixation under ambient conditions.

We have also performed a screening analysis of dopant metals on rutile (110). We find that the metal substitution energy of dopant sites on the surface is correlated to the transition metals' d-band center. We hypothesize this is due to the favorable interaction between the metal and oxygen, which exists in transition metals. We have also shown that the binding of nitrogen species shows a parabolic structure across the periodic table row, correlating strongly with the metals' cohesive energies. This parabolic trend has the metals in the center of the row binding nitrogen species the strongest, and the metals on the edges of the row binding them more weakly. We hypothesize that the cohesive energy measures a metal's relative instability and, therefore, the propensity to form bonds with gas-phase species. Finally, we analyze the binding energies and reaction energies to search for scaling relations. We find Reasonably accurate linear scaling relations in the system, with the scaling relations generated having an overall RMSE of 0.2eV. We conclude that a few metals (Rh and Mo) are predicted to slightly improve the rate of N_2 reduction, but none improve the rate significantly.

We also analyzed the possibility that adventitious surface carbon on rutile (110) surface helps catalyze the nitrogen reduction reaction. We utilize ambient pressure XPS to observe the rutile (110) surface under reaction conditions, finding that reduced nitrogen species are present only when adventitious surface carbon is present. We then analyze several possible carbon-based active sites on the rutile (110) surface, finding that sites containing carbon tend to bind nitrogen strongly, but are relatively unstable. We then analyze one particular active site: a carbon substituted onto a bridging oxygen site. We investigate this active site's ability to selectively adsorb N_2 over O_2 and H_2O, finding that N_2 adsorption is

competitive under ambient conditions. We demonstrate that the nitrogen reduction reaction can proceed through this active site, but requires an oxidative regeneration step to close the catalytic cycle. Finally, we show that this carbon active site is meta-stable under reaction conditions, requiring illumination to be generated from adventitious surface carbon.

7.2 Analysis and Future Work

While the technology of photocatalytic nitrogen fixation is viable, there are substantial challenges to overcome to enable low-cost solar fertilizers generated from photocatalysis Chapters 4-6 have focused on the TiO_2 surface, laying out the thermodynamics of N_2 reduction and oxidation on the surface. However, this work suggests that the rutile TiO_2 (110) surface is fundamentally limited as a material for photocatalytic nitrogen fixation. Rates initially reported were low [71] and remain low in more recent work [59] ($\sim$2 $\mu mol/h$) despite attempts to improve its activity. The large bandgap of TiO_2 (roughly 3 eV, see Figure 1.5) limits its ability to utilize sunlight for photocatalytic reactions. TiO_2 also has relatively unfavorable band alignment, meaning that the reducing potential of photoexcited electrons is relatively small. Additionally, Chapter 4 shows that the reaction cannot proceed on the pristine rutile (110) surface, requiring complicated reactions involving radical carbon species as shown in Chapter 6. This leads to the challenging task of engineering surface carbon to improve reaction rates. The need to ensure that surface carbon is present in the proper form and amount is a significant barrier to practical reactor design.

The difficulties with engineering TiO_2 for photocatalytic nitrogen fixation and lack of progress over several decades suggest that researchers should search for novel materials. Computational analysis can provide an advantage, since if good descriptors can be found many materials can be screened rapidly to narrow the field of possible catalysts. The descriptors that have been identified in the literature [107] and in our work (Chapter 5) are the binding energies of O_2, N_2, N_2H, and NH_2. In particular, our work suggests that the relative binding of O_2 and N_2 is important. If a surface binds O_2 much stronger than N_2, the

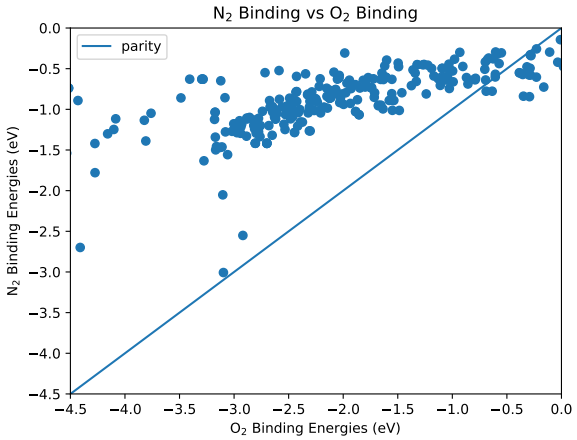

Figure 7.1: The binding of N_2 vs. the binding of O_2 for screened surfaces. Surfaces include metal oxides, borides, and phosphides. Bulk materials were obtained from the materials project database [346]. The diagonal line represents equivalent binding of O_2 and N_2.

surface will be poisoned by O_2 even if N_2 binds strongly, necessitating capital-intensive air separation. N_2 binding is relevant as N_2 coverage is a prerequisite to obtaining reasonable rates under ambient conditions. Finally, the binding energies of N_2H and NH_2 are relevant, as they are involved in the two steps that are normally rate-limiting under electrochemical conditions (N_2* $\rightarrow$ N_2H*, and NH_2* $\rightarrow$ NH_3 + *).

In most practical applications of photo- and electrocatalytic nitrogen reduction, the feed gas will be air. Thus, O_2 will be present alongside N_2 and compete for surface adsorption sites. This competition necessitates the use of materials that will adsorb N_2 more favorably than O_2. It is generally accepted that O_2 is more reactive than N_2 in most circumstances, as it is a relatively unstable molecule in a triplet spin state [347]. Because of the instability of O_2, future work should focus on finding materials able to adsorb N_2 more favorably than O_2. This will be a challenging endeavor, due to the relative reactivity of these molecules. However, a preliminary analysis of N_2 and O_2 adsorption over 2000 candidate oxide, (oxy)boride, and (oxy)phosphide surfaces has yielded at least 25 promising candidate surfaces (see Figure 7.1). .

To perform this screening, a variety of surface oxide, phosphites, and boride surfaces

were tested to study the competitive binding of oxygen and nitrogen. Bulk materials were selected from the Materials Project database [346]. The chosen materials were specified to be all materials that contain one of the metals Sc, Ru, V, Sn, Nb, Zr, Mo, Ti and one of the non-metals O, B, P. These metals were selected as all of them can form rutile oxides so a baseline of comparison will exist in the dataset[107]. Additionally, borides have shown promise for nitrogen fixation reactions[348]. From these bulk structures, surfaces were generated with all possible combinations of Miller indices where the maximum index was one (i.e. 110, 111, 100). Voronoi polygon analysis was used to determine all surface active sites on all generated surfaces[349, 350]. These active sites include bridge, ontop, and hollow sites. With this information, for each active site N_2 and O_2 were adsorbed to generate a full set of adsorption structures.

DFT calculations were performed on each surface to obtain ground state energies. The surfaces were fully frozen to simplify the study initial candidate materials. Each adsorption structure was then relaxed to obtain the lowest energy structures. Systems in which one or more calculations did not converge, O_2 $\mathring{A}$ dissociated, or N_2 and O_2 were not bound to the same site were discarded. In total, calculations were performed on 2078 systems, of which 300 were found to be physically relevant.

Figure 7.1 shows the 300 systems obtained from the preliminary screening analysis. An interesting trend emerges from the calculated bindings. There is a weak linear correlation between the binding of N_2 and O_2 across the studied surfaces. This trend has the binding of O_2 increasing much faster than N_2. This trend matches the expectation that O_2 is more reactive than N_2 and highlights the challenge posed by this problem. Additionally, there existed 25 systems that bound N_2 favorably and bound stronger than O_2 and also bound N_2 stronger than -0.5eV. These surfaces represent a pool of candidate materials for future study. While subsequent work is required to ensure that these are not false positives, this encouraging result indicates the promise of computational screening in the discovery of air-stable photocatalysts for nitrogen fixation.

Appendices

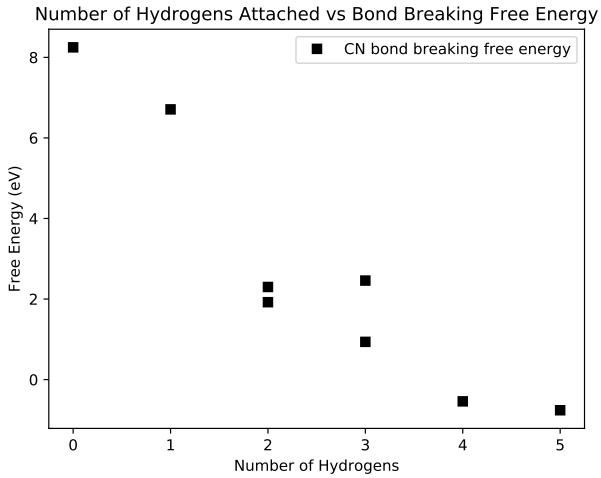

Figure A2: Reaction free energy of of breaking the C–N bond vs the number of hydrogens.

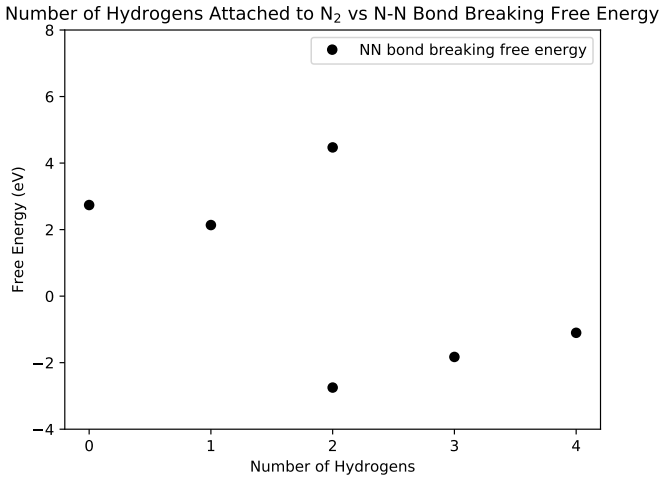

Figure A3: The reaction free energy of breaking the N–N bond vs the number of hydrogens.

Table A1: The calculated relative energies of all 2+ surface species on all metal substituents at standard state. All energies are referenced with respect to N_2 gas and H_2 gas at 300K and 1 bar of pressure. Blank spaces represent calculations that could not be converged

Element	H_2NNH_2	HNNH	N	N_2	N_2H	N_2H_2	N_2H_3	NH	NH_2	NH_3	Formation Energy
V	1.5	1.52	0.0	0.35	1.11	0.79	0.95	0.5	-0.94	-0.71	1.9
Ni	1.6	2.17	3.5	0.14	1.78	1.91	1.25	2.57	0.06	-0.51	4.94
Au	1.79	2.49	4.34	0.27	2.65	2.85	2.28	3.07	0.8	-0.03	6.89
Re	1.04	0.8	-1.44	-0.78	-0.32	-0.03	0.4	-0.13	-1.17	-0.92	5.77
Hf	1.32	1.46	1.85	0.0	1.1	0.72	0.32	0.07	-1.38	-0.9	-0.79
Nb	1.3	0.55	-1.02	-0.18	0.47	-0.25	0.06	-0.79	-1.66	-0.83	2.08
Pd	1.65	2.24	3.62	0.25	2.13	2.38	1.83	2.58	0.35	-0.16	5.69
Mo	1.36	1.07	-1.14	-0.27	0.13	0.02	0.49	-0.18	-1.15	-0.7	4.1
Tc	1.13	1.08	-0.8	-0.61	0.09	0.38	0.77	0.0	-1.39	-0.87	5.21
Cr	1.37	1.61	0.7	0.03	1.58	0.98	0.74	1.12	-0.91	-0.76	2.62
Ti	1.52	1.79	1.97	0.13	1.4	0.97	0.73	0.43	-0.93	-0.56	-0.0
W	1.34	0.97	-1.74	-0.3	-0.12	-0.62	0.11	-1.01	-1.56	-0.75	4.25
Fe	1.82	2.25	11.57	0.63	1.78	1.77	1.62	2.09	-0.01	-0.47	3.3
Sc	1.16	1.91	4.47	0.05	1.81	1.71	1.1	2.57	-0.57	-0.71	-1.24
Ru	0.92	0.89	0.55	-0.78	0.75	0.29	0.57	0.91	-1.0	-1.08	5.83
Os	0.72	0.53	-0.63	-1.11	-0.04	-0.24	0.18	0.12	-1.38	-1.23	6.85
Ag	1.55	2.45	5.38	0.25	2.71	2.76	2.16	3.89	1.15	-0.14	6.39
Y	1.11	1.82	2.9	0.04		2.12	1.42	2.98	-0.12	-0.73	-0.93
Zr	1.33	1.53	1.76	0.01	1.19	0.86	0.47	0.2	-1.21	-0.83	-0.42
Pt	1.75	2.28	3.01	0.27	1.89	2.2	1.56	1.75	-0.04	-0.06	6.01
Co	1.61	2.01	2.76	0.16	1.51	1.5	1.27	2.05	-0.32	-0.3	4.38
Cu	1.44	2.2	5.14	0.19	2.43	2.51	1.79	3.72	0.84	-0.4	5.31
Ir	1.06	0.99	1.23	-0.53	0.5	0.44	0.22	0.72	-1.35	-1.02	6.55
Rh	1.39	1.54	2.27	-0.03	0.93	1.07	0.67	1.36	-0.9	-0.7	5.63
Ta	1.26	0.44	-0.96	-0.1	0.54	-0.19	-0.11	-0.88	-1.81	-0.81	1.52

Table A2: The calculated relative energies of all 4+ surface species on all metal substituents at standard state. All energies are referenced with respect to N_2 gas and H_2 gas at 300K and 1 bar of pressure. Blank spaces represent calculations that could not be converged

Element	N_2	N_2H	Formation Energy
V	0.07	3.17	2.37
Ni	0.1	2.15	8.14
Au	0.16		9.39
Re	-0.01	2.24	6.15
Hf	-0.05	2.84	-1.08
Nb	-0.01	3.01	1.62
Pd	-0.06	2.06	8.89
Mo	0.02	3.01	4.3
Tc	-0.01	2.53	6.04
Cr	0.09	2.21	4.5
Ti	0.04	3.21	-0.0
W	0.02		4.14
Fe	0.07	1.82	6.29
Ru	-0.13	2.28	7.35
Sc	-0.03	2.71	0.71
Os	-0.33	2.4	7.77
Ag	0.13		9.62
Y	-0.09		1.14
Mn	0.09		
Zr	-0.04	3.16	-0.66
Pt	-0.4	2.06	8.72
Co	0.08		7.13
Cu	0.11		8.75
Ir	-0.52		8.24
Rh	-0.24	2.56	7.86
Ta	-0.01	2.91	1.06

Table A3: The limiting potentials and limiting steps for each dopant metal on 2+ surfaces

Element	Limiting Potential	Limiting Step
Sc	-1.81	$N_2 \rightarrow N_2H^*$
Ti	-1.4	$N_2 \rightarrow N_2H^*$
V	-1.11	$N_2 \rightarrow N_2H^*$
Cr	-1.58	$N_2 \rightarrow N_2H^*$
Fe	-1.78	$N_2 \rightarrow N_2H^*$
Co	-1.51	$N_2 \rightarrow N_2H^*$
Ni	-1.78	$N_2 \rightarrow N_2H^*$
Cu	-2.43	$N_2 \rightarrow N_2H^*$
Zr	-1.19	$N_2 \rightarrow N_2H^*$
Nb	-1.35	$NH_2^*+NH_3 \rightarrow 2NH_3$
Mo	-0.83	$NH_2^*+NH_3 \rightarrow 2NH_3$
Tc	-1.08	$NH_2^*+NH_3 \rightarrow 2NH_3$
Ru	-1.53	$N_2^* \rightarrow N_2H^*$
Rh	-0.95	$N_2^* \rightarrow N_2H^*$
Pd	-2.13	$N_2 \rightarrow N_2H^*$
Ag	-2.71	$N_2 \rightarrow N_2H^*$
Hf	-1.1	$N_2 \rightarrow N_2H^*$
Ta	-1.5	$NH_2^*+NH_3 \rightarrow 2NH_3$
W	-1.25	$NH_2^*+NH_3 \rightarrow 2NH_3$
Re	-0.86	$NH_2^*+NH_3 \rightarrow 2NH_3$
Os	-1.07	$N_2^* \rightarrow N_2H^*$
Ir	-1.04	$N_2^* \rightarrow N_2H^*$
Pt	-1.89	$N_2 \rightarrow N_2H^*$
Au	-2.65	$N_2 \rightarrow N_2H^*$

Table A4: The largest barrier for thermochemical steps and corresponding steps for each dopant metal on 2+ surfaces

Element	Largest Thermodynamic Step	Limiting Step
Sc	0.4	NH_3*+NH_3 $\rightarrow$ 2NH_3
Ti	0.62	NH_3*+NH_3 $\rightarrow$ 2NH_3
V	0.63	NH_3*+NH_3 $\rightarrow$ 2NH_3
Cr	0.59	NH_3*+NH_3 $\rightarrow$ 2NH_3
Fe	0.63	N_2 $\rightarrow$ N_2*
Co	0.16	N_2 $\rightarrow$ N_2*
Ni	0.62	H_2NNH_2* $\rightarrow$ 2NH_2*
Cu	1.21	H_2NNH_2* $\rightarrow$ 2NH_2*
Zr	0.9	NH_3*+NH_3 $\rightarrow$ 2NH_3
Nb	1.35	NH_3*+NH_3 $\rightarrow$ 2NH_3
Mo	0.83	NH_3*+NH_3 $\rightarrow$ 2NH_3
Tc	1.08	NH_3*+NH_3 $\rightarrow$ 2NH_3
Ru	0.77	NH_3*+NH_3 $\rightarrow$ 2NH_3
Rh	0.58	NH_3*+NH_3 $\rightarrow$ 2NH_3
Pd	0.51	H_2NNH_2* $\rightarrow$ 2NH_2*
Ag	1.41	H_2NNH_2* $\rightarrow$ 2NH_2*
Hf	1.06	NH_3*+NH_3 $\rightarrow$ 2NH_3
Ta	1.5	NH_3*+NH_3 $\rightarrow$ 2NH_3
W	1.25	NH_3*+NH_3 $\rightarrow$ 2NH_3
Re	0.86	NH_3*+NH_3 $\rightarrow$ 2NH_3
Os	1.07	NH_3*+NH_3 $\rightarrow$ 2NH_3
Ir	1.03	NH_3*+NH_3 $\rightarrow$ 2NH_3
Pt	0.27	N_2 $\rightarrow$ N_2*
Au	0.82	H_2NNH_2* $\rightarrow$ 2NH_2*

Table A5: The largest thermodynamic barrier and corresponding steps for each dopant metal on 2+ surfaces when set at the band edge of rutile, -0.142V

Element	Rate Limiting Step	Limiting Step
Sc	1.66	$N_2 \rightarrow N_2H^*$
Ti	1.26	$N_2 \rightarrow N_2H^*$
V	0.97	$N_2 \rightarrow N_2H^*$
Cr	1.43	$N_2 \rightarrow N_2H^*$
Fe	1.63	$N_2 \rightarrow N_2H^*$
Co	1.37	$N_2 \rightarrow N_2H^*$
Ni	1.64	$N_2 \rightarrow N_2H^*$
Cu	2.29	$N_2 \rightarrow N_2H^*$
Zr	1.05	$N_2 \rightarrow N_2H^*$
Nb	1.27	$N_2H_2^* \rightarrow H_2NNH_2^*$
Mo	1.06	$N_2H_2^* \rightarrow H_2NNH_2^*$
Tc	1.17	$N_2^* \rightarrow H_2NNH_2^*$
Ru	1.39	$N_2^* \rightarrow N_2H^*$
Rh	0.82	$N_2^* \rightarrow N_2H_2^*$
Pd	2.1	$N_2 \rightarrow N_2H_2^*$
Ag	2.57	$N_2 \rightarrow N_2H^*$
Hf	0.96	$N_2 \rightarrow N_2H^*$
Ta	1.36	$NH_2^*+NH_3 \rightarrow 2NH_3$
W	1.67	$N_2H_2^* \rightarrow H_2NNH_2^*$
Re	1.25	$N_2^* \rightarrow H_2NNH_2^*$
Os	0.93	$N_2^* \rightarrow N_2H^*$
Ir	0.89	$N_2^* \rightarrow N_2H^*$
Pt	1.91	$N_2 \rightarrow N_2H_2^*$
Au	2.57	$N_2 \rightarrow N_2H_2^*$

Table A6: N1s peak area, FWHM and Peak Position for TiO_2 110 (Rutile)

	Dark			Light		
	N_{red}	FWHM	Position	N_{red}	FWHM	Position
No Carbon	-	-	-	-	-	-
Carbon	-	-	-	15558	2.4	398.2

Table A7: O1s peak area, FWHM and Peak Position for TiO_2 110 (Rutile)

	Dark			Light		
	Lattice O	FWHM	Position	Lattice O	FWHM	Position
No Carbon	389063	1.12	529.9	388158	1.13	529.9
Carbon	659853	1.3	529.9	709855	1.31	529.9
	OH	FWHM	Position	OH	FWHM	Position
No Carbon	467438	2.4	531.9	427399	2.77	531.8
Carbon	367047	2.36	531.6	331613	2.18	531.7

Table A8: Ti2p peak area, FWHM and Peak Position for TiO_2 110 (Rutile)

	Dark			Light		
	$Ti2P_{3/2}$	FWHM	Position	$Ti2P_{3/2}$	FWHM	Position
No Carbon	421563	1.02	458.5	3999645	1	458.5
Carbon	494951	1.11	458.2	514699	1.09	458.58
	$Ti2P_{1/2}$	FWHM	Position	$Ti2P_{1/2}$	FWHM	Position
No Carbon	180339	1.99	464.2	220096	2.05	463.9
Carbon	220563.1	2.04	463.9	200931.3	2.04	464.3

Table A9: C1s peak area, FWHM and Peak Position for TiO_2 110 (Rutile)

	Dark			Light		
	C1s	FWHM	Position	C1s	FWHM	Position
No Carbon	1455	1.17	284.5	2450	1.87	284.5
Carbon	74294	1.96	283.5	92449	2.04	284.2

REFERENCES

[1] T. Kelly, G. Matos, D. with Buckingham, C. DiFrancesco, K. Porter, C. Berry, M. Crane, T. Goonan, and J. Sznopek, *Historical statistics for mineral and material commodities in the united states*, 2016.

[2] M. Roser and H. Ritchie, "Hunger and undernourishment," *Our World in Data*, 2019, https://ourworldindata.org/hunger-and-undernourishment.

[3] ——, "Fertilizers," *Our World in Data*, 2013, https://ourworldindata.org/fertilizers.

[4] R. Schloegl, "Catalytic synthesis of ammonia — a "never-ending story"?" *ChemInform*, vol. 34, no. 27, 2003.

[5] V. Smil, "Detonator of the population explosion," *Nature*, vol. 400, no. 6743, pp. 415–415, 1999.

[6] S. Pinker, *Enlightenment Now: The Case for Reason, Science, Humanism, and Progress*. Viking, 2018.

[7] Z. J. Schiffer and K. Manthiram, "Electrification and decarbonization of the chemical industry," *Joule*, vol. 1, no. 1, pp. 10–14, 2017.

[8] S. L. Foster, S. I. P. Bakovic, R. D. Duda, S. Maheshwari, R. D. Milton, S. D. Minteer, M. J. Janik, J. N. Renner, and L. F. Greenlee, "Catalysts for nitrogen reduction to ammonia," *Nature Catalysis*, vol. 1, no. 7, pp. 490–500, 2018.

[9] B. E. Smith, "Nitrogenase reveals its inner secrets," *Science*, vol. 297, no. 5587, pp. 1654–1655, 2002.

[10] H. F. Abbas and W. W. Daud, "Hydrogen production by methane decomposition: A review," *International Journal of Hydrogen Energy*, vol. 35, no. 3, pp. 1160–1190, 2010.

[11] J. W. McArthur and G. C. McCord, "Fertilizing growth: Agricultural inputs and their effects in economic development," *Journal of Development Economics*, vol. 127, pp. 133–152, 2017.

[12] J. R. Bartels, "A feasibility study of implementing an ammonia economy," PhD thesis, Iowa State University, 2008.

[13] T. O. West and G. Marland, "A synthesis of carbon sequestration, carbon emissions, and net carbon flux in agriculture: Comparing tillage practices in the united states," *Agriculture, Ecosystems & Environment*, vol. 91, no. 1-3, pp. 217–232, 2002.

[14] N. Gilbert, "African agriculture: Dirt poor," *Nature*, vol. 483, no. 7391, pp. 525–527, 2012.

[15] N. D. Mueller, J. S. Gerber, M. Johnston, D. K. Ray, N. Ramankutty, and J. A. Foley, "Closing yield gaps through nutrient and water management," *Nature*, vol. 490, no. 7419, pp. 254–257, 2012.

[16] M. Van der Velde, C. Folberth, J. Balkovič, P. Ciais, S. Fritz, I. A. Janssens, M. Obersteiner, L. See, R. Skalský, W. Xiong, and J. Peñuelas, "African crop yield reductions due to increasingly unbalanced Nitrogen and Phosphorus consumption," *Global Change Biology*, vol. 20, no. 4, pp. 1278–1288, 2014.

[17] R. J. Diaz and R. Rosenberg, "Spreading dead zones and consequences for marine ecosystems," *Science*, vol. 321, no. 5891, pp. 926–929, 2008. eprint: `http://science.sciencemag.org/content/321/5891/926.full.pdf`.

[18] C. J. Stevens, "Nitrogen in the environment," *Science*, vol. 363, no. 6427, pp. 578–580, 2019.

[19] G. Marlair and M.-A. Kordek, "Safety and security issues relating to low capacity storage of AN-based fertilizers," *Journal of Hazardous Materials*, vol. 123, no. 1-3, pp. 13–28, 2005.

[20] N. Ramankutty, A. T. Evan, C. Monfreda, and J. A. Foley, "Farming the planet: 1. geographic distribution of global agricultural lands in the year 2000," *Global Biogeochemical Cycles*, vol. 22, no. 1, n/a–n/a, 2008.

[21] N. Ramankutty, A. T. Evan, C. Monfreda, and J. A. Foley, *Global agricultural lands: Croplands, 2000*, Palisades, NY, 2010.

[22] *Africafertilizer.org*, Web Database, https://africafertilizer.org/production/, 2018.

[23] I. J. McPherson, T. Sudmeier, J. Fellowes, and S. C. E. Tsang, "Materials for electrochemical ammonia synthesis," *Dalton Trans.*, vol. 48, pp. 1562–1568, 5 2019.

[24] S. Burén and L. M. Rubio, "State of the art in eukaryotic nitrogenase engineering," *FEMS Microbiology Letters*, vol. 365, no. 2, 2017.

[25] R. Hawtof, S. Ghosh, E. Guarr, C. Xu, R. M. Sankaran, and J. N. Renner, "Catalyst-free, highly selective synthesis of ammonia from nitrogen and water by a plasma electrolytic system," *Science Advances*, vol. 5, no. 1, eaat5778, 2019.

[26] R. Michalsky, A. M. Avram, B. A. Peterson, P. H. Pfromm, and A. A. Peterson, "Chemical looping of metal nitride catalysts: Low-pressure ammonia synthesis for energy storage," *Chemical Science*, vol. 6, no. 7, pp. 3965–3974, 2015.

[27] M. Jewess and R. H. Crabtree, "Electrocatalytic nitrogen fixation for distributed fertilizer production?" *ACS Sustainable Chemistry & Engineering*, vol. 4, no. 11, pp. 5855–5858, 2016.

[28] A. J. Medford and M. C. Hatzell, "Photon-driven nitrogen fixation: Current progress, thermodynamic considerations, and future outlook," *ACS Catalysis*, pp. 2624–2643, 2017.

[29] V. Kyriakou, I. Garagounis, E. Vasileiou, A. Vourros, and M. Stoukides, "Progress in the electrochemical synthesis of ammonia," *Catalysis Today*, vol. 286, pp. 2–13, 2017.

[30] J. G. Chen, R. M. Crooks, L. C. Seefeldt, K. L. Bren, R. M. Bullock, M. Y. Darensbourg, P. L. Holland, B. Hoffman, M. J. Janik, A. K. Jones, M. G. Kanatzidis, P. King, K. M. Lancaster, S. V. Lymar, P. Pfromm, W. F. Schneider, and R. R. Schrock, "Beyond fossil fuel–driven nitrogen transformations," *Science*, vol. 360, no. 6391, eaar6611, 2018.

[31] H. Tao, C. Choi, L.-X. Ding, Z. Jiang, Z. Han, M. Jia, Q. Fan, Y. Gao, H. Wang, A. W. Robertson, S. Hong, Y. Jung, S. Liu, and Z. Sun, "Nitrogen fixation by ru single-atom electrocatalytic reduction," *Chem*, vol. 5, no. 1, pp. 204–214, 2019.

[32] P. Song, H. Wang, L. Kang, B. Ran, H. Song, and R. Wang, "Electrochemical nitrogen reduction to ammonia at ambient conditions on nitrogen and phosphorus co-doped porous carbon," *Chemical Communications*, vol. 55, no. 5, pp. 687–690, 2019.

[33] Y. Luo, G.-F. Chen, L. Ding, X. Chen, L.-X. Ding, and H. Wang, "Efficient electrocatalytic N_2 fixation with MXene under ambient conditions," *Joule*, 2018.

[34] D. Wang, L. M. Azofra, M. Harb, L. Cavallo, X. Zhang, B. H. R. Suryanto, and D. R. MacFarlane, "Energy-efficient nitrogen reduction to ammonia at low overpotential in aqueous electrolyte under ambient conditions," *ChemSusChem*, vol. 11, no. 19, pp. 3356–3356, 2018.

[35] M. G. Walter, E. L. Warren, J. R. McKone, S. W. Boettcher, Q. Mi, E. A. Santori, and N. S. Lewis, "Solar water splitting cells," *Chemical reviews*, vol. 110, no. 11, pp. 6446–6473, 2010.

[36] B. A. Pinaud, J. D. Benck, L. C. Seitz, A. J. Forman, Z. Chen, T. G. Deutsch, B. D. James, K. N. Baum, G. N. Baum, S. Ardo, H. Wang, E. Miller, and T. F. Jaramillo,

"Technical and economic feasibility of centralized facilities for solar hydrogen production via photocatalysis and photoelectrochemistry," *Energy & Environmental Science*, vol. 6, no. 7, p. 1983, 2013.

[37] E. V. Kondratenko, G. Mul, J. Baltrusaitis, G. O. Larrazábal, and J. Pérez-Ramírez, "Status and perspectives of CO2 conversion into fuels and chemicals by catalytic, photocatalytic and electrocatalytic processes," *Energy & Environmental Science*, vol. 6, no. 11, p. 3112, 2013.

[38] M. R. Shaner, H. A. Atwater, N. S. Lewis, and E. W. McFarland, "A comparative technoeconomic analysis of renewable hydrogen production using solar energy," *Energy & Environmental Science*, vol. 9, no. 7, pp. 2354–2371, 2016.

[39] N. S. Lewis, "Progress towards a synergistically integrated, scalable solar fuels generator," in *Nanotechnology: Delivering on the Promise Volume 2*, American Chemical Society, 2016, pp. 3–22.

[40] J. H. Montoya, L. C. Seitz, P. Chakthranont, A. Vojvodic, T. F. Jaramillo, and J. K. Nørskov, "Materials for solar fuels and chemicals," *Nature Materials*, vol. 16, no. 1, pp. 70–81, 2017.

[41] A. R. Singh, B. A. Rohr, J. A. Schwalbe, M. Cargnello, K. Chan, T. F. Jaramillo, I. Chorkendorff, and J. K. Nørskov, "Electrochemical ammonia synthesis-the selectivity challenge," *ACS Catal.*, vol. 7, no. 1, pp. 706–709, 2017.

[42] Atmonia. (2020). Sustainable nitrogen fertilizer. https://atmonia.com/, (visited on 08/31/2020).

[43] Y. Song, D. Johnson, R. Peng, D. K. Hensley, P. V. Bonnesen, L. Liang, J. Huang, F. Yang, F. Zhang, R. Qiao, A. P. Baddorf, T. J. Tschaplinski, N. L. Engle, M. C. Hatzell, Z. Wu, D. A. Cullen, H. M. Meyer, B. G. Sumpter, and A. J. Rondinone, "A physical catalyst for the electrolysis of nitrogen to ammonia," *Science Advances*, vol. 4, no. 4, e1700336, 2018.

[44] K. Kim, N. Lee, C.-Y. Yoo, J.-N. Kim, H. C. Yoon, and J.-I. Han, "Communication—electrochemical reduction of nitrogen to ammonia in 2-propanol under ambient temperature and pressure," *Journal of The Electrochemical Society*, vol. 163, no. 7, F610–F612, 2016.

[45] N. Lazouski, Z. J. Schiffer, K. Williams, and K. Manthiram, "Understanding continuous lithium-mediated electrochemical nitrogen reduction," *Joule*, 2019.

[46] D. Krishnamurthy, N. Lazouski, M. L. Gala, K. Manthiram, and V. Viswanathan, "Closed-Loop Design of Proton Donors for Lithium-Mediated Ammonia Synthesis

with Interpretable Models and Molecular Machine Learning," 2020. arXiv: 2008.08078.

[47] V. Smil, "Nitrogen in crop production: An account of global flows adds recycled in organic up by harvested and Quantification of N losses from crop to 26-60," *Global Biogeochemical Cycles*, vol. 13, no. 2, pp. 647–662, 1999.

[48] L. C. Seefeldt, B. M. Hoffman, and D. R. Dean, "Mechanism of Mo-dependent nitrogenase," *Annual Review of Biochemistry*, vol. 78, no. 1, pp. 701–722, 2009.

[49] S. L. Foster, S. I. Bakovic, R. D. Duda, S. Maheshwari, R. D. Milton, S. D. Minteer, M. J. Janik, J. N. Renner, and L. F. Greenlee, "Catalysts for nitrogen reduction to ammonia," *Nature Catalysis*, vol. 1, no. 7, pp. 490–500, 2018.

[50] R. D. Milton, S. Abdellaoui, N. Khadka, D. R. Dean, D. Leech, L. C. Seefeldt, and S. D. Minteer, "Nitrogenase bioelectrocatalysis: Heterogeneous ammonia and hydrogen production by MoFe protein," *Energy & Environmental Science*, vol. 9, no. 8, pp. 2550–2554, 2016.

[51] K. Birkeland, "On the oxidation of atmospheric nitrogen in electric arcs," *Transactions of the Faraday Society*, vol. 2, no. December, p. 98, 1906.

[52] P. Mehta, P. Barboun, F. A. Herrera, J. Kim, P. Rumbach, D. B. Go, J. C. Hicks, and W. F. Schneider, "Overcoming ammonia synthesis scaling relations with plasma-enabled catalysis," *Nature Catalysis*, vol. 1, no. 4, pp. 269–275, 2018.

[53] Nitricity. (2020). Renewable on-site nitrogen fertilizer production. https://www.nitricity.co/, (visited on 09/03/2020).

[54] M. P. Shaver and M. D. Fryzuk, "Activation of molecular nitrogen: Coordination, cleavage and functionalization of n2 mediated by metal complexes," *ChemInform*, vol. 34, no. 51, 2003.

[55] K. P. Kepp, "Accuracy of theoretical catalysis from a model of iron-catalyzed ammonia synthesis," *Communications Chemistry*, vol. 1, no. 1, 2018.

[56] M. Appl, "Ammonia," in *Ullmann's Encyclopedia of Industrial Chemistry*, John Wiley & Sons, Inc, 2006, ISBN: 9783527306732. eprint: https://onlinelibrary.wiley.com/doi/pdf/10.1002/14356007.a02_143.pub2.

[57] E. Skúlason, T. Bligaard, S. Gudmundsdóttir, F. Studt, J. Rossmeisl, F. Abild-Pedersen, T. Vegge, H. Jónsson, and J. K. Nørskov, "A theoretical evaluation of possible transition metal electro-catalysts for n 2 reduction," *Phys. Chem. Chem. Phys.*, vol. 14, no. 3, pp. 1235–1245, 2012.

[58] J. M. McEnaney, A. R. Singh, J. A. Schwalbe, J. Kibsgaard, J. C. Lin, M. Cargnello, T. F. Jaramillo, and J. K. Nørskov, "Ammonia synthesis from n2 and H_2O using a lithium cycling electrification strategy at atmospheric pressure," *Energy & Environmental Science*, vol. 10, no. 7, pp. 1621–1630, 2017.

[59] H. Hirakawa, M. Hashimoto, Y. Shiraishi, and T. Hirai, "Photocatalytic conversion of nitrogen to ammonia with water on surface oxygen vacancies of titanium dioxide," *Journal of the American Chemical Society*, vol. 139, no. 31, pp. 10 929–10 936, 2017.

[60] Y. Jiao, Y. Zheng, M. Jaroniec, and S. Z. Qiao, "Design of electrocatalysts for oxygen- and hydrogen-involving energy conversion reactions," *Chemical Society Reviews*, vol. 44, no. 8, pp. 2060–2086, 2015.

[61] Z. W. Seh, J. Kibsgaard, C. F. Dickens, I. Chorkendorff, J. K. Nørskov, and T. F. Jaramillo, "Combining theory and experiment in electrocatalysis: Insights into materials design," *Science*, vol. 355, no. 6321, eaad4998, 2017.

[62] F. Wiesler, "Comparative assessment of the efficacy of various nitrogen fertilizers," *Journal of Crop Production*, vol. 1, no. 2, pp. 81–114, 1998.

[63] B. Yao, J. Cao, C. Zhao, and Z. Rengel, "Influence of ammonium and nitrate supply on growth, nitrate reductase activity and n-use efficiency in a natural hybrid pine and its parents," *Journal of Plant Ecology*, vol. 4, no. 4, pp. 275–282, 2011.

[64] C. Mancino and J. Troll, "Nitrate and ammonium leaching losses from n fertilizers applied to 'penncross' creeping bentgrass," *HortScience*, vol. 25, no. 2, pp. 194–196, 1990.

[65] N. R. Council, "Nitrate and nitrite in drinking water," in. Washington, DC: The National Academies Press, 1995, ch. Chapter: 2 Hazard Identification, ISBN: 978-0-309-08370-6.

[66] R. I. Bickley and V. Vishwanathan, "Photocatalytically induced fixation of molecular nitrogen by near UV radiation," *Nature*, vol. 280, no. 5720, pp. 306–308, 1979.

[67] S.-J. Yuan, J.-J. Chen, Z.-Q. Lin, W.-W. Li, G.-P. Sheng, and H.-Q. Yu, "Nitrate formation from atmospheric nitrogen and oxygen photocatalysed by nano-sized titanium dioxide," *Nat. Commun.*, vol. 4, 2013.

[68] C. Dai, Y. Sun, G. Chen, A. C. Fisher, and Z. J. Xu, "Electrochemical oxidation of nitrogen towards direct nitrate production on spinel oxides," *Angewandte Chemie*, vol. 132, no. 24, pp. 9504–9508, 2020.

[69] K. Nakata and A. Fujishima, "TiO_2 photocatalysis: Design and applications," *Journal of Photochemistry and Photobiology C: Photochemistry Reviews*, vol. 13, no. 3, pp. 169–189, 2012.

[70] A. Fujishima and K. Honda, "Electrochemical photolysis of water at a semiconductor electrode," *Nature*, vol. 238, no. 5358, pp. 37–38, 1972.

[71] G. Schrauzer and T. Guth, "Photocatalytic reactions. 1. Photolysis of water and photoreduction of nitrogen on titanium dioxide," *J. Am. Chem. Soc.*, vol. 99, no. 22, pp. 7189–7193, 1977.

[72] T. Inoue, A. Fujishima, S. Konishi, and K. Honda, *Photoelectrocatalytic reduction of carbon dioxide in aqueous suspensions of semiconductor powders*, 1979.

[73] C. C. Mao and H. S. Weng, "Promoting effect of adding carbon black to TiO_2 for aqueous photocatalytic degradation of methyl orange," *Chemical Engineering Journal*, vol. 155, no. 3, pp. 744–749, 2009.

[74] D. Bahnemann, "Photocatalytic water treatment: Solar energy applications," *Solar Energy*, vol. 77, no. 5, pp. 445–459, 2004.

[75] N. Dhar, E. Seshacharyulu, and N. Biswas, "New aspects of nitrogen fixation and loss in soils," *Proceedings of the National institute of sciences of India*, vol. 7, pp. 115–131, 1941.

[76] C. T. Campbell and J. Sauer, "Introduction: Surface chemistry of oxides," *Chemical Reviews*, vol. 113, no. 6, pp. 3859–3862, 2013.

[77] U. Diebold, "The surface science of titanium dioxide," *Surface Science Reports*, vol. 48, no. 5-8, 2003.

[78] M. A. Henderson, "A surface science perspective on TiO_2 photocatalysis," *Surface Science Reports*, vol. 66, no. 6-7, pp. 185–297, 2011.

[79] J. Schneider, M. Matsuoka, M. Takeuchi, J. Zhang, Y. Horiuchi, M. Anpo, and D. W. Bahnemann, "Understanding TiO_2 photocatalysis: Mechanisms and materials," *Chemical Reviews*, vol. 114, no. 19, pp. 9919–9986, 2014.

[80] C. L. Pang, R. Lindsay, and G. Thornton, "Chemical reactions on rutile TiO_2(110).," *Chemical Society reviews*, vol. 37, no. 10, pp. 2328–2353, 2008.

[81] H. Chen, A. Nambu, Wen, J. Graciani, Zhong, J. C. Hanson, E. Fujita, and J. A. Rodriguez, "Reaction of NH_3 with titania: n-doping of the oxide and TiN formation," *The Journal of Physical Chemistry C*, vol. 111, no. 3, pp. 1366–1372, 2007.

[82] C. Sun, L.-m. Liu, A. Selloni, G. Q. M. Lu, and S. C. Smith, "Titania-water interactions: a review of theoretical studies," *Journal of Materials Chemistry*, vol. 20, no. 46, p. 10 319, 2010.

[83] L. A. Harris and A. A. Quong, "Molecular Chemisorption as the Theoretically Preferred Pathway for Water Adsorption on Ideal Rutile TiO_2(110)," *Physical Review Letters*, no. 8, p. 086 105, 2004.

[84] N. Kumar, P. R. C. Kent, D. J. Wesolowski, and J. D. Kubicki, "Modeling water adsorption on rutile (110) using van der waals density functional and DFT+U methods," *Journal of Physical Chemistry C*, vol. 117, no. 45, pp. 23 638–23 644, 2013.

[85] C. L. Pang, R. Lindsay, and G. Thornton, "Structure of clean and adsorbate-covered single-crystal rutile TiO_2surfaces," *Chemical Reviews*, vol. 113, no. 6, pp. 3887–3948, 2013.

[86] S. Benkoula, O. Sublemontier, M. Patanen, C. Nicolas, F. Sirotti, A. Naitabdi, F. Gaie-Levrel, E. Antonsson, D. Aureau, F.-X. Ouf, S.-I. Wada, A. Etcheberry, K. Ueda, and C. Miron, "Water adsorption on TiO_2 surfaces probed by soft X-ray spectroscopies: bulk materials vs. isolated nanoparticles," *Scientific Reports*, vol. 5, no. January, p. 15 088, 2015.

[87] P. Lindan, N. Harrison, J. Holender, and M. Gillan, "First-principles molecular dynamics simulation of water dissociation on TiO_2 (110)," *Chemical Physics Letters*, vol. 261, no. 3, pp. 246–252, 1996.

[88] S. Bates, G Kresse, and M. Gillan, "The adsorption and dissociation of ROH molecules on TiO_2(110)," *Surface Science*, vol. 409, no. 2, pp. 336–349,

[89] R. Schaub, P. Thostrup, N. Lopez, E. Lægsgaard, I. Stensgaard, J. K. Nørskov, and F. Besenbacher, "Oxygen vacancies as active sites for water dissociation on rutile TiO 2 (110)," *Phys. Rev. Lett.*, vol. 87, no. 26, 2001.

[90] P. J. D. Lindan and C. Zhang, "Exothermic water dissociation on the rutileTiO2(110)surface," *Physical Review B*, vol. 72, no. 7, 2005.

[91] P. M. Kowalski, B. Meyer, and D. Marx, "Composition, structure, and stability of the rutile TiO_2(110)surface: Oxygen depletion, hydroxylation, hydrogen migration, and water adsorption," *Physical Review B*, vol. 79, no. 11, 2009.

[92] L. E. Walle, A. Borg, P. Uvdal, and A. Sandell, "Experimental evidence for mixed dissociative and molecular adsorption of water on a rutile TiO_2 (110) surface without oxygen vacancies," *Physical Review B*, vol. 80, no. 23, p. 235 436, 2009.

[93] M. A. Henderson, "An HREELS and TPD study of water on TiO_2(110): the extent of molecular versus dissociative adsorption," *Surface Science*, vol. 355, no. 1-3, pp. 151–166, 1996.

[94] S Krischok, O Höfft, J Günster, J Stultz, D. Goodman, and V Kempter, "H_2O interaction with bare and li-precovered TiO_2: Studies with electron spectroscopies (MIES and UPS(HeI and II))," *Surface Science*, vol. 495, no. 1-2, pp. 8–18, 2001.

[95] G. Ketteler, S. Yamamoto, H. Bluhm, K. Andersson, D. E. Starr, D. F. Ogletree, H. Ogasawara, A. Nilsson, and M. Salmeron, "The nature of water nucleation sites on TiO_2(110) surfaces revealed by ambient pressure x-ray photoelectron spectroscopy," *The Journal of Physical Chemistry C*, vol. 111, no. 23, pp. 8278–8282, 2007.

[96] M. B. Hugenschmidt, L. Gamble, and C. T. Campbell, "The interaction of H_2O with a TiO_2(110) surface," *Surface Science*, vol. 302, no. 3, pp. 329–340, 1994.

[97] K. ichi Ishibashi, A. Fujishima, T. Watanabe, and K. Hashimoto, "Quantum yields of active oxidative species formed on TiO_2 photocatalyst," *Journal of Photochemistry and Photobiology A: Chemistry*, vol. 134, no. 1-2, pp. 139–142, 2000.

[98] Q. Xiang, J. Yu, and P. K. Wong, "Quantitative characterization of hydroxyl radicals produced by various photocatalysts," *Journal of Colloid and Interface Science*, vol. 357, no. 1, pp. 163–167, 2011.

[99] J. Yan, G. Wu, N. Guan, L. Li, Z. Li, and X. Cao, "Understanding the effect of surface/bulk defects on the photocatalytic activity of TiO_2: Anatase versus rutile," *Physical Chemistry Chemical Physics*, vol. 15, no. 26, p. 10 978, 2013.

[100] G Lu, a Linsebigler, and J. T. Yates, "Ti^{3+} Defect Sites on TiO_2(110): Production and Chemical Detection of Active Sites," *Journal of Physical Chemistry*, vol. 98, no. 45, pp. 11 733–11 738, 1994.

[101] C. N. Rusu and J. T. Yates, "Photochemistry of NO Chemisorbed on TiO_2 (110) and TiO_2 Powders," *The journal of physical chemistry. B*, vol. 104, no. 8, pp. 1729–1737, 2000.

[102] C. N. Rusu and J. T. Yates Jr., "N_2O Adsorption and Photochemistry on High Area TiO_2 Powder," *J. Phys. Chem. B*, vol. 105, no. 13, pp. 2596–2603, 2001.

[103] D. Stodt, H. Noei, C. Hättig, and Y. Wang, "A combined experimental and computational study on the adsorption and reactions of NO on rutile TiO_2.," *Physical chemistry chemical physics : PCCP*, vol. 15, no. 2, pp. 466–72, 2013.

[104] D. Sorescu, C. Rusu, and J. Yates, "Adsorption of NO on the TiO_2 (110) Surface: An Experimental and Theoretical Study," *The Journal of Physical Chemistry B*, vol. 2, no. 110, pp. 4408–4417, 2000.

[105] D. Cheng, J. Lan, D. Cao, and W. Wang, "Adsorption and dissociation of ammonia on clean and metal-covered TiO_2 rutile (110) surfaces: A comparative DFT study," *Applied Catalysis B: Environmental*, vol. 106, no. 3-4, pp. 510–519, 2011.

[106] U. Diebold, "The surface science of titanium dioxide," *Surface Science Reports*, vol. 48, no. 5-8, pp. 53–229, 2003.

[107] Á. B. Höskuldsson, Y. Abghoui, A. B. Gunnarsdóttir, and E. Skúlason, "Computational screening of rutile oxides for electrochemical ammonia formation," *ACS Sustainable Chemistry & Engineering*, vol. 5, no. 11, pp. 10 327–10 333, 2017.

[108] X.-Y. Xie, Q. Wang, W.-H. Fang, and G. Cui, "DFT study on reaction mechanism of nitric oxide to ammonia and water on a hydroxylated rutile TiO_2(110) surface," *The Journal of Physical Chemistry C*, vol. 121, no. 30, pp. 16 373–16 380, 2017.

[109] I. Onal, S. Soyer, and S. Senkan, "Adsorption of water and ammonia on TiO_2-anatase cluster models," *Surface Science*, vol. 600, no. 12, pp. 2457–2469, 2006.

[110] R. Erdogan, O. Ozbek, and I. Onal, "A periodic DFT study of water and ammonia adsorption on anatase TiO_2 (001) slab," *Surface Science*, vol. 604, no. 11-12, pp. 1029–1033, 2010.

[111] R. Erdogan and I. Onal, "An ONIOM and DFT study of water and ammonia adsorption on anatase TiO_2 (001) cluster," *International Journal of Quantum Chemistry*, vol. 111, no. 9, pp. 2149–2159, 2011.

[112] A. Markovits, J. Ahdjoudj, and C. Minot, "A theoretical analysis of NH3 adsorption on TiO_2," *Surface Science*, vol. 365, no. 3, pp. 649–661, 1996.

[113] Y. Ji and Y. Luo, "First-Principles Study on the Mechanism of Photoselective Catalytic Reduction of NO by NH_3 on Anatase TiO_2(101) Surface," *Journal of Physical Chemistry C*, vol. 118, no. 12, 6359–6364, 2014.

[114] X. jing Guo, W. Liu, W. Fang, L. Cai, Y. Zhu, L. Lu, and X. Lu, "DFT study of coverage-depended adsorption of NH3 on TiO_2-b (100) surface," *Physical Chemistry Chemical Physics*, vol. 14, no. 48, p. 16 618, 2012.

[115] B. Kim, Z. Dohnálek, J. Szanyi, B. D. Kay, and Y. K. Kim, "Temperature-programmed desorption study of NO reactions on rutile TiO_2(110)-1x1," *Surface Science*, vol. 652, pp. 148–155, 2016.

[116] B. Kim, Z. Li, B. D. Kay, Z. Dohnálek, and Y. K. Kim, "Low-Temperature Desorption of N 2 O from NO on Rutile TiO 2 (110)-1 x 1," *The Journal of Physical Chemistry C*, vol. 118, no. 18, pp. 9544–9550, 2014.

[117] B. Karunagaran, P. Uthirakumar, S. Chung, S. Velumani, and E.-K. Suh, "TiO_2 thin film gas sensor for monitoring ammonia," *Materials Characterization*, vol. 58, no. 8-9, pp. 680–684, 2007.

[118] S. Suganuma, Y. Murakami, J. Ohyama, T. Torikai, K. Okumura, and N. Katada, "Assignments of bending vibrations of ammonia adsorbed on surfaces of metal oxides," *Catalysis Letters*, vol. 145, no. 10, pp. 1904–1912, 2015.

[119] G Busca, "Chemical and mechanistic aspects of the selective catalytic reduction of NOx by ammonia over oxide catalysts: A review," *Applied Catalysis B: Environmental*, vol. 18, no. 1-2, pp. 1–36, 1998.

[120] G. Ramis, G. Busca, V. Lorenzelli, and P. Forzatti, "Fourier transform infrared study of the adsorption and coadsorption of nitric oxide, nitrogen dioxide and ammonia on TiO_2 anatase," *Applied Catalysis*, vol. 64, pp. 243–257, 1990.

[121] F. Giraud, C. Geantet, N. Guilhaume, S. Gros, L. Porcheron, M. Kanniche, and D. Bianchi, "Experimental Microkinetic Approach of De-NOx by NH_3 on V2O5/ WO3/ TiO_2 Catalysts. 1. Individual Heats of Adsorption of Adsorbed NH_3 Species on a Sulfate-Free TiO_2 Support Using Adsorption Isobars," *Journal of Physical Chemistry C*, vol. 118, no. 29, 15664–15676, 2014.

[122] J. Liu, J. Meeprasert, S. Namuangruk, K. Zha, H. Li, L. Huang, P. Maitarad, L. Shi, and D. Zhang, "Facet–activity relationship of TiO_2 in fe2o3/TiO_2 nanocatalysts for selective catalytic reduction of NO with NH3: In situ DRIFTs and DFT studies," *The Journal of Physical Chemistry C*, vol. 121, no. 9, pp. 4970–4979, 2017.

[123] N.-Y. Topsoe, "Mechanism of the selective catalytic reduction of nitric oxide by ammonia elucidated by in situ on-line fourier transform infrared spectroscopy," *Science*, vol. 265, no. 5176, pp. 1217–1219, 1994.

[124] T Tanaka, K Teramura, K Arakaki, and T Funabiki, "Photoassisted NO reduction with NH_3 over TiO_2 photocatalyst," *Chemical Communications*, no. 22, 2742–2743, 2002.

[125] K Teramura, T Tanaka, and T Funabiki, "EPR study of photoinduced electron transfer between adsorbent and adsorbed species in photo-SCR with NH_3," *Chemistry Letters*, vol. 32, no. 12, 1184–1185, 2003.

[126] K Teramura, T Tanaka, S Yamazoe, K Arakaki, and T Funabiki, "Kinetic study of photo-SCR with NH_3 over TiO_2," *Applied Catalysis B-Environmental*, vol. 53, no. 1, 29–36, 2004.

[127] S Yamazoe, T Okumura, K Teramura, and T Tanaka, "Development of the efficient TiO_2 photocatalyst in photoassisted selective catalytic reduction of NO with NH_3," *Catalysis Today*, vol. 111, no. 3-4, 266–270, 2006, 10th Japan-Korea Symposium on Catalysis, Matsue, JAPAN, MAY 10-12, 2005.

[128] S. Yamazoe, K. Teramura, Y. Hitomi, T. Shishido, and T. Tanaka, "Visible light absorbed NH2 species derived from NH_3 adsorbed on TiO_2 for photoassisted selective catalytic reduction," *Journal of Physical Chemistry C*, vol. 111, no. 38, 14189–14197, 2007.

[129] A. Yamamoto, Y. Mizuno, K. Teramura, T. Shishido, and T. Tanaka, "Effects of reaction temperature on the photocatalytic activity of photo-SCR of NO with NH_3 over a TiO_2 photocatalyst," *CATALYSIS SCIENCE & TECHNOLOGY*, vol. 3, no. 7, 1771–1775, 2013.

[130] J. Lasek, Y.-H. Yu, and J. C. S. Wu, "Removal of NOx by photocatalytic processes," *Journal of Photochemistry and Photobiology C-Photochemistry Reviews*, vol. 14, 29–52, 2013.

[131] S. Z. Andersen, V. Čolić, S. Yang, J. A. Schwalbe, A. C. Nielander, J. M. McEnaney, K. Enemark-Rasmussen, J. G. Baker, A. R. Singh, B. A. Rohr, M. J. Statt, S. J. Blair, S. Mezzavilla, J. Kibsgaard, P. C. K. Vesborg, M. Cargnello, S. F. Bent, T. F. Jaramillo, I. E. L. Stephens, J. K. Nørskov, and I. Chorkendorff, "A rigorous electrochemical ammonia synthesis protocol with quantitative isotope measurements," *Nature*, vol. 570, no. 7762, pp. 504–508, 2019.

[132] V Augugliaro, A Lauricella, L Rizzuti, M Schiavello, and A Sclafani, "Conversion of solar energy to chemical energy by photoassisted processes—I. Preliminary results on ammonia production over doped titanium dioxide catalysts in a fluidized bed reactor," *Int. J. Hydrogen Energy*, vol. 7, no. 11, pp. 845–849, 1982.

[133] J. Soria, J. C. Conesa, V. Augugliaro, L. Palmisano, M. Schiavello, and A. Sclafani, "Dinitrogen photoreduction to ammonia over titanium dioxide powders doped with ferric ions," *J. Phys. Chem.*, vol. 95, no. 1, pp. 274–282, 1991.

[134] G. N. Schrauzer, "Photoreduction of Nitrogen on TiO_2 and TiO_2-Containing Minerals," in *Energy Efficiency and Renewable Energy Through Nanotechnology*, Springer, 2011, pp. 601–623.

[135] C. Li, T. Wang, Z.-J. Zhao, W. Yang, J.-F. Li, A. Li, Z. Yang, G. A. Ozin, and J. Gong, "Promoted fixation of molecular nitrogen with surface oxygen vacancies

on plasmon-enhanced TiO_2 photoelectrodes," *Angewandte Chemie International Edition*, 2018.

[136] P. P. Radford and C. G. Francis, "Photoreduction of nitrogen by metal doped titanium dioxide powders: A novel use for metal vapour techniques," *Journal of the Chemical Society, Chemical Communications*, no. 24, p. 1520, 1983.

[137] J. G. Edwards, J. A. Davies, D. L. Boucher, and A. Mennad, "An Opinion on the Heterogeneous Photoreactions of N2 with H2O," *Angew. Chem. Int. Ed.*, vol. 31, no. 4, pp. 480–482, 1992.

[138] J. A. Davies and J. G. Edwards, "Reply: Standards of Demonstration for the Heterogeneous Photoreactions of N2 with H2O," *Angew. Chem. Int. Ed.*, vol. 32, no. 4, pp. 552–553, 1993.

[139] D. L. Boucher, J. A. Davies, J. G. Edwards, and A. Mennad, "An investigation of the putative photosynthesis of ammonia on iron-doped titania and other metal oxides," *Journal of Photochemistry and Photobiology A: Chemistry*, vol. 88, no. 1, pp. 53–64, 1995.

[140] J. A. Davies, D. L. Boucher, and J. G. Edwards, "The question of artificial photosynthesis of ammonia on heterogeneous catalysts," in *Advances in Photochemistry*, John Wiley & Sons, Inc., 1995, pp. 235–310.

[141] G. N. Schrauzer, N. Strampach, L. N. Hui, M. R. Palmer, and J. Salehi, "Nitrogen photoreduction on desert sands under sterile conditions," *Proc. Natl. Acad. Sci. U.S.A.*, vol. 80, no. 12, pp. 3873–3876, 1983.

[142] Y. Huang, W. Ho, S. Lee, L. Zhang, G. Li, and J. C. Yu, "Effect of carbon doping on the mesoporous structure of nanocrystalline titanium dioxide and its solar-light-driven photocatalytic degradation of NOx," *Langmuir*, vol. 24, no. 7, pp. 3510–3516, 2008.

[143] A. Hellman and B. Wang, "First-Principles View on Photoelectrochemistry: Water-Splitting as Case Study," *Inorganics*, vol. 5, no. 2, p. 37, 2017.

[144] Y. Zhao, R. Shi, X. Bian, C. Zhou, Y. Zhao, S. Zhang, F. Wu, G. I. N. Waterhouse, L.-Z. Wu, C.-H. Tung, and T. Zhang, "Ammonia detection methods in photocatalytic and electrocatalytic experiments: How to improve the reliability of NH_3 production rates?" *Advanced Science*, p. 1 802 109, 2019.

[145] L. F. Greenlee, J. N. Renner, and S. L. Foster, "The use of controls for consistent and accurate measurements of electrocatalytic ammonia synthesis from dinitrogen," *ACS Catalysis*, vol. 8, no. 9, pp. 7820–7827, 2018.

[146] X. Gao, Y. Wen, D. Qu, L. An, S. Luan, W. Jiang, X. Zong, X. Liu, and Z. Sun, "Interference effect of alcohol on nessler's reagent in photocatalytic nitrogen fixation," *ACS Sustainable Chemistry & Engineering*, vol. 6, no. 4, pp. 5342–5348, 2018.

[147] X. Cui, C. Tang, and Q. Zhang, "A review of electrocatalytic reduction of dinitrogen to ammonia under ambient conditions," *Advanced Energy Materials*, vol. 8, no. 22, p. 1 800 369, 2018.

[148] B. H. R. Suryanto, H.-L. Du, D. Wang, J. Chen, A. N. Simonov, and D. R. MacFarlane, "Challenges and prospects in the catalysis of electroreduction of nitrogen to ammonia," *Nature Catalysis*, 2019.

[149] S. Licht, B. Cui, B. Wang, F.-F. Li, J. Lau, and S. Liu, "Ammonia synthesis by n2 and steam electrolysis in molten hydroxide suspensions of nanoscale fe2o3," *Science*, vol. 345, no. 6197, pp. 637–640, 2014.

[150] W. Zhao, J. Zhang, X. Zhu, M. Zhang, J. Tang, M. Tan, and Y. Wang, "Enhanced nitrogen photofixation on fe-doped TiO_2 with highly exposed (101) facets in the presence of ethanol as scavenger," *Applied Catalysis B: Environmental*, vol. 144, pp. 468–477, 2014.

[151] S. Wang, X. Hai, X. Ding, K. Chang, Y. Xiang, X. Meng, Z. Yang, H. Chen, and J. Ye, "Photocatalysis: Light-switchable oxygen vacancies in ultrafine bi5 o7 br nanotubes for boosting solar-driven nitrogen fixation in pure water (adv. mater. 31/2017)," *Advanced Materials*, vol. 29, no. 31, 2017.

[152] O. Linnik and H. Kisch, "On the mechanism of nitrogen photofixation at nanostructured iron titanate films," *Photochemical & Photobiological Sciences*, vol. 5, no. 10, p. 938, 2006.

[153] M. Andersen, A. J. Medford, J. K. Nørskov, and K. Reuter, "Analyzing the case for bifunctional catalysis," *Angewandte Chemie International Edition*, vol. 55, no. 17, pp. 5210–5214, 2016.

[154] D. J. C. MacKay, "Solar energy in the context of energy use, energy transportation and energy storage," *Philosophical Transactions of the Royal Society A: Mathematical, Physical and Engineering Sciences*, vol. 371, no. 1996, pp. 20 110 431–20 110 431, 2013.

[155] P. G. Levi and J. M. Cullen, "Mapping global flows of chemicals: From fossil fuel feedstocks to chemical products," *Environmental Science & Technology*, vol. 52, no. 4, pp. 1725–1734, 2018.

[156] M. Yousaf, J. Li, J. Lu, T. Ren, R. Cong, S. Fahad, and X. Li, "Effects of fertilization on crop production and nutrient-supplying capacity under rice-oilseed rape rotation system," *Scientific Reports*, vol. 7, no. 1, pp. 1–9, 2017.

[157] E. J. Vicente and D. R. Dean, "Keeping the nitrogen-fixation dream alive," *Proceedings of the National Academy of Sciences*, vol. 114, no. 12, pp. 3009–3011, 2017.

[158] K. C. MacLeod and P. L. Holland, "Recent developments in the homogeneous reduction of dinitrogen by molybdenum and iron," *Nature Chemistry*, vol. 5, no. 7, pp. 559–565, 2013.

[159] B. Bar-Yosef, "Advances in fertigation," in *Advances in Agronomy*, Elsevier, 1999, pp. 1–77.

[160] U. Kafkafi, *Fertigation: a tool for efficient fertilizer and water management*. Paris (28 rue Marbeuf, 75008) Horgen (Switzerland: International fertilizer industry Association International potash Institute, 2011, ISBN: 978-2-9523139-8-8.

[161] FAOSTAT, *Cropland*, Web Database, Data retrieved from FAOSTAT: `http://www.fao.org/faostat/en/#data/RL`, 2019.

[162] FAO, *The state of food and agriculture: Innovation in family farming*, Rome, Italy, 2014.

[163] S. K. Lowder, J. Skoet, and T. Raney, "The number, size, and distribution of farms, smallholder farms, and family farms worldwide," *World Development*, vol. 87, pp. 16–29, 2016.

[164] P. M. Berthouex, "Evaluating economy of scale," *Journal (Water Pollution Control Federation)*, vol. 44, no. 11, pp. 2111–2119, 1972.

[165] Northern Plains Nitrogen, *Northern plains nitrogen to construct $1.5 billion nitrogen fertilizer production facility northwest of grand forks*, Press Release, 2013.

[166] R Sommer, D Bossio, L Desta, J Dimes, J Kihara, S Koala, N Mango, D Rodriguez, C Thierfelder, and L Winowiecki, *Profitable and sustainable nutrient management systems for east and southern african smallholder farming systems challenges and opportunities: A synthesis of the eastern and southern africa situation in terms of past experiences, present and future opportunities in promoting nutrients use in africa*, 2013.

[167] W. Huang, "Impact of Rising Natural Gas Prices on U . S . Ammonia Supply," *Management*, vol. WRS-0702, WRS–0702, 2007.

[168] X. L. Etienne, A. Trujillo-Barrera, and S. Wiggins, "Price and volatility transmissions between natural gas, fertilizer, and corn markets," *Agricultural Finance Review*, vol. 76, no. 1, pp. 151–171, 2016.

[169] K. S. A. Czuppon T. A. and J. M. Rovner, "Ammonia," in *Kirk-Othmer Encyclopedia of Chemical Technology*, John Wiley & Sons, Inc., 2000, ISBN: 9780471238966. eprint: https://onlinelibrary.wiley.com/doi/pdf/10.1002/0471238961.0113131503262116.a01.

[170] *Fertilizer manual*. Dordrecht Norwell, MA Vienna, Austria Muscle Shoals, Ala: Kluwer Academic in cooperation with UNIDO IFDC, 1998, ISBN: 978-0-7923-5032-3.

[171] M. Wanzala and R. Groot, "Fertilizer market development in sub-saharian Africa," *Conference International Fertiliser Society*, vol. 4, no. May, pp. 12–14, 2013.

[172] J. N. Chianu, J. N. Chianu, and F. Mairura, "Mineral fertilizers in the farming systems of sub-saharan africa. a review," *Agronomy for Sustainable Development*, vol. 32, no. 2, pp. 545–566, 2011.

[173] P.A. Fuentes, B. Bumb, and M. Johnson, "Improving fertilizer markets in west africa: The fertilizer supply chain in senegal," International Fertilizer Development Center and International Food Policy Research Institute, Muscle Shoals, Alabama, Tech. Rep., 2012, pp. 17–18.

[174] ——, "International fertilizer development center and international food policy research institute," US Agency for International Development and International Fertilizer Development Center, Muscle Shoals, Alabama, Tech. Rep., 2012.

[175] ——, "Improving fertilizer markets in west africa: The fertilizer supply chain in nigeria," International Fertilizer Development Center and International Food Policy Research Institute, Muscle Shoals, Alabama, Tech. Rep., 2012.

[176] B. L. Bumb, M. E. Johnson, P. A. Fuentes, "Policy options for improving regional fertilizer markets in west africa," International Food Policy Research Institute and International Fertilizer Development Center, Washington DC, Discussion Paper 01084, 2011, p. 40.

[177] P. A. Fuentes, "Transitioning from government control to a larger private sector participation in the ghanaian fertilizer market," US Agency for International Development and International Fertilizer Development Center, Muscle Shoals, Alabama, Policy Brief, 2018.

[178] FAO, IFAD, UNICEF, WFP and WHO, *The state of food security and nutrition in the world 2017. building resilience for peace and food security.* Rome, Italy, 2017.

[179] *Urea price in ghana 2017*, Web Database, https://africafertilizer.org/ghana/#tab-id-3, 2017.

[180] T. Weyrauch and C. Herstatt, "What is frugal innovation? three defining criteria," *Journal of Frugal Innovation*, vol. 2, no. 1, 2016.

[181] J. Lonnen, S. Kilvington, S. Kehoe, F. Al-Touati, and K. McGuigan, "Solar and photocatalytic disinfection of protozoan, fungal and bacterial microbes in drinking water," *Water Research*, vol. 39, no. 5, pp. 877–883, 2005.

[182] K. G. McGuigan, R. M. Conroy, H.-J. Mosler, M. du Preez, E. Ubomba-Jaswa, and P. Fernandez-Ibañez, "Solar water disinfection (SODIS): A review from bench-top to roof-top," *Journal of Hazardous Materials*, vol. 235-236, pp. 29–46, 2012.

[183] Argus, "Argus monthly urea outlook 2018," Argus Media Group, London UK, Tech. Rep. Issue 18-8, 2018, p. 9.

[184] T Grundt, "Hydrogen by water electrolysis as basis for small scale ammonia production. a comparison with hydrocarbon based technologies," *International Journal of Hydrogen Energy*, vol. 7, no. 3, pp. 247–257, 1982.

[185] P. H. Pfromm, "Towards sustainable agriculture: Fossil-free ammonia," *Journal of Renewable and Sustainable Energy*, vol. 9, no. 3, p. 034 702, 2017.

[186] J. Lehmann, "Bio-energy in the black," *Frontiers in Ecology and the Environment*, vol. 5, no. 7, pp. 381–387, 2007.

[187] ——, "A handful of carbon," *Nature*, vol. 447, no. 7141, pp. 143–144, 2007.

[188] B. Glaser, J. Lehmann, and W. Zech, "Ameliorating physical and chemical properties of highly weathered soils in the tropics with charcoal - A review," *Biology and Fertility of Soils*, vol. 35, no. 4, pp. 219–230, 2002. arXiv: `bk-21`.

[189] M. M. Wright, J. A. Satrio, R. C. Brown, D. E. Daugaard, and D. D. Hsu, "Techno-economic analysis of biomass fast pyrolysis to transportation fuels," Tech. Rep., 2010.

[190] S. P. Galinato, J. K. Yoder, and D. Granatstein, "The economic value of biochar in crop production and carbon sequestration," *Energy Policy*, vol. 39, no. 10, pp. 6344–6350, 2011.

[191] Y. Bicer and I. Dincer, "Exergoeconomic analysis and optimization of a concentrated sunlight-driven integrated photoelectrochemical hydrogen and ammonia production system," *International Journal of Hydrogen Energy*, 2018.

[192] ——, "Assessment of a sustainable electrochemical ammonia production system using photoelectrochemically produced hydrogen under concentrated sunlight," *ACS Sustainable Chemistry & Engineering*, vol. 5, no. 9, pp. 8035–8043, 2017.

[193] B. L. Keeler, J. D. Gourevitch, S. Polasky, F. Isbell, C. W. Tessum, J. D. Hill, and J. D. Marshall, "The social costs of nitrogen," *Science advances*, vol. 2, no. 10, e1600219, 2016.

[194] B. L. Meyer and N. S. Shepherd, "Nutrient balance and nitrogen cycling in a multi-stage, multispecies space farm," in *AIAA SPACE 2016*, American Institute of Aeronautics and Astronautics, 2016.

[195] M. J. Unkovich, J. Baldock, and M. B. Peoples, "Prospects and problems of simple linear models for estimating symbiotic N_2 fixation by crop and pasture legumes," *Plant and Soil*, vol. 329, no. 1-2, pp. 75–89, 2009.

[196] D. F. Herridge, M. B. Peoples, and R. M. Boddey, "Global inputs of biological nitrogen fixation in agricultural systems," *Plant and Soil*, vol. 311, no. 1-2, pp. 1–18, 2008.

[197] M. Goyal, *Water and fertigation management in micro irrigation*. Oakville, ON: Apple Academic Press, 2016, ISBN: 978-1-4987-2003-8.

[198] D. M. Kadyampakeni, K. T. Morgan, P. Nkedi-Kizza, and G. N. Kasozi, "Nutrient management options for florida citrus: A review of NPK application and analytical methods," *Journal of plant nutrition*, vol. 38, no. 4, pp. 568–583, 2015.

[199] K. T. Morgan, T. A. Wheaton, W. S. Castle, and L. R. Parsons, "Response of young and maturing citrus trees grown on a sandy soil to irrigation scheduling, nitrogen fertilizer rate, and nitrogen application method," *HortScience*, vol. 44, no. 1, pp. 145–150, 2009.

[200] M. J. Mohammad and S. Zuraiqi, "Enhancement of yield and nitrogen and water use efficiencies by nitrogen drip-fertigation of garlic," *Journal of Plant Nutrition*, vol. 26, no. 9, pp. 1749–1766, 2002.

[201] Z. Feng, Y. Kang, S. Wan, and S. Liu, "Effect of drip fertigation on potato productivity with basal application of loss control fertilizer in sandy soil," *Irrigation and Drainage*, vol. 67, no. 2, pp. 210–221, 2017.

[202] L. E. Willis, F. S. Davies, and D. A. Graetz, "Fertigation and Growth of Young Hamlin Orange Trees in Florida," *Hortscience*, vol. 26, no. 2, pp. 106–109, 1991.

[203] D. R. Bryla, E. Dickson, R. Shenk, R. S. Johnson, C. H. Crisosto, and T. J. Trout, "Influence of irrigation method and scheduling on patterns of soil and tree water

status and its relation to yield and fruit quality in peach," *HortScience*, vol. 40, no. 7, pp. 2118–2124, 2005.

[204] A. Phocaides, "Fertigation," in *Handbook on pressurized irrigation techniques*, Rome, Italy: Food and Agriculture Organization of the United Nations, 2007, ch. 16, ISBN: 978-92-5-105817-6.

[205] I. Papadopoulos, "Nitrogen fertigation of trickle-irrigated potato," *Fertilizer Research*, vol. 16, no. 2, pp. 157–167, 1988.

[206] L. You, C. Ringler, U. Wood-Sichra, R. Robertson, S. Wood, T. Zhu, G. Nelson, Z. Guo, and Y. Sun, "What is the irrigation potential for africa? a combined biophysical and socioeconomic approach," *Food Policy*, vol. 36, no. 6, pp. 770–782, 2011.

[207] M. Gonçalves, L. Sánchez-García, E. de Oliveira Jardim, J. Silvestre-Albero, and F. Rodríguez-Reinoso, "Ammonia removal using activated carbons: Effect of the surface chemistry in dry and moist conditions," *Environmental Science & Technology*, vol. 45, no. 24, pp. 10 605–10 610, 2011.

[208] J. Heckman, "A history of organic farming: Transitions from sir albert howard's war in the soil to USDA national organic program," *Renewable Agriculture and Food Systems*, vol. 21, no. 3, 143–150, 2006.

[209] Y. Li, F. Zhang, M. Yang, J. Zhang, and Y. Xie, "Impacts of biochar application rates and particle sizes on runoff and soil loss in small cultivated loess plots under simulated rainfall," *Science of the Total Environment*, vol. 649, pp. 1403–1413, 2018.

[210] E. Chidumayo, "Effects of wood carbonization on soil and initial development of seedlings in miombo woodland, zambia," *Forest Ecology and Management*, vol. 70, no. 1-3, pp. 353–357, 1994.

[211] W. Ye, "Application of near-infrared spectroscopy for determination of nutrient contents in manure," PhD thesis, Iowa State University, 2003.

[212] M. P. McHenry, "Agricultural bio-char production, renewable energy generation and farm carbon sequestration in Western Australia: Certainty, uncertainty and risk," *Agriculture, Ecosystems and Environment*, vol. 129, no. 1-3, pp. 1–7, 2009.

[213] M. Y. Naz and S. A. Sulaiman, "Slow release coating remedy for nitrogen loss from conventional urea: A review," *Journal of Controlled Release*, vol. 225, pp. 109–120, 2016.

[214] D. J. Conley, H. W. Paerl, R. W. Howarth, D. F. Boesch, S. P. Seitzinger, K. E. Havens, C. Lancelot, and G. E. Likens, "ECOLOGY: Controlling eutrophication: Nitrogen and phosphorus," *Science*, vol. 323, no. 5917, pp. 1014–1015, 2009.

[215] J. Shindo, K. Okamoto, and H. Kawashima, "Prediction of the environmental effects of excess nitrogen caused by increasing food demand with rapid economic growth in eastern asian countries, 1961–2020," *Ecological Modelling*, vol. 193, no. 3-4, pp. 703–720, 2006.

[216] A. R. Ravishankara, J. S. Daniel, and R. W. Portmann, "Nitrous oxide (N_2O): The dominant ozone-depleting substance emitted in the 21st century," *Science*, vol. 326, no. 5949, pp. 123–125, 2009.

[217] J. Angle, *Role of fertilisers for climate-resilient agriculture / by J.S. Angle, U. Singh, C.O. Dimkpa, D. Hellums and P.S. Bindraban*. Colchester: International Fertiliser Society, 2017, ISBN: 978-0-85310-439-1.

[218] M. Flink, R. Pettersson, and O. Andrén, "Growth dynamics of winter wheat in the field with daily fertilization and irrigation," *Journal of Agronomy and Crop Science*, vol. 174, no. 4, pp. 239–252, 1995.

[219] N. D. McDaniel and S. Bernhard, "Solar fuels: Thermodynamics, candidates, tactics, and figures of merit," *Dalton Transactions*, vol. 39, no. 42, p. 10 021, 2010.

[220] J. Highfield, "Advances and recent trends in heterogeneous photo(electro)-catalysis for solar fuels and chemicals," *Molecules*, vol. 20, no. 4, pp. 6739–6793, 2015.

[221] S. J. Davis, N. S. Lewis, M. Shaner, S. Aggarwal, D. Arent, I. L. Azevedo, S. M. Benson, T. Bradley, J. Brouwer, Y.-M. Chiang, C. T. M. Clack, A. Cohen, S. Doig, J. Edmonds, P. Fennell, C. B. Field, B. Hannegan, B.-M. Hodge, M. I. Hoffert, E. Ingersoll, P. Jaramillo, K. S. Lackner, K. J. Mach, M. Mastrandrea, J. Ogden, P. F. Peterson, D. L. Sanchez, D. Sperling, J. Stagner, J. E. Trancik, C.-J. Yang, and K. Caldeira, "Net-zero emissions energy systems," *Science*, vol. 360, no. 6396, 2018. eprint: `http://science.sciencemag.org/content/360/6396/eaas9793.full.pdf`.

[222] J. A. Herron, J. Kim, A. A. Upadhye, G. W. Huber, and C. T. Maravelias, "A general framework for the assessment of solar fuel technologies," *Energy & Environmental Science*, vol. 8, no. 1, pp. 126–157, 2015.

[223] A. Nakamura, Y. Ota, K. Koike, Y. Hidaka, K. Nishioka, M. Sugiyama, and K. Fujii, "A 24.4% solar to hydrogen energy conversion efficiency by combining concentrator photovoltaic modules and electrochemical cells," *Applied Physics Express*, vol. 8, no. 10, p. 107 101, 2015.

[224] J. Jia, L. C. Seitz, J. D. Benck, Y. Huo, Y. Chen, J. W. D. Ng, T. Bilir, J. S. Harris, and T. F. Jaramillo, "Solar water splitting by photovoltaic-electrolysis with a solar-to-hydrogen efficiency over 30%," *Nature Communications*, vol. 7, no. 1, 2016.

[225] Y. Liu, Y. Su, X. Quan, X. Fan, S. Chen, H. Yu, H. Zhao, Y. Zhang, and J. Zhao, "Facile Ammonia Synthesis from Electrocatalytic N_2 Reduction under Ambient Conditions on N-Doped Porous Carbon," *ACS Catalysis*, acscatal.7b02165, 2018.

[226] W. Qiu, X.-Y. Xie, J. Qiu, W.-H. Fang, R. Liang, X. Ren, X. Ji, G. Cui, A. M. Asiri, G. Cui, B. Tang, and X. Sun, "High-performance artificial nitrogen fixation at ambient conditions using a metal-free electrocatalyst," *Nature Communications*, vol. 9, no. 1, 2018.

[227] R. Zhang, X. Ren, X. Shi, F. Xie, B. Zheng, X. Guo, and X. Sun, "Enabling effective electrocatalytic N_2 conversion to NH_3 by the TiO_2 nanosheets array under ambient conditions," *ACS Applied Materials & Interfaces*, vol. 10, no. 34, pp. 28 251–28 255, 2018.

[228] H. S. Burney, "Membrane chlor-alkali process," in *Modern Aspects of Electrochemistry*, R. E. White, B. E. Conway, and J. O. Bockris, Eds., Boston, MA: Springer US, 1993, pp. 393–438, ISBN: 978-1-4615-3022-0.

[229] R Leroy, "Industrial water electrolysis: Present and future," *International Journal of Hydrogen Energy*, vol. 8, no. 6, pp. 401–417, 1983.

[230] "Proton OnSite MW electrolyser passes half-million cell hours," *Fuel Cells Bulletin*, vol. 2016, no. 2, p. 8, 2016.

[231] K. L. Hardee and A. J. Bard, "Semiconductor electrodes V. the application of chemically vapor deposited iron oxide films to photosensitized electrolysis," *Journal of The Electrochemical Society*, vol. 123, no. 7, pp. 1024–1026, 1976.

[232] M. Birnie, S. Riffat, and M. Gillott, "Photocatalytic reactors: design for effective air purification," *International Journal of Low-Carbon Technologies*, vol. 1, no. 1, pp. 47–58, 2006.

[233] D. S. Bhatkhande, V. G. Pangarkar, and A. A. Beenackers, "Photocatalytic degradation for environmental applications - a review," *Journal of Chemical Technology & Biotechnology*, vol. 77, no. 1, pp. 102–116, 2001.

[234] I. P. Parkin and R. G. Palgrave, "Self-cleaning coatings," *Journal of Materials Chemistry*, vol. 15, no. 17, p. 1689, 2005.

[235] L. C. Seitz, Z. Chen, A. J. Forman, B. A. Pinaud, J. D. Benck, and T. F. Jaramillo, "Modeling practical performance limits of photoelectrochemical water splitting

based on the current state of materials research," *ChemSusChem*, vol. 7, no. 5, pp. 1372–1385, 2014.

[236] B. Seger, O. Hansen, and P. C. K. Vesborg, "A flexible web-based approach to modeling tandem photocatalytic devices," *Solar RRL*, vol. 1, no. 1, e201600013, 2016.

[237] N. Furuya and H. Yoshiba, "Electroreduction of nitrogen to ammonia on gas-diffusion electrodes modified by fe-phthalocyanine," *Journal of Electroanalytical Chemistry and Interfacial Electrochemistry*, vol. 263, no. 1, pp. 171–174, 1989.

[238] R. Lan, J. T. Irvine, and S. Tao, "Synthesis of ammonia directly from air and water at ambient temperature and pressure," *Scientific reports*, vol. 3, p. 1145, 2013.

[239] L. Wang, M. Xia, H. Wang, K. Huang, C. Qian, C. T. Maravelias, and G. A. Ozin, "Greening ammonia toward the solar ammonia refinery," *Joule*, 2018.

[240] M. Taniguchi, H. Asaoka, and T. Ayuhara, "Energy Saving Air-Separation Plant Based on Exergy Analysis," *Kobelco Technology Review*, no. 33, pp. 34–38, 2015.

[241] T. L. Hardenburger and M. a. Ennis, "Nitrogen," in *Kirk–Othmer Encyclopedia of Chemical Technology*, John Wiley & Sons, Inc, 2005, ISBN: 9780471238966. eprint: `https://onlinelibrary.wiley.com/doi/pdf/10.1002/0471238961.1409201808011804.a01.pub2`.

[242] A. R. Smith and J. Klosek, "A review of air separation technologies and their integration with energy conversion processes," *Fuel Processing Technology*, vol. 70, no. 2, pp. 115–134, 2001.

[243] P. M. Ndegwa, V. K. Vaddella, A. N. Hristov, and H. S. Joo, "Measuring concentrations of ammonia in ambient air or exhaust air stream using acid traps," *Journal of Environment Quality*, vol. 38, no. 2, p. 647, 2009.

[244] S. Yin, K. Chen, C. Srinivasakannan, S. Guo, S. Li, J. Peng, and L. Zhang, "Enhancing recovery of ammonia from rare earth wastewater by air stripping combination of microwave heating and high gravity technology," *Chemical Engineering Journal*, vol. 337, pp. 515–521, 2018.

[245] L. Kinidi, I. A. W. Tan, N. B. A. Wahab, K. F. B. Tamrin, C. N. Hipolito, and S. F. Salleh, "Recent development in ammonia stripping process for industrial wastewater treatment," *International Journal of Chemical Engineering*, vol. 2018, pp. 1–14, 2018.

[246] A. Hasanoğlu, J. Romero, B. Pérez, and A. Plaza, "Ammonia removal from wastewater streams through membrane contactors: Experimental and theoretical analy-

sis of operation parameters and configuration," *Chemical Engineering Journal*, vol. 160, no. 2, pp. 530–537, 2010.

[247] Y. Hu and U. Schmidhalter, "Drought and salinity: A comparison of their effects on mineral nutrition of plants," *Journal of Plant Nutrition and Soil Science*, vol. 168, no. 4, pp. 541–549, 2005.

[248] D. J. Cole-Hamilton, "Homogeneous catalysis - New approaches to catalyst separation, recovery, and recycling," *Science*, vol. 299, no. 5613, pp. 1702–1706, 2003.

[249] I. Vural Gürsel, T. Noël, Q. Wang, and V. Hessel, "Separation/recycling methods for homogeneous transition metal catalysts in continuous flow," *Green Chemistry*, vol. 17, no. 4, pp. 2012–2026, 2015. arXiv: 1612.08814.

[250] Z. Chen, T. F. Jaramillo, T. G. Deutsch, A. Kleiman-Shwarsctein, A. J. Forman, N. Gaillard, R. Garland, K. Takanabe, C. Heske, M. Sunkara, E. W. McFarland, K. Domen, E. L. Miller, J. A. Turner, and H. N. Dinh, "Accelerating materials development for photoelectrochemical hydrogen production: Standards for methods, definitions, and reporting protocols," *Journal of Materials Research*, vol. 25, no. 01, pp. 3–16, 2010.

[251] C. C. L. McCrory, S. Jung, J. C. Peters, and T. F. Jaramillo, "Benchmarking heterogeneous electrocatalysts for the oxygen evolution reaction," *Journal of the American Chemical Society*, vol. 135, no. 45, pp. 16 977–16 987, 2013.

[252] C. C. L. McCrory, S. Jung, I. M. Ferrer, S. M. Chatman, J. C. Peters, and T. F. Jaramillo, "Benchmarking hydrogen evolving reaction and oxygen evolving reaction electrocatalysts for solar water splitting devices," *Journal of the American Chemical Society*, vol. 137, no. 13, pp. 4347–4357, 2015.

[253] W. A. Smith, "Photoelectrochemical cell design, efficiency, definitions, standards, and protocols," in *Photoelectrochemical Solar Fuel Production*, Springer International Publishing, 2016, pp. 163–197.

[254] T. Bligaard, R. M. Bullock, C. T. Campbell, J. G. Chen, B. C. Gates, R. J. Gorte, C. W. Jones, W. D. Jones, J. R. Kitchin, and S. L. Scott, "Toward benchmarking in catalysis science: Best practices, challenges, and opportunities," *ACS Catalysis*, vol. 6, no. 4, pp. 2590–2602, 2016.

[255] A. J. Martín, T. Shinagawa, and J. Pérez-Ramírez, "Electrocatalytic reduction of nitrogen: From haber-bosch to ammonia artificial leaf," *Chem*, 2018.

[256] Y. Shiraishi, S. Shiota, Y. Kofuji, M. Hashimoto, K. Chishiro, H. Hirakawa, S. Tanaka, S. Ichikawa, and T. Hirai, "Nitrogen fixation with water on carbon-nitride-

based metal-free photocatalysts with 0.1% solar-to-ammonia energy conversion efficiency," *ACS Applied Energy Materials*, vol. 1, no. 8, pp. 4169–4177, 2018.

[257] S. Huang, Y. Miao, Q. Cao, Y. Yao, G. Zhao, W. Yu, J. Shen, K. Yu, and G. Bareth, "A new critical nitrogen dilution curve for rice nitrogen status diagnosis in northeast china," *Pedosphere*, vol. 28, no. 5, pp. 814–822, 2018.

[258] P. Waller and M. Yitayew, "Chemigation," in *Irrigation and Drainage Engineering*, Springer International Publishing, 2016, pp. 327–341.

[259] C. Stockle and P Debaeke, "Modeling crop nitrogen requirements: A critical analysis," *European Journal of Agronomy*, vol. 7, no. 1-3, pp. 161–169, 1997.

[260] "Manufacturing Cost Analysis of PEM Fuel Cell Systems for 5- and 10-kW Backup Power Applications," Department of Energy, Tech. Rep., 2016.

[261] K. P. Kuhl, E. R. Cave, D. N. Abram, and T. F. Jaramillo, "New insights into the electrochemical reduction of carbon dioxide on metallic copper surfaces," *Energy & Environmental Science*, vol. 5, no. 5, p. 7050, 2012.

[262] A. International, *Standard tables for reference solar spectral irradiances: Direct normal and hemispherical on 37° tilted surface*, ASTM Standard, 2012.

[263] F. Zhou, L. M. Azofra, M. Ali, M. Kar, A. N. Simonov, C. McDonnell-Worth, C. Sun, X. Zhang, and D. R. MacFarlane, "Electro-synthesis of ammonia from nitrogen at ambient temperature and pressure in ionic liquids," *Energy & Environmental Science*, vol. 10, no. 12, pp. 2516–2520, 2017.

[264] B. L. Sheets and G. G. Botte, "Electrochemical nitrogen reduction to ammonia under mild conditions enabled by a polymer gel electrolyte," *Chemical Communications*, vol. 54, no. 34, pp. 4250–4253, 2018.

[265] P. Hohenberg and W. Kohn, "Inhomogeneous electron gas," *Physical Review*, vol. 136, no. 3B, B864–B871, 1964.

[266] W. Kohn and L. J. Sham, "Self-consistent equations including exchange and correlation effects," *Physical Review*, vol. 140, no. 4A, A1133–A1138, 1965.

[267] J. Wellendorff, K. T. Lundgaard, A. Møgelhøj, V. Petzold, D. D. Landis, J. K. Nørskov, T. Bligaard, and K. W. Jacobsen, "Density functionals for surface science: Exchange-correlation model development with bayesian error estimation," *Physical Review B*, vol. 85, no. 23, pp. 235 149–235 149, 2012.

[268] J. P. Perdew, K. Burke, and M. Ernzerhof, "Generalized gradient approximation made simple," *Phys. Rev. Lett.*, vol. 77, pp. 3865–3868, 18 1996.

[269] P. Giannozzi, S. Baroni, N. Bonini, M. Calandra, R. Car, C. Cavazzoni, D. Ceresoli, G. L. Chiarotti, M. Cococcioni, I. Dabo, A. Dal Corso, S. de Gironcoli, S. Fabris, G. Fratesi, R. Gebauer, U. Gerstmann, C. Gougoussis, A. Kokalj, M. Lazzeri, L. Martin-Samos, N. Marzari, F. Mauri, R. Mazzarello, S. Paolini, A. Pasquarello, L. Paulatto, C. Sbraccia, S. Scandolo, G. Sclauzero, A. P. Seitsonen, A. Smogunov, P. Umari, and R. M. Wentzcovitch, "Quantum espresso: A modular and open-source software project for quantum simulations of materials," *Journal of Physics: Condensed Matter*, vol. 21, no. 39, 395502 (19pp), 2009.

[270] A. H. Larsen, J. J. Mortensen, J. Blomqvist, I. E. Castelli, R. Christensen, M. Dułak, J. Friis, M. N. Groves, B. Hammer, C. Hargus, E. D. Hermes, P. C. Jennings, P. B. Jensen, J. Kermode, J. R. Kitchin, E. L. Kolsbjerg, J. Kubal, K. Kaasbjerg, S. Lysgaard, J. B. Maronsson, T. Maxson, T. Olsen, L. Pastewka, A. Peterson, C. Rostgaard, J. Schiøtz, O. Schütt, M. Strange, K. S. Thygesen, T. Vegge, L. Vilhelmsen, M. Walter, Z. Zeng, and K. W. Jacobsen, "The atomic simulation environment—a python library for working with atoms," *Journal of Physics: Condensed Matter*, vol. 29, no. 27, p. 273 002, 2017.

[271] J. K. Nørskov, J. Rossmeisl, A. Logadottir, L. Lindqvist, J. R. Kitchin, T. Bligaard, and H. Jónsson, "Origin of the overpotential for oxygen reduction at a fuel-cell cathode," *The Journal of Physical Chemistry B*, vol. 108, no. 46, pp. 17 886–17 892, 2004.

[272] ——, "Origin of the overpotential for oxygen reduction at a fuel-cell cathode," *J. Phys. Chem. B*, vol. 108, no. 46, pp. 17 886–17 892, 2004.

[273] A. A. Peterson, F. Abild-Pedersen, F. Studt, J. Rossmeisl, and J. K. Nørskov, "How copper catalyzes the electroreduction of carbon dioxide into hydrocarbon fuels," *Energy & Environmental Science*, vol. 3, no. 9, p. 1311, 2010.

[274] A. J. Nozik and R. Memming, "Physical chemistry of semiconductor-liquid interfaces," *The Journal of Physical Chemistry*, vol. 100, no. 31, pp. 13 061–13 078, 1996.

[275] F. Calle-Vallejo and M. T. Koper, "First-principles computational electrochemistry: Achievements and challenges," *Electrochimica Acta*, vol. 84, pp. 3–11, 2012.

[276] M. E. A. de Dompablo, A. Morales-García, and M. Taravillo, "DFT+U calculations of crystal lattice, electronic structure, and phase stability under pressure of TiO_2 polymorphs," *The Journal of Chemical Physics*, vol. 135, no. 5, p. 054 503, 2011.

[277] K. Reuter and M. Scheffler, "Composition, structure, and stability of RuO2(110) as a function of oxygen pressure," *Physical Review B*, vol. 65, no. 3, 2001.

[278] D. Zhu, L. Zhang, R. E. Ruther, and R. J. Hamers, "Photo-illuminated diamond as a solid-state source of solvated electrons in water for nitrogen reduction," *Nature Materials*, vol. 12, no. 9, pp. 836–841, 2013.

[279] M. Vettraino, M. Trudeau, A. Y. H. Lo, R. W. Schurko, and D. Antonelli, "Room-temperature ammonia formation from dinitrogen on a reduced mesoporous titanium oxide surface with metallic properties," *Journal of the American Chemical Society*, vol. 124, no. 32, pp. 9567–9573, 2002.

[280] M. Ali, F. Zhou, K. Chen, C. Kotzur, C. Xiao, L. Bourgeois, X. Zhang, and D. R. MacFarlane, "Nanostructured photoelectrochemical solar cell for nitrogen reduction using plasmon-enhanced black silicon," *Nature Communications*, vol. 7, p. 11 335, 2016.

[281] J. H. Montoya, C. Tsai, A. Vojvodic, and J. K. Nørskov, "The challenge of electrochemical ammonia synthesis: A new perspective on the role of nitrogen scaling relations," *ChemSusChem*, vol. 8, no. 13, pp. 2180–2186, 2015.

[282] P. H. Emmett and S. Brunauer, "The adsorption of nitrogen by iron synthetic ammonia catalysts," *Journal of the American Chemical Society*, vol. 55, no. 4, pp. 1738–1739, 1933.

[283] G. Ertl, M. Grunze, and M. Weiss, "Chemisorption of n2 on an fe(100) surface," *Journal of Vacuum Science and Technology*, vol. 13, no. 1, pp. 314–317, 1976.

[284] N. D. Spencer, R. C. Schoonmaker, and G. A. Somorjai, "Structure sensitivity in the iron single-crystal catalysed synthesis of ammonia," *Nature*, vol. 294, no. 5842, pp. 643–644, 1981.

[285] K. Honkala, "Ammonia synthesis from first-principles calculations," *Science*, vol. 307, no. 5709, pp. 555–558, 2005.

[286] A. Vojvodic, A. J. Medford, F. Studt, F. Abild-Pedersen, T. S. Khan, T. Bligaard, and J. K. Nørskov, "Exploring the limits: A low-pressure, low-temperature haber-bosch process," *Chemical Physics Letters*, vol. 598, pp. 108–112, 2014.

[287] G. S. Karlberg, J. Rossmeisl, and J. K. Nørskov, "Estimations of electric field effects on the oxygen reduction reaction based on the density functional theory," *Physical Chemistry Chemical Physics*, vol. 9, no. 37, p. 5158, 2007.

[288] Z.-D. He, S. Hanselman, Y.-X. Chen, M. T. M. Koper, and F. Calle-Vallejo, "Importance of solvation for the accurate prediction of oxygen reduction activities of pt-based electrocatalysts," *The Journal of Physical Chemistry Letters*, vol. 8, no. 10, pp. 2243–2246, 2017.

[289] C. J. M. van der Ham, M. T. M. Koper, and D. G. H. Hetterscheid, "Challenges in reduction of dinitrogen by proton and electron transfer," *Chem. Soc. Rev.*, vol. 43, no. 15, p. 5183, 2014.

[290] Y. Abghoui, A. L. Garden, J. G. Howalt, T. Vegge, and E. Skúlason, "Electroreduction of n_2 to ammonia at ambient conditions on mononitrides of zr, nb, cr, and v: A DFT guide for experiments," *ACS Catalysis*, vol. 6, no. 2, pp. 635–646, 2016.

[291] J. T. Yates, A. Szabó, and M. A. Henderson, "The influence of surface defect sites on chemisorption and catalysis," in *Structure-Activity and Selectivity Relationships in Heterogeneous Catalysis, Proceedings of the ACS Symposium on Structure-Activity Relationships in Heterogeneous Catalysis*, Elsevier, 1991, pp. 273–290.

[292] E. W. McFarland and H. Metiu, "Catalysis by doped oxides," *Chemical Reviews*, vol. 113, no. 6, pp. 4391–4427, 2013.

[293] G Hobiger, P Herzig, R Eibler, F Schlapansky, and A Neckel, "The influence of titanium and oxygen vacancies on the chemical bonding in titanium oxide," *Journal of Physics: Condensed Matter*, vol. 2, no. 20, pp. 4595–4612, 1990.

[294] B. R. Goldsmith, E. D. Sanderson, D. Bean, and B. Peters, "Isolated catalyst sites on amorphous supports: A systematic algorithm for understanding heterogeneities in structure and reactivity," *J. Chem. Phys.*, vol. 138, no. 20, p. 204 105, 2013.

[295] K. Ranjit and B. Viswanathan, "Photocatalytic reduction of nitrite and nitrate ions to ammonia on m/TiO_2 catalysts," *Journal of Photochemistry and Photobiology A: Chemistry*, vol. 108, no. 1, pp. 73–78, 1997.

[296] K. Kobwittaya and S. Sirivithayapakorn, "Photocatalytic reduction of nitrate over TiO_2 and ag-modified TiO_2," *Journal of Saudi Chemical Society*, vol. 18, no. 4, pp. 291–298, 2014.

[297] H. Kominami, H. Gekko, and K. Hashimoto, "Photocatalytic disproportionation of nitrite to dinitrogen and nitrate in an aqueous suspension of metal-loaded titanium(iv) oxide nanoparticles," *Physical Chemistry Chemical Physics*, vol. 12, no. 47, p. 15 423, 2010.

[298] M. Shand and J. A. Anderson, "Aqueous phase photocatalytic nitrate destruction using titania based materials: Routes to enhanced performance and prospects for visible light activation," *Catalysis Science & Technology*, vol. 3, no. 4, p. 879, 2013.

[299] A. V. Lozovskii, I. V. Stolyarova, R. V. Prikhod'ko, and V. V. Goncharuk, "Research of photocatalytic activity of the ag/TiO_2 catalysts in the reduction reaction of nitrate-ions in aqueous media," *Journal of Water Chemistry and Technology*, vol. 31, no. 6, pp. 360–366, 2009.

[300] C. H. Pollema, E. B. Milosavljević, J. L. Hendrix, L. Solujić, and J. H. Nelson, "Photocatalytic oxidation of aqueous ammonia (ammonium ion) to nitrite or nitrate at TiO_2 particles," *Monatshefte für Chemie Chemical Monthly*, vol. 123, no. 4, pp. 333–339, 1992.

[301] A. Wang, J. G. Edwards, and J. A. Davies, "Photooxidation of aqueous ammonia with titania-based heterogeneous catalysts," *Solar Energy*, vol. 52, no. 6, pp. 459–466, 1994.

[302] H. Kominami, K. Kitsui, Y. Ishiyama, and K. Hashimoto, "Simultaneous removal of nitrite and ammonia as dinitrogen in aqueous suspensions of a titanium(iv) oxide photocatalyst under reagent-free and metal-free conditions at room temperature," *RSC Adv.*, vol. 4, no. 93, pp. 51 576–51 579, 2014.

[303] K Urabe, "Isotopic equilibration of nitrogen on potassium-promoted transition metal catalysts," *Journal of Catalysis*, vol. 54, no. 3, pp. 436–438, 1978.

[304] S. U. M. Khan, M. Al-Shahry, and W. B. Ingler Jr., "Efficient photochemical water splitting by a chemically modified n-tio2," *Advancement Of Science*, vol. 297, no. September, pp. 2243–2245, 2002.

[305] X. Yang, C. Cao, K. Hohn, L. Erickson, R. Maghirang, D. Hamal, and K. Klabunde, "Highly visible-light active C- and V-doped $TiO_2$for degradation of acetaldehyde," *Journal of Catalysis*, vol. 252, no. 2, pp. 296–302, 2007.

[306] A Ruban, B Hammer, P Stoltze, H. Skriver, and J. Nørskov, "Surface electronic structure and reactivity of transition and noble metals1communication presented at the first francqui colloquium, brussels, 19–20 february 1996.1," *Journal of Molecular Catalysis A: Chemical*, vol. 115, no. 3, pp. 421–429, 1997.

[307] B. Hammer and J. K. Norskov, "Why gold is the noblest of all the metals," *Nature*, vol. 376, no. 6537, pp. 238–240, 1995.

[308] A. Nilsson and L. G. Pettersson, "Adsorbate electronic structure and bonding on metal surfaces," in *Chemical Bonding at Surfaces and Interfaces*, Elsevier, 2008, pp. 57–142.

[309] B. Hammer and J. Nørskov, "Theoretical surface science and catalysis—calculations and concepts," in *Advances in Catalysis*, Elsevier, 2000, pp. 71–129.

[310] Z. Xu and J. R. Kitchin, "Relationships between the surface electronic and chemical properties of doped 4d and 5d late transition metal dioxides," *The Journal of Chemical Physics*, vol. 142, no. 10, p. 104 703, 2015.

[311] N. J. O'Connor, A. S. M. Jonayat, M. J. Janik, and T. P. Senftle, "Interaction trends between single metal atoms and oxide supports identified with density functional theory and statistical learning," *Nature Catalysis*, vol. 1, no. 7, pp. 531–539, 2018.

[312] M. García-Mota, A. Vojvodic, H. Metiu, I. C. Man, H.-Y. Su, J. Rossmeisl, and J. K. Nørskov, "Tailoring the activity for oxygen evolution electrocatalysis on rutile TiO_2(110) by transition-metal substitution," *ChemCatChem*, vol. 3, no. 10, pp. 1607–1611, 2011.

[313] V. Iliev, D. Tomova, L. Bilyarska, A. Eliyas, and L. Petrov, "Photocatalytic properties of TiO_2 modified with platinum and silver nanoparticles in the degradation of oxalic acid in aqueous solution," *Applied Catalysis B: Environmental*, vol. 63, no. 3-4, pp. 266–271, 2006.

[314] T. M. D. Dang, T. M. H. Nguyen, and H. P. Nguyen, "The preparation of nano-gold catalyst supported on iron doped titanium oxide," *Advances in Natural Sciences: Nanoscience and Nanotechnology*, vol. 1, no. 2, p. 025 011, 2010.

[315] V. M. Shinde and G. Madras, "CO methanation toward the production of synthetic natural gas over highly active Ni/TiO_2catalyst," *AIChE Journal*, vol. 60, no. 3, pp. 1027–1035, 2013.

[316] J. Yu, J. Yu, Z. Shi, Q. Guo, X. Xiao, H. Mao, and D. Mao, "The effects of the nature of TiO_2 supports on the catalytic performance of Rh–Mn/TiO_2 catalysts in the synthesis of C2 oxygenates from syngas," *Catalysis Science & Technology*, vol. 9, no. 14, pp. 3675–3685, 2019.

[317] S. Bagheri, N. M. Julkapli, and S. B. A. Hamid, "Titanium dioxide as a catalyst support in heterogeneous catalysis," *The Scientific World Journal*, vol. 2014, pp. 1–21, 2014.

[318] M. A. Turchanin and P. G. Agraval, "Cohesive energy, properties, and formation energy of transition metal alloys," *Powder Metallurgy and Metal Ceramics*, vol. 47, no. 1-2, pp. 26–39, 2008.

[319] U. Mizutani, M. Inukai, H. Sato, and E. Zijlstra, "2 - electron theory of complex metallic alloys," in *Physical Metallurgy (Fifth Edition)*, D. E. Laughlin and K. Hono, Eds., Fifth Edition, Oxford: Elsevier, 2014, pp. 103 –202, ISBN: 978-0-444-53770-6.

[320] T. Z. H. Gani and H. J. Kulik, "Understanding and breaking scaling relations in single-site catalysis: Methane to methanol conversion by Fe^{IV}=O," *ACS Catalysis*, vol. 8, no. 2, pp. 975–986, 2018.

[321] M. T. Darby, M. Stamatakis, A. Michaelides, and E. C. H. Sykes, "Lonely atoms with special gifts: Breaking linear scaling relationships in heterogeneous catalysis with single-atom alloys," *The Journal of Physical Chemistry Letters*, vol. 9, no. 18, pp. 5636–5646, 2018.

[322] S. Wang, V. Petzold, V. Tripkovic, J. Kleis, J. G. Howalt, E. Skúlason, E. M. Fernández, B. Hvolbæk, G. Jones, A. Toftelund, H. Falsig, M. Björketun, F. Studt, F. Abild-Pedersen, J. Rossmeisl, J. K. Nørskov, and T. Bligaard, "Universal transition state scaling relations for (de)hydrogenation over transition metals," *Physical Chemistry Chemical Physics*, vol. 13, no. 46, p. 20 760, 2011.

[323] P. C. K. Vesborg and T. F. Jaramillo, "Addressing the terawatt challenge: Scalability in the supply of chemical elements for renewable energy," *RSC Advances*, vol. 2, no. 21, p. 7933, 2012.

[324] J. A. Hernandez, S. J. George, and L. M. Rubio, "Molybdenum trafficking for nitrogen fixation," *Biochemistry*, vol. 48, no. 41, pp. 9711–9721, 2009.

[325] Y. Roux, C. Duboc, and M. Gennari, "Molecular catalysts for n 2 reduction: State of the art, mechanism, and challenges," *ChemPhysChem*, vol. 18, no. 19, pp. 2606–2617, 2017.

[326] K. Ranjit, T. Varadarajan, and B. Viswanathan, "Photocatalytic reduction of dinitrogen to ammonia over noble-metal-loaded TiO_2," *Journal of Photochemistry and Photobiology A: Chemistry*, vol. 96, no. 1-3, pp. 181–185, 1996.

[327] J. Yang, Y. Guo, R. Jiang, F. Qin, H. Zhang, W. Lu, J. Wang, and J. C. Yu, "High-efficiency "working-in-tandem" nitrogen photofixation achieved by assembling plasmonic gold nanocrystals on ultrathin titania nanosheets," *Journal of the American Chemical Society*, vol. 140, no. 27, pp. 8497–8508, 2018.

[328] F. Larkins and A Lubenfeld, "The auger spectrum of solid ammonia," *Journal of Electron Spectroscopy and Related Phenomena*, vol. 15, no. 1, pp. 137–144, 1979.

[329] X. Chen and C. Burda, "Photoelectron spectroscopic investigation of nitrogen-doped titania nanoparticles," *The Journal of Physical Chemistry B*, vol. 108, no. 40, pp. 15 446–15 449, 2004.

[330] M. Lazarus and T. Sham, "X-ray photoelectron spectroscopy (xps) studies of hydrogen reduced rutile (tio_2-x) surfaces," *Chemical Physics Letters*, vol. 92, no. 6, pp. 670–674, 1982.

[331] Y. Park, W. Kim, H. Park, T. Tachikawa, T. Majima, and W. Choi, "Carbon-doped TiO_2 photocatalyst synthesized without using an external carbon precursor and

the visible light activity," *Applied Catalysis B: Environmental*, vol. 91, no. 1-2, pp. 355–361, 2009.

[332] "Retraction for chanmanee et al., solar photothermochemical alkane reverse combustion," *Proceedings of the National Academy of Sciences*, vol. 115, no. 3, E557–E557, 2018.

[333] W Göpel, J. Anderson, D Frankel, M Jaehnig, K Phillips, J. Schäfer, and G Rocker, "Surface defects of tio_2 (110): A combined xps, xaes and els study," *Surface science*, vol. 139, no. 2-3, pp. 333–346, 1984.

[334] T. L. Barr and S. Seal, "Nature of the use of adventitious carbon as a binding energy standard," *Journal of Vacuum Science & Technology A: Vacuum, Surfaces, and Films*, vol. 13, no. 3, pp. 1239–1246, 1995.

[335] R. F. W. Bader, "A quantum theory of molecular structure and its applications," *Chemical Reviews*, vol. 91, no. 5, pp. 893–928, 1991.

[336] C. T. Brigden, S. Poulston, M. V. Twigg, A. P. Walker, and A. J. Wilkins, "Photooxidation of short-chain hydrocarbons over titania," *Applied Catalysis B: Environmental*, vol. 32, no. 1-2, pp. 63–71, 2001.

[337] W. Tu, Y. Zhou, and Z. Zou, "Photocatalytic conversion of CO_2 into renewable hydrocarbon fuels: State-of-the-art accomplishment, challenges, and prospects," *Advanced Materials*, vol. 26, no. 27, pp. 4607–4626, 2014.

[338] H. Kisch, "Nitrogen Photofixation at Nanostructured Iron Titanate Films," in *Energy Efficiency and Renewable Energy Through Nanotechnology*, Springer Science + Business Media, 2011, pp. 585–599.

[339] O. Rusina, A. Eremenko, G. Frank, H. P. Strunk, and H. Kisch, "Nitrogen Photofixation at Nanostructured Iron Titanate Films," *Angew. Chem. Int. Ed.*, vol. 113, no. 21, pp. 4115–4117, 2001.

[340] N. M. Dimitrijevic, B. K. Vijayan, O. G. Poluektov, T. Rajh, K. A. Gray, H. He, and P. Zapol, "Role of water and carbonates in photocatalytic transformation of CO 2 to CH4 on titania," *Journal of the American Chemical Society*, vol. 133, no. 11, pp. 3964–3971, 2011.

[341] M. Anpo, H. Yamashita, Y. Ichihashi, and S. Ehara, "Photocatalytic reduction of CO2 with H_2O on various titanium oxide catalysts," *Journal of Electroanalytical Chemistry*, vol. 396, no. 1-2, pp. 21–26, 1995.

[342] L. Yu and D. Li, "Photocatalytic methane conversion coupled with hydrogen evolution from water over pd/TiO_2," *Catal. Sci. Technol.*, vol. 7, pp. 635–640, 3 2017.

[343] X.-F. Li, Q.-K. Li, J. Cheng, L. Liu, Q. Yan, Y. Wu, X.-H. Zhang, Z.-Y. Wang, Q. Qiu, and Y. Luo, "Conversion of dinitrogen to ammonia by FeN_3-embedded graphene," *Journal of the American Chemical Society*, vol. 138, no. 28, pp. 8706–8709, 2016.

[344] I. Y. Jeon, H. J. Choi, M. J. Ju, I. T. Choi, K. Lim, J. Ko, H. K. Kim, J. C. Kim, J. J. Lee, D. Shin, S. M. Jung, J. M. Seo, M. J. Kim, N. Park, L. Dai, and J. B. Baek, "Direct nitrogen fixation at the edges of graphene nanoplatelets as efficient electrocatalysts for energy conversion," *Scientific Reports*, vol. 3, pp. 1–7, 2013.

[345] T. Hirakawa and Y. Nosaka, "Properties of O_2^- and OH formed in TiO_2 aqueous suspensions by photocatalytic reaction and the influence of h_2o_2 and some ions," *Langmuir*, vol. 18, no. 8, pp. 3247–3254, 2002.

[346] A. Jain, S. P. Ong, G. Hautier, W. Chen, W. D. Richards, S. Dacek, S. Cholia, D. Gunter, D. Skinner, G. Ceder, and K. a. Persson, "The Materials Project: A materials genome approach to accelerating materials innovation," *APL Materials*, vol. 1, no. 1, p. 011 002, 2013.

[347] P. L. Holland, "Metal–dioxygen and metal–dinitrogen complexes: Where are the electrons?" *Dalton Transactions*, vol. 39, no. 23, p. 5415, 2010.

[348] Q. Li, C. Liu, S. Qiu, F. Zhou, L. He, X. Zhang, and C. Sun, "Exploration of iron borides as electrochemical catalysts for the nitrogen reduction reaction," *Journal of Materials Chemistry A*, vol. 7, no. 37, pp. 21 507–21 513, 2019.

[349] R. Tran, Z. Xu, B. Radhakrishnan, D. Winston, W. Sun, K. A. Persson, and S. P. Ong, "Surface energies of elemental crystals," *Scientific Data*, vol. 3, no. 1, 2016.

[350] W. Sun and G. Ceder, "Efficient creation and convergence of surface slabs," *Surface Science*, vol. 617, pp. 53–59, 2013.